

Model-independent bounds on new physics effects in non-leptonic tree-level decays of B-mesons

Alexander Lenz^a Gilberto Tetlalmatzi-Xolocotzi^{1b,c}

^a*Institute for Particle Physics Phenomenology, Durham University,
DH1 3LE Durham, United Kingdom*

^b*Theoretische Physik 1, Naturwissenschaftlich-Technische Fakultät, Universität Siegen,
Walter-Flex-Strasse 3, D-57068 Siegen, Germany*

^c*Nikhef, Theory Group, Science Park 105, 1098 XG, Amsterdam, The Netherlands*

E-mail: alexander.lenz@durham.ac.uk, gtx@physik.uni-siegen.de

ABSTRACT: We present a considerably improved analysis of model-independent bounds on new physics effects in non-leptonic tree-level decays of B-mesons. Our main finding is that contributions of about ± 0.1 to the Wilson coefficient of the colour-singlet operator Q_2 of the effective weak Hamiltonian and contributions in the range of ± 0.5 (both for real and imaginary part) to Q_1 can currently not be excluded at the 90% C.L.. Effects of such a size can modify the direct experimental extraction of the CKM angle γ by up to 10° and they could lead to an enhancement of the decay rate difference $\Delta\Gamma_d$ of up to a factor of 5 over its SM value - a size that could explain the D^0 dimuon asymmetry. Future more precise measurements of the semi-leptonic asymmetries a_{sl}^q and the lifetime ratio $\tau(B_s)/\tau(B_d)$ will allow to shrink the bounds on tree-level new physics effects considerably. Due to significant improvements in the precision of the non-perturbative input we update all SM predictions for the mixing observables in the course of this analysis, obtaining: $\Delta M_s = (18.77 \pm 0.86) \text{ ps}^{-1}$, $\Delta M_d = (0.543 \pm 0.029) \text{ ps}^{-1}$, $\Delta\Gamma_s = (9.1 \pm 1.3) \cdot 10^{-2} \text{ ps}^{-1}$, $\Delta\Gamma_d = (2.6 \pm 0.4) \cdot 10^{-3} \text{ ps}^{-1}$, $a_{sl}^s = (2.06 \pm 0.18) \cdot 10^{-5}$ and $a_{sl}^d = (-4.73 \pm 0.42) \cdot 10^{-4}$.

KEYWORDS: New Physics, B-Physics, CP violation

¹Corresponding author.

Contents

1	Introduction	1
2	Basic formalism	3
2.1	Effective Hamiltonian	3
2.2	Heavy Quark Expansion	5
2.3	QCD Factorization	7
3	Strategy	11
3.1	Statistical analysis	12
4	Individual Constraints	13
4.1	Observables constraining $b \rightarrow c\bar{u}d$ transitions	14
4.1.1	$\bar{B}_d^0 \rightarrow D^{*+}\pi^-$	14
4.2	Observables constraining $b \rightarrow u\bar{u}d$ transitions	16
4.2.1	$R_{\pi\pi}$	16
4.2.2	$S_{\pi\pi}$	19
4.2.3	$S_{\rho\pi}$	20
4.2.4	$R_{\rho\rho}$	24
4.3	Observables constraining $b \rightarrow c\bar{c}s$ transitions	26
4.3.1	$\bar{B} \rightarrow X_s\gamma$	26
4.3.2	$\Delta\Gamma_s$: Bounds and SM update	28
4.3.3	$S_{J/\psi\phi}$	36
4.3.4	τ_{B_s}/τ_{B_d}	37
4.4	Observables constraining $b \rightarrow c\bar{c}d$ transitions	39
4.4.1	$\sin(2\beta_d)$ and SM update of ΔM_q	39
4.4.2	$\bar{B} \rightarrow X_d\gamma$	42
4.5	Observables constraining multiple channels	44
4.5.1	a_{sl}^s and a_{sl}^d : Bounds and SM update	44
5	Global χ^2-fit results	44
5.1	χ^2 -fit for the $b \rightarrow u\bar{u}d$ channel and bounds on $\Delta\Gamma_d$	48
5.2	χ^2 -fit for the $b \rightarrow c\bar{u}d$ channel and bounds on $\Delta\Gamma_d$	49
5.3	χ^2 -fit for the $b \rightarrow c\bar{c}d$ channel and bounds on $\Delta\Gamma_d$	50
5.4	Universal fit on $\Delta C_1(M_W)$ and $\Delta C_2(M_W)$	51
5.5	NP in non-leptonic tree-level decays and its interplay with the CKM angle γ	53
6	Future prospects	54
6.1	τ_{B_s}/τ_{B_d}	55
6.2	Semi-leptonic CP asymmetries	55
6.3	Rare decays	56

7	Conclusions and outlook	57
A	Numerical Inputs	58
B	QCD-Factorization formulas	63
B.1	Generic parameters	63
B.1.1	Vertices for the $B \rightarrow \pi\pi, \rho\pi, \pi\rho, \rho\rho$ decays	64
B.1.2	Vertices for the $B \rightarrow J/\psi\phi$ decay.	64
B.1.3	Penguin functions	65
B.1.4	Hard Scattering functions for the $B \rightarrow \pi\pi, \rho\pi, \pi\rho, \rho\rho$ decays.	68
B.1.5	Hard scattering function for the $B \rightarrow J/\psi\phi$	68
B.2	Annihilation coefficients	70
B.3	Annihilation kernels	70

1 Introduction

Motivations for flavour physics are manifold. Standard model parameters, like the elements of the Cabibbo-Kobayashi-Maskawa (CKM) matrix [1, 2] or quark masses are determined very accurately in this field. Moreover the quark-sector is the only sector, where CP violating effects have been detected so far - since 1964 in the Kaon sector [3] and since 2001 also in the B-sector [4, 5]. Very recently CP violation has been measured for the first time in the charm sector [6], which might actually be an indication for physics beyond the standard model (BSM) [7, 8]. Considering that CP violation is a necessary ingredient for creating a baryon asymmetry in the universe [9], flavour physics might shed some light on this unsolved problem. In addition flavour physics is perfectly suited for indirect new physics (NP) searches, because there are many processes strongly suppressed in the standard model (SM) but not necessarily in hypothetical NP models. And, last but not least, a comparison between experiment and theory predictions can provide a deeper insight into the dynamics of QCD.

In recent years experimental flavour physics entered a new precision era, which was initiated by the B-factories at KEK and SLAC (see e.g. [10]) and the Tevatron at Fermilab [11, 12]. Currently this field is dominated by the results of the LHCb collaboration [13, 14], but also complemented by competing results from the general purpose detectors ATLAS and CMS, see e.g. [15, 16].

The corresponding dramatic increase in experimental precision, demands complementary improvements in theory. Besides calculating higher orders in perturbative QCD or more precise lattice evaluations, this also means revisiting some common approximations by investigating questions like: How large are penguin contributions? How well does QCD-factorization [17–20] work? How large can duality violation in the Heavy Quark Expansion (HQE) (see e.g. [21–28] for pioneering papers and [29] for a recent review) be? How sizeable NP effects in tree-level decays can be? Some of these questions have been studied in

detail for quite some time. There is e.g. a huge literature on penguin contributions, see e.g. [30, 31] for reviews. Others gained interest recently, for instance duality violations [32]. In principle all these questions are interwoven, but as a starting point it is reasonable to consider them separately. The assumption of no NP effects at tree-level in non-leptonic b -decays was already challenged after the measurement of the dimuon asymmetry by the D0-collaboration [33–36], see e.g. [37]. And after the measurements of $B \rightarrow D^{(*)}\tau\nu$ by BaBar, Belle and LHCb [38–41] for the case of semi-leptonic b -decays.

Compared to numerous systematic studies of NP effects in the Wilson coefficients of the electromagnetic dipole and the semi-leptonic penguin operators $Q_{7\gamma}$ and Q_9 , Q_{10} respectively, see e.g. [42–54], we are not aware of systematic studies for NP effects in the Wilson coefficients for non-leptonic tree-level decays, except the ones in [55–60]¹.

The aim of the current paper is to considerably extend the studies in [55, 57] by incorporating two main improvements:

1. A full χ^2 -fit is performed instead of a simple parameter scan. To implement this step we use the package MyFitter [63] and allow the different nuisance parameters to run independently. This will allow us to account properly for the corresponding statistical correlations.
2. Instead of simplified theoretical equations we include full expressions for the observables under investigation.

The recent work in [58, 60] concentrates exclusively on the transition $b \rightarrow c\bar{c}s$, while we consider in this paper all different hadronic decays, that occur in the SM on tree-level. Moreover in this work we consider only BSM effects to the tree-level operators Q_1 and Q_2 , while [58, 60] investigates also effects of four-quark operators that do not exist in the SM. Whenever there is some direct overlap between the work in [58, 60] we directly compare the results. Any realistic BSM model that gives rise to new tree-level effects will also give new effects at the loop-level, which are not considered in the current model independent approach. In that respect this work can be considered as an important building block of future model dependent studies.

The paper is organised as follows: In Section 2 we describe briefly the theoretical tools to be used: we start with the effective Hamiltonian in Section 2.1, then in Section 2.2 we introduce the Heavy Quark Expansion and in Section 2.3 we review basic concepts in QCD factorization relevant to this project. Next in Section 3, we outline our strategy for performing the χ^2 -fit. We discuss all our different constraints on NP effects in non-leptonic tree-level decays in Section 4. The bounds on individual decay channels are organized as follows: $b \rightarrow c\bar{u}d$ in Section 4.1, $b \rightarrow u\bar{u}d$ in Section 4.2, $b \rightarrow c\bar{c}s$ in Section 4.3, $b \rightarrow c\bar{c}d$ in Section 4.4. Additionally, in Section 4.5 we present observables constraining more decay channels. Our main results are presented in Section 5: fits for the allowed size

¹ In [61] NP entering inside Q_5 and Q_6 is explored, establishing a link between the $B \rightarrow K\pi$ puzzle and the ε'/ε ratio. This is further addressed in [62] within the context of simplified Z' models with $U(2)^3$ flavour symmetry.

of BSM effects in the tree-level Wilson coefficients based on individual decay channels will be discussed in Sections 5.1 - 5.3. In particular we focus on the channels which can enhance the decay rate difference of neutral B_d^0 -mesons $\Delta\Gamma_d$ and we calculate these enhancements. Flavour-universal bounds on the tree level Wilson coefficients will be presented in Section 5.5, with an emphasis on the consequences of tree-level NP effects on the precision in the direct extraction of the CKM angle γ . In Section 6 we study observables that seem to be most promising in shrinking the space for new effects in C_1 and C_2 . Finally we conclude in Section 7 and give additional information in the appendices.

Since there has been tremendous progress (see e.g.[64, 65]) in the theoretical precision of the mixing observables, we will present in this work numerical updates of all mixing observables: $\Delta\Gamma_q$ in Section 4.3.2, ΔM_q in Section 4.4.1 and the semi-leptonic CP asymmetries a_{sl}^q and mixing phases ϕ_q in Section 4.5.

2 Basic formalism

In this section we provide an overview of the basic theoretical tools required for the description of our different flavour observables, this includes: the effective Hamiltonian, the Heavy Quark Expansion for inclusive decays and mixing observables. A quick review of QCD factorization for exclusive, non-leptonic decays is also provided. In addition we fix the notation to be used during this work.

2.1 Effective Hamiltonian

We start by introducing the effective Hamiltonian describing a b -quark decay into a $p\bar{p}'q$ final state via electroweak interactions, with $p, p' = u, c$ and $q = s, d$:

$$\begin{aligned} \hat{\mathcal{H}}_{eff}^{|\Delta B|=1} = \frac{G_F}{\sqrt{2}} \left\{ \sum_{p,p'=u,c} \lambda_{pp'}^{(q)} \sum_{i=1,2} C_i^{q,pp'}(\mu) \hat{Q}_i^{q,pp'} \right. \\ \left. + \sum_{p=u,c} \lambda_p^{(q)} \left[\sum_{i=3}^{10} C_i^q(\mu) \hat{Q}_i^q + C_{7\gamma}^q \hat{Q}_{7\gamma}^q + C_{8g}^q \hat{Q}_{8g}^q \right] \right\} + h.c.. \end{aligned} \quad (2.1)$$

The Fermi constant is denoted by G_F , additionally we have introduced the following CKM combinations

$$\begin{aligned} \lambda_p^{(q)} &= V_{pb} V_{pq}^*, \\ \lambda_{pp'}^{(q)} &= V_{pb} V_{p'q}^*. \end{aligned} \quad (2.2)$$

Moreover C_i denote the Wilson coefficients of the following dimension six operators:

$$\begin{aligned}
\hat{Q}_1^{q,pp'} &= (\bar{\hat{p}}_\beta \hat{b}_\alpha)_{V-A} (\bar{\hat{q}}_\alpha \hat{p}'_\beta)_{V-A}, & \hat{Q}_2^{q,pp'} &= (\bar{\hat{p}} \hat{b})_{V-A} (\bar{\hat{q}} \hat{p}')_{V-A}, \\
\hat{Q}_3^q &= (\bar{\hat{q}} \hat{b})_{V-A} \sum_k (\bar{\hat{k}} \hat{k})_{V-A}, & \hat{Q}_4^q &= (\bar{\hat{q}}_\alpha \hat{b}_\beta)_{V-A} \sum_k (\bar{\hat{k}}_\beta \hat{k}_\alpha)_{V-A}, \\
\hat{Q}_5^q &= (\bar{\hat{q}} \hat{b})_{V-A} \sum_k (\bar{\hat{k}} \hat{k})_{V+A}, & \hat{Q}_6^q &= (\bar{\hat{q}}_\alpha \hat{b}_\beta)_{V-A} \sum_k (\bar{\hat{k}}_\beta \hat{k}_\alpha)_{V+A}, \\
\hat{Q}_7^q &= (\bar{\hat{q}} \hat{b})_{V-A} \sum_k \frac{3}{2} e_k (\bar{\hat{k}} \hat{k})_{V+A}, & \hat{Q}_8^q &= (\bar{\hat{q}}_\alpha \hat{b}_\beta)_{V-A} \sum_k \frac{3}{2} e_k (\bar{\hat{k}}_\beta \hat{k}_\alpha)_{V+A}, \\
\hat{Q}_9^q &= (\bar{\hat{q}} \hat{b})_{V-A} \sum_k \frac{3}{2} e_k (\bar{\hat{k}} \hat{k})_{V-A}, & \hat{Q}_{10}^q &= (\bar{\hat{q}}_\alpha \hat{b}_\beta)_{V-A} \sum_k \frac{3}{2} e_k (\bar{\hat{k}}_\beta \hat{k}_\alpha)_{V-A}, \\
\hat{Q}_{7\gamma}^q &= \frac{e}{8\pi^2} m_b \bar{\hat{q}} \sigma_{\mu\nu} (1 + \gamma_5) \hat{F}^{\mu\nu} \hat{b}, & \hat{Q}_{8g}^q &= \frac{g_s}{8\pi^2} m_b \bar{\hat{q}} \sigma_{\mu\nu} (1 + \gamma_5) \hat{G}^{\mu\nu} \hat{b}. \quad (2.3)
\end{aligned}$$

Here α and β are colour indices, e_k is the electric charge of the quark k (in the penguin operators the quark flavours are summed over $k = u, d, s, c, b$), e is the $U(1)_{\text{em}}$ coupling and g_s the $SU(3)_C$ one, m_b is the mass of the b -quark and $F^{\mu\nu}$ and $G^{\mu\nu}$ are the electro-magnetic and chromo-magnetic field strength tensors respectively. In this work we consider NP effects that will affect the tree-level operators $\hat{Q}_1^{q,pp'}$ and $\hat{Q}_2^{q,pp'}$ by modifying their corresponding Wilson coefficients. In our notation $\hat{Q}_1^{q,pp'}$ is colour non diagonal and $\hat{Q}_2^{q,pp'}$ is the colour singlet, the QCD penguin operators correspond to \hat{Q}_{3-6}^q and the electro-weak penguin interactions are described by \hat{Q}_{7-10}^q . Different bases compared to the one in Eq. (2.3) are used in the literature. Our notation agrees with the one used in [66] and [67], here C_{8g} is negative because we are considering $-ig\gamma_\mu T^a$ as the Feynman rule for the quark-gluon vertex. In [19] a different basis is used, where \hat{Q}_1 and \hat{Q}_2 are interchanged and $\hat{Q}_{7\gamma}$ and \hat{Q}_{8g} have a different sign (this is equivalent to the sign convention $iD^\mu = i\partial^\mu + g_s A_a^\mu T^a$ for the gauge-covariant derivative)². A nice introduction on effective Hamiltonians can be found in [69], and a concise review up to NLO-QCD in [66].

The Wilson coefficients C_i with $i = 1, 2, \dots, 10, 7\gamma, 8g$ in Eq. (2.1) are obtained by matching the calculations of the effective theory and the full SM at the scale $\mu = M_W$ and then evolving down to the scale $\mu \sim m_b$ using the renormalisation group equations according to

$$\vec{C}(\mu) = \mathbf{U}(\mu, M_W, \alpha) \vec{C}(M_W), \quad (2.4)$$

where the NLO evolution matrix is given by [19]

$$\mathbf{U}(\mu, M_W, \alpha) = \mathbf{U}(\mu, \mu_W) + \frac{\alpha}{4\pi} \mathbf{R}(\mu, \mu_W). \quad (2.5)$$

The matrix $\mathbf{U}(\mu, \mu_W)$ accounts for pure QCD evolution, on the other hand $\mathbf{R}(\mu, \mu_W)$

²A minimal basis of dimension six operators for $\Delta B \neq 0$ processes has been introduced in [68]. This extends our set of operators in Eq. (2.3). For the purposes of studying NP in tree-level non-leptonic operators the basis in Eq. (2.3) is enough. However, future extension which include NP in other operators as well, should be done paying attention to the results presented in [68].

introduces QED effects as well. We write at NLO [19]

$$\begin{aligned} \mathbf{U}(\mu, M_W, \alpha) = & \left[\mathbf{U}_0 + \frac{\alpha_s(\mu)}{4\pi} \mathbf{J} \mathbf{U}_0 - \frac{\alpha_s(M_W)}{4\pi} \mathbf{U}_0 \mathbf{J} \right. \\ & \left. + \frac{\alpha}{4\pi} \left(\frac{4\pi}{\alpha_s(\mu)} \mathbf{R}_0 + \mathbf{R}_1 \right) \right], \end{aligned} \quad (2.6)$$

where $\alpha_s(\mu)$ denotes the strong coupling at the scale μ calculated up to NLO-QCD precision and α is the electro-magnetic coupling. The matrix \mathbf{U}_0 is the LO of the pure QCD evolution component $\mathbf{U}(\mu, \mu_W)$. At LO the evolution matrix $\mathbf{U}(\mu, M_W, \alpha)$ reduces to

$$\mathbf{U}^{\text{LO}}(\mu, \mu_W, \alpha) = \mathbf{U}_0 + \frac{\alpha}{\alpha_s(\mu)} \mathbf{R}_0. \quad (2.7)$$

The NLO-QCD corrections are then introduced through \mathbf{J} . The explicit expressions for \mathbf{U}_0 and \mathbf{J} are given in Eqns. (3.94)-(3.98) of [66]. The anomalous dimension matrices $\gamma_s^{(0)}$ and $\gamma_s^{(1)}$ required for these evaluations can be found in Eqn. (6.25) and Tables XIV and XV of [66]. To introduce QED corrections we calculate \mathbf{R}_0 and \mathbf{R}_1 using Eqns. (7.24)-(7.28) of [66], the anomalous dimension matrices used are $\gamma_e^{(0)}$ and $\gamma_e^{(1)}$ and are given in Tables XVI and XVII of [66].

The initial conditions for the Wilson coefficients have the following expansion at NLO

$$\begin{aligned} \vec{C}(M_W) = & \vec{C}_s^{(0)}(M_W) + \frac{\alpha_s(M_W)}{4\pi} \vec{C}_s^{(1)}(M_W) \\ & + \frac{\alpha}{4\pi} \left[\vec{C}_e^{(0)}(M_W) + \frac{\alpha_s(M_W)}{4\pi} \vec{C}_e^{(1)}(M_W) + \vec{R}_e^{(0)}(M_W) \right], \end{aligned} \quad (2.8)$$

as pointed out in [19] the electroweak contributions $\vec{C}_e^{(0)}$ and $\vec{C}_e^{(1)}$ in Eq. (2.8) can be x_t and/or $1/\sin^2 \theta_W$ enhanced. Consequently it is fair to treat the product between α and $\vec{C}_e^{(0)}$ as a LO contribution and the product between α and $\vec{C}_e^{(1)}$ as a NLO effect. The remainder, denoted by $\vec{R}_e^{(0)}$, is numerically smaller in comparison with $\vec{C}_e^{(0)}$ and it is therefore treated as a NLO effect, it contains the NLO scheme dependency. This approach differs from the one followed by [66], where the contribution of $\vec{C}_e^{(0)}(M_W) + \vec{R}_e^{(0)}(M_W)$ is introduced as a NLO effect and then $\vec{C}_e^{(1)}$ is omitted. The explicit expressions for $\vec{C}_s^{(0)}$, $\vec{C}_s^{(1)}$, $\vec{C}_e^{(0)}$, $\vec{C}_e^{(1)}$ and $\vec{R}_e^{(0)}$ of $\vec{C}(M_W)$ are given in Section VII.B of [66] and Section 3.1 of [19], the results presented for $\vec{C}_e^{(1)}$ in [19] are based on the calculations of [70].

It should be further stressed that when applying Eq. (2.4) we consistently dropped products between NLO contributions from $\mathbf{U}(\mu, M_W, \alpha)$ and NLO effects from $\vec{C}(M_W)$ but we have taken into account products between NLO contributions from $\mathbf{U}(\mu, M_W, \alpha)$ and LO contributions from $\vec{C}(M_W)$ and vice versa.

2.2 Heavy Quark Expansion

The effective Hamiltonian can be used to calculate inclusive decays of a heavy hadron B_q into an inclusive final state X via

$$\Gamma(B_q \rightarrow X) = \frac{1}{2m_{B_q}} \sum_X \int_{\text{PS}} (2\pi)^4 \delta^{(4)}(p_{B_q} - p_X) |\langle X | \hat{\mathcal{H}}_{eff} | B_q \rangle|^2. \quad (2.9)$$

With the help of the optical theorem the total decay rate in Eq. (2.9) can be rewritten as

$$\Gamma(B_q \rightarrow X) = \frac{1}{2m_{B_q}} \langle B_q | \hat{\mathcal{T}} | B_q \rangle, \quad (2.10)$$

with the transition operator

$$\hat{\mathcal{T}} = \text{Im } i \int d^4x \hat{T} \left[\hat{\mathcal{H}}_{eff}(x) \hat{\mathcal{H}}_{eff}(0) \right], \quad (2.11)$$

consisting of a non-local double insertion of the effective Hamiltonian. Expanding this bi-local object in local operators gives the Heavy Quark Expansion (see e.g. [21–28] for pioneering papers and [29] for a recent review). The total decay rate Γ of a b -hadron can then be expressed as products of perturbatively calculable coefficients Γ_i times non-perturbative matrix elements $\langle O_D \rangle$ of $\Delta B = 0$ -operators of dimension $D = i + 3$:

$$\begin{aligned} \Gamma = & \Gamma_0 \langle \hat{O}_{D=3} \rangle + \Gamma_2 \frac{\langle \hat{O}_{D=5} \rangle}{m_b^2} + \tilde{\Gamma}_3 \frac{\langle \tilde{\hat{O}}_{D=6} \rangle}{m_b^3} + \dots \\ & + 16\pi^2 \left[\Gamma_3 \frac{\langle \hat{O}_{D=6} \rangle}{m_b^3} + \Gamma_4 \frac{\langle \hat{O}_{D=7} \rangle}{m_b^4} + \Gamma_5 \frac{\langle \hat{O}_{D=8} \rangle}{m_b^5} + \dots \right], \end{aligned} \quad (2.12)$$

with $\langle \hat{O}_D \rangle = \langle B_q | \hat{O}_D | B_q \rangle / (2M_{B_q})$. The leading term Γ_0 describes the decay of a free b -quark and is free of non-perturbative uncertainties, since $\langle \hat{O}_{D=3} \rangle = 1 + \mathcal{O}(\langle \hat{O}_{D=5} \rangle / m_b^2)$. At order $1/m_b^2$ small corrections due to the kinetic and chromomagnetic operator are arising, at order $1/m_b^3$ we get e.g. the Darwin term in $\tilde{\Gamma}_3$, but also phase space enhanced terms Γ_3 , stemming from weak exchange, weak annihilation and Pauli interference. The numerical values of the matrix elements are expected to be of the order the hadronic scale Λ_{QCD} , thus the HQE is an expansion in the small parameter Λ_{QCD}/m_b . Each of the terms Γ_i with $i = 0, 2, 3, \dots$ can be expanded as

$$\Gamma_i = \Gamma_i^{(0)} + \frac{\alpha_s}{4\pi} \Gamma_i^{(1)} + \left(\frac{\alpha_s}{4\pi} \right)^2 \Gamma_i^{(2)} + \dots \quad (2.13)$$

In our investigation of the lifetimes we will use $\Gamma_0^{(0)}$ and $\Gamma_0^{(1)}$ from [71], which is based on [72–77], $\Gamma_3^{(0)}$ from [58] based on [78, 79] and $\Gamma_3^{(1)}$ from [80, 81]. The matrix elements of the dimension six operators were recently determined in [82].

The HQE can also be used to describe the off-diagonal element Γ_{12} of the meson mixing matrix

$$\Gamma_{12}^q = \left[\Gamma_{12,3}^{q,(0)} + \frac{\alpha_s}{4\pi} \Gamma_{12,3}^{q,(1)} + \dots \right] \frac{\langle \hat{Q}_{D=6} \rangle}{m_b^3} + \left[\Gamma_{12,4}^{q,(0)} + \frac{\alpha_s}{4\pi} \Gamma_{12,4}^{q,(1)} + \dots \right] \frac{\langle \hat{Q}_{D=7} \rangle}{m_b^4} + \dots, \quad (2.14)$$

with $\langle \hat{Q}_D \rangle = \langle B_q | \hat{Q}_D | \bar{B}_q \rangle / (2M_{B_q})$, where \hat{Q}_D are $\Delta B = 2$ -operators of dimension D . The matrix element Γ_{12}^q can be used together with M_{12}^q to predict physical observables like mass differences, decay rate differences or semi-leptonic CP-asymmetries, see e.g. [31]

$$\Delta M_q = 2|M_{12}^q|, \quad (2.15)$$

$$\Delta \Gamma_q = 2|\Gamma_{12}^q| \cos \phi_{12}^q = -\text{Re} \left(\frac{\Gamma_{12}^q}{M_{12}^q} \right) \Delta M_q, \quad (2.16)$$

$$a_{sl}^q = \left| \frac{\Gamma_{12}^q}{M_{12}^q} \right| \sin \phi_{12}^q = \text{Im} \left(\frac{\Gamma_{12}^q}{M_{12}^q} \right), \quad (2.17)$$

with the phase $\phi_{12}^q = \arg(-M_{12}^q/\Gamma_{12}^q)$. For our numerical analysis we use results for $\Gamma_{12,3}^{q,(0)}$, $\Gamma_{12,3}^{q,(1)}$ and $\Gamma_{12,4}^{q,(0)}$ from [67, 80, 83–87], results for M_{12}^q from [88, 89] and for the hadronic matrix elements of dimension six the averages presented in [65] based on [82, 90, 91] and [92–95]. Recently also the first non-perturbative evaluation of dimension seven matrix elements became available [96], which we will use for Γ_{12}^q .

2.3 QCD Factorization

In our analysis we included different observables based on non-leptonic B meson decays such as: $B \rightarrow D\pi$, $B \rightarrow \pi\pi$, $B \rightarrow \pi\rho$ and $B \rightarrow \rho\rho$. To calculate the corresponding amplitudes we used the expressions available in the literature obtained within the QCD Factorization (QCDF) framework [17–20]. In this section we briefly summarise the QCDF results relevant for the evaluation of some of our flavour constraints. Consider the process $B \rightarrow M_1 M_2$, in which a B meson decays into the final states M_1 and M_2 , where either M_1 and M_2 are two “light” mesons or M_1 is “heavy” and M_2 is “light”³.

If both M_1 and M_2 are light, then the matrix element $\langle M_1 M_2 | \hat{Q}_i | B \rangle$ of the dimension six effective operators in Eq. (2.3) can be written as

$$\begin{aligned} \langle M_1 M_2 | \hat{Q}_i | B \rangle = & \sum_j F_j^{B \rightarrow M_1}(0) \int_0^1 du T_{ij}^I(u) \Phi_{M_2}(u) + (M_1 \leftrightarrow M_2) \\ & + \int_0^1 d\xi du dv T_i^{II}(\xi, u, v) \Phi_B(\xi) \Phi_{M_1}(v) \Phi_{M_2}(u). \end{aligned} \quad (2.18)$$

In the right hand side of Eq. (2.18) $F_j^{B \rightarrow M_{1,2}}(m_{2,1}^2)$ represents the relevant form factor to account for the transition $B \rightarrow M_1$ (and correspondingly for $B \rightarrow M_2$) and $\Phi_M(u)$ is the non-perturbative Light-Cone Distribution Amplitude (LCDA) for the meson M , see Fig. 1.

Notice that Eq. (2.18) is written in such a way that it can be applied to situations where the spectator quark can end in any of the two final state light mesons. If the spectator can go into only one of the final mesons, this one will be labelled as M_1 and just the first and the third terms on the right hand side of Eq. (2.18) should be included. The functions $T^{I,II}$ are called hard-scattering kernels and can be calculated perturbatively. The kernel T^I contains, at higher order in α_s , nonfactorizable contributions from hard gluon exchange or penguin topologies. On the other hand, nonfactorizable hard interactions involving the spectator quark are part of T^{II} .

When in the final state the mesons M_1 is “heavy” and M_2 is “light”, then the corresponding QCDF formula for the matrix element $\langle M_1 M_2 | \hat{Q}_i | B \rangle$ becomes

$$\langle M_1 M_2 | \hat{Q}_i | B \rangle = \sum_j F_j^{B \rightarrow M_1}(m_2^2) \int_0^1 du T_{ij}^I(u) \Phi_{M_2}(u), \quad (2.19)$$

where the meaning of the different terms in Eq. (2.19) are analogous to those given for Eq. (2.18).

³ A meson with mass m is considered “heavy” if m scales with m_b in the heavy quark limit such that m/m_b remains fixed. On the other hand a meson is regarded as “light” if its mass remains finite in the heavy quark limit, for a light meson $m \sim \mathcal{O}(\Lambda_{QCD})$ [18].

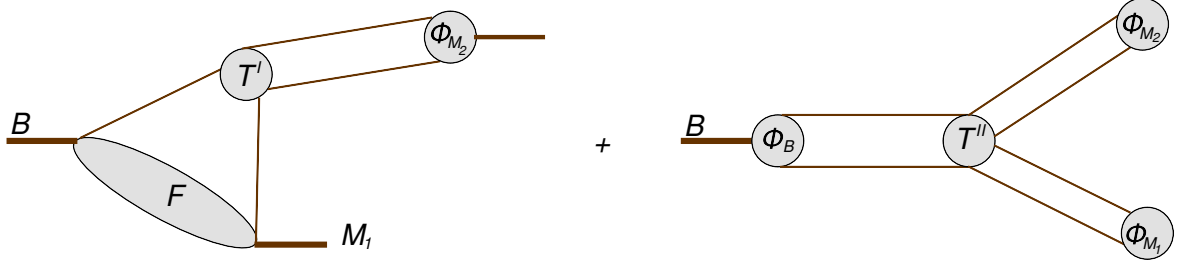


Figure 1: Factorization of matrix elements for B meson decays into “light”-“light” mesons (both diagrams included) and “heavy”-“light” (only left diagram) in QCDF.

To determine the decay amplitude $\mathcal{A}(B \rightarrow M_1 M_2)$, the matrix element $\langle M_1 M_2 | \hat{\mathcal{H}}_{eff} | B \rangle$ should be calculated, with $\hat{\mathcal{H}}_{eff}$ being the effective Hamiltonian introduced in Eq. (2.1). In QCDF the final expression for $\mathcal{A}(B \rightarrow M_1 M_2)$ is written as a linear combination of sub-amplitudes $\alpha_i^{p, M_1 M_2}$ and $\beta_i^{p, M_1 M_2}$, which for the purposes of our discussion will be termed “Topological Amplitudes” (TA). The TA $\alpha_i^p(M_1 M_2)$, for $p = u, c$, have the following generic structure at NLO in α_s [20]

$$\begin{aligned} \alpha_i^{p, M_1 M_2} = & \left[C_i(\mu_b) + \frac{C_{i\pm 1}(\mu_b)}{N_c} \right] N_i(M_2) \\ & + \frac{\alpha_s(\mu_b)}{4\pi} \frac{C_F}{N_c} C_{i\pm 1}(\mu_b) V_i(M_2) + P_i^p(M_2) \\ & + \frac{\alpha_s(\mu_h)}{4\pi} \frac{4\pi^2 C_F}{N_c^2} C_{i\pm 1}(\mu_h) H_i(M_1 M_2), \end{aligned} \quad (2.20)$$

where C_i are the Wilson coefficients calculated at the scale $\mu \sim m_b$, and the subindex in the coefficient $C_{i\pm 1}$ is assigned following the rule

$$C_{i\pm 1} = \begin{cases} C_{i+1} : & \text{if } i \text{ is odd,} \\ C_{i-1} : & \text{if } i \text{ is even.} \end{cases}$$

The Wilson coefficients inside the squared bracket in Eq. (2.20) will be modified to allow for NP contributions as discussed below, see Section 3, and N_c denotes the number of colours under consideration and will be taken as $N_c = 3$. The global factor $N_i(M_2)$ multiplying the square bracket corresponds to the normalisation of the light cone distribution for the meson M_2 , and is evaluated according to the following rule

$$N_i(M_2) = \begin{cases} 0 : & \text{if } i = 6, 8 \text{ and } M_2 \text{ is a vector meson,} \\ 1 : & \text{in any other case.} \end{cases}$$

The symbol $V_i(M_2)$ in Eq. (2.20) stands for the one loop vertex corrections illustrated in Fig. 2. Additionally, the contributions from Penguin diagrams such as those shown in Fig. 3 are included in $P_i^p(M_2)$, with $p = u, c$. Finally the hard spectator interactions shown in Fig. 4 are accounted for by the term $H_i(M_1 M_2)$. If M_1 and M_2 are both pseudoscalar mesons or if one of them is a pseudoscalar and the other is a vector meson, then the hard

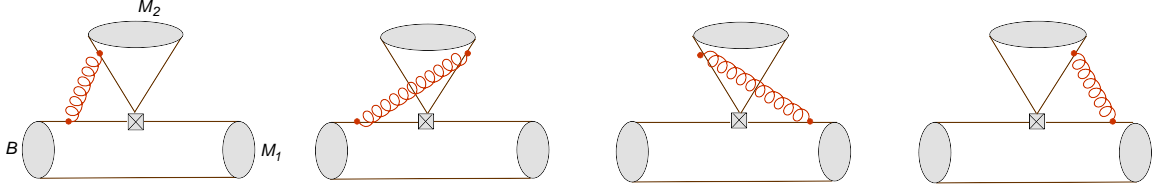


Figure 2: NLO Vertex contributions to the process $B \rightarrow M_1 M_2$.

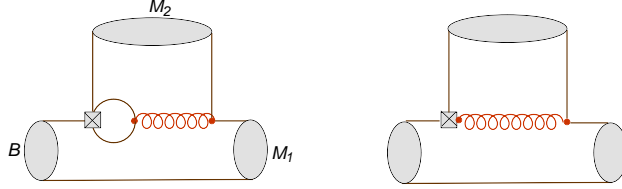


Figure 3: NLO penguin contributions to the process $B \rightarrow M_1 M_2$.

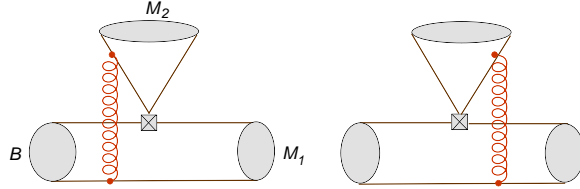


Figure 4: Hard spectator-scattering contributions to the decay $B \rightarrow M_1 M_2$.

spectator function $H_i(M_1 M_2)$ can be written in terms of the leading twist LCDAs of M_1 and M_2 , Φ_{M_1} and Φ_{M_2} respectively, and the twist-3 LCDA of M_1 , Φ_{m_1} , as [20]:

$$\begin{aligned}
H_i(M_1 M_2) &= \frac{B_{M_1 M_2}}{A_{M_1 M_2}} \int_0^1 d\xi \frac{\Phi_B(\xi)}{\xi} \int_0^1 dx \int_0^1 dy \left[\frac{\Phi_{M_2}(x) \Phi_{M_1}(y)}{\bar{x}\bar{y}} \right. \\
&\quad \left. + r_\chi^{M_1} \frac{\Phi_{M_2}(x) \Phi_{m_1}(y)}{x\bar{y}} \right], \quad (\text{for } i = 1, \dots, 4, 9, 10), \\
H_i(M_1 M_2) &= -\frac{B_{M_1 M_2}}{A_{M_1 M_2}} \int_0^1 d\xi \frac{\Phi_B(\xi)}{\xi} \int_0^1 dx \int_0^1 dy \left[\frac{\Phi_{M_2}(x) \Phi_{M_1}(y)}{x\bar{y}} \right. \\
&\quad \left. + r_\chi^{M_1} \frac{\Phi_{M_2}(x) \Phi_{m_1}(y)}{\bar{x}\bar{y}} \right], \quad (\text{for } i = 5, 7), \\
H_i(M_1 M_2) &= 0, \quad (\text{for } i = 6, 8).
\end{aligned} \tag{2.21}$$

The analogous expressions for $H_i(M_1 M_2)$ when M_1 and M_2 are two longitudinally polarised light vector mesons can be found in [97, 98]. We provide the functions $H_i(M_1 M_2)$ for the processes relevant to this project in Appendix B. The global coefficients $A_{M_1 M_2}$ and $B_{M_1 M_2}$ presented in Eqs. (2.21) depend on form factors and decay constants and are given in Eq. (B.1) also in Appendix B.

We want to highlight two sources of uncertainty arising in Eq. (2.21). The first one stems from the contribution of the twist-3 LCDA $\Phi_{m_1}(y)$. Since this function does not vanish at $y = 1$, the integral $\int_0^1 dy \Phi_{m_1}(y)/\bar{y}$ is divergent. To isolate the divergence we follow the

prescription given in [20] and write

$$\begin{aligned}\int_0^1 \frac{dy}{\bar{y}} \Phi_{m_1}(y) &= \Phi_{m_1}(1) \int_0^1 \frac{dy}{\bar{y}} + \int_0^1 \frac{dy}{\bar{y}} [\Phi_{m_1}(y) - \Phi_{m_1}(1)] \\ &= \Phi_{m_1}(1) X_H + \int_0^1 \frac{dy}{[\bar{y}]_+} \Phi_{m_1}(y).\end{aligned}\quad (2.22)$$

The divergent piece of Eq. (2.22) is contained in X_H . The remaining integral $\int_0^1 dy/[\bar{y}]_+ \Phi_{m_1}(y)$ is finite (for instance for a pseudo scalar meson $\Phi_{m_1}(y) = 1$ and trivially $\int_0^1 dy/[\bar{y}]_+ \Phi_{m_1}(y) = 0$). Physically X_H represents a soft gluon interaction with the spectator quark. It is expected that $X_H \approx \ln(m_b/\Lambda_{QCD})$ because the divergence appearing is regulated by a physical scale of the order Λ_{QCD} . A complex coefficient cannot be excluded since multiple soft scattering can introduce a strong interaction phase. Here we use the standard parameterisation for X_H introduced by Beneke-Buchalla-Neubert-Sachrajda (BBNS) [18]

$$X_H = \left(1 + \rho_H e^{i\phi_H}\right) \ln \frac{m_B}{\Lambda_h}, \quad (2.23)$$

where $\Lambda_h \approx \mathcal{O}(\Lambda_{QCD})$ and $\rho_H \approx \mathcal{O}(1)$.

The second source of theoretical uncertainty in Eqs. (2.21) that deserves special attention is the inverse moment of the LCDA Φ_B corresponding to the B meson. Following [17] we write

$$\int_0^1 d\xi \frac{\Phi_B(\xi)}{\xi} \equiv \frac{m_B}{\lambda_B}, \quad (2.24)$$

where λ_B is expected to be of $\mathcal{O}(\Lambda_{QCD})$. We provide more details about the values for X_H and λ_B used in this work at the end of this subsection.

Next we address the contributions from weak annihilation topologies, see Fig. 5, which are power suppressed in the Λ_{QCD}/m_b expansion with respect to the factorizable amplitudes. Although they do not appear in Eq. (2.18), they are included in terms of subamplitudes denoted as $\beta_k^{p,M_1 M_2}$. The numerical subscript k describes the Dirac structure under consideration: $k = 1$ for $(V - A) \otimes (V - A)$, $k = 2$ for $(V - A) \otimes (V + A)$ and $k = 3$ for $(-2)(S - P) \otimes (S + P)$. The annihilation coefficients are expressed in terms of a set of basic “building blocks” denoted by $A_k^{i,f}$. Where the subindex k also denotes the Dirac structure being considered as previously explained, and the superindices i and f denote the emission of a gluon by an initial or a final state quark as shown in Fig. 5. The coefficients $A_k^{i,f}$ relevant for this work can be found in Appendix B. The final expressions for annihilation are the result of the convolution of twist-2 and twist-3 LCDA with the corresponding hard scattering kernels; as in the case of hard spectator scattering, there are also endpoint singularities that are treated in a model dependent fashion. To parameterize these divergences, we follow once more the approach of BBNS. Thus, in analogy with hard spectator scattering we introduce [18]

$$X_A = \left(1 + \rho_A e^{i\phi_A}\right) \ln \frac{m_B}{\Lambda_h}. \quad (2.25)$$

To finalize this subsection we discuss the numerical inputs used in our evaluations of λ_B , X_H and X_A . As indicated in Eq. (2.24), the inverse moment of the LCDA of the B meson

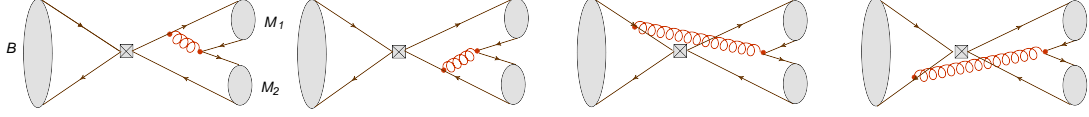


Figure 5: Annihilation topologies contributing to the decay process $B \rightarrow M_1 M_2$.

introduces the parameter λ_B . The description of non-leptonic B decays based on QCDF requires $\lambda_B \sim 200$ MeV [20, 99]. In contrast, QCD sum rules calculations give a higher value. For instance, in [100] the result $\lambda_B = (460 \pm 110)$ MeV was found. In [101] the usage of the channel $B \rightarrow \gamma \ell \nu_\ell$ was proposed in order to extract λ_B experimentally. This study was updated in [102–104] where further effects, including subleading power corrections in $1/E_\gamma$ and $1/m_b$, were accounted for. Based on this idea, the Belle collaboration found [105]

$$\lambda_B \Big|_{\text{Belle}} > 238 \text{ MeV}, \quad (2.26)$$

at the 90% C.L. and it is expected that the Belle II experiment improves this result [103]. Interestingly the experimental bound in Eq. (2.26) is compatible with the QCD sum rules value quoted above and other theoretical approaches, including the one in [106] where the value $\lambda_B = (476.19 \pm 113.38)$ MeV was obtained. For the purposes of our analysis, we consider the following result calculated in [107] with QCD sum rules:

$$\lambda_B = (400 \pm 150) \text{ MeV}. \quad (2.27)$$

As discussed above, the calculation of hard spectator interactions and the evaluation of annihilation topologies, leads to extra sources of uncertainty associated with endpoint singularities that are power suppressed. As indicated in Eqs. (2.23) and (2.25) they can be parameterized through the functions $X_H(\rho_H, \phi_H)$ and $X_A(\rho_A, \phi_A)$ respectively. Using these models, we account for the hard spectator scattering power suppressed singularities through the parameters ρ_H and ϕ_H . Correspondingly, we introduce ρ_A and ϕ_A to address the analogous effects from annihilation topologies. Based on phenomenological considerations we will take into account the intervals [56, 108]

$$0 < \rho_{H,A} < 2, \quad 0 < \phi_{H,A} < 2\pi, \quad (2.28)$$

which correspond to a 200% uncertainty on $|X_H|$ and $|X_A|$.

To evaluate the central values of our observables we take $\rho_{H,A} = 0$, or equivalently $X_H = X_A = \ln m_B/\Lambda_h$. Finally, we calculate the percentual error from X_A and X_H , by estimating the difference between the maximum and the minimum values reached by the hadronic observables when considering the intervals in Eq. (2.28), and then we normalize by two times the corresponding central values.

3 Strategy

Consider the effective Hamiltonian in Eq. (2.1) written in terms of the basis in Eq. (2.3). We introduce “new physics” in the Wilson coefficients $\{C_1, C_2\}$ of the operators \hat{Q}_1 and

\hat{Q}_2 following the prescription

$$\begin{aligned} C_1(M_W) &:= C_1^{\text{SM}}(M_W) + \Delta C_1(M_W), \\ C_2(M_W) &:= C_2^{\text{SM}}(M_W) + \Delta C_2(M_W), \end{aligned} \quad (3.1)$$

where in the SM

$$\begin{aligned} \Delta C_1(M_W) &= 0, \\ \Delta C_2(M_W) &= 0. \end{aligned} \quad (3.2)$$

In this paper we present possible bounds on ΔC_1 and ΔC_2 at the matching scale $\mu = M_W$ and consider changes to each Wilson coefficient independently, e.g. to establish constraints on $\Delta C_1(M_W)$ we fix $\Delta C_2(M_W) = 0$ and vice versa. This is a conservative approach, if we allow both parameters to change simultaneously this can result into partial cancellations leading to potentially bigger NP allowed regions for $\{\Delta C_1(M_W), \Delta C_2(M_W)\}$. Since the theoretical formulae for our observables are calculated at the scale $\mu = m_b$, we evolve down the modified Wilson coefficients $C_1(M_W)$ and $C_2(M_W)$ up to this scale using the renormalisation group formalism described in Section 2.1. We consider NP to be leading order only, therefore we treat the SM contribution $\{C_1^{\text{SM}}(M_W), C_2^{\text{SM}}(M_W)\}$ and the NP components $\{\Delta C_1(M_W), \Delta C_2(M_W)\}$ differently under the renormalisation group equations. For instance the evolution of $\{C_1^{\text{SM}}(M_W), C_2^{\text{SM}}(M_W)\}$ is done using the full NLO expressions in Eq. (2.5), on the other hand $\{\Delta C_1(M_W), \Delta C_2(M_W)\}$ are evolved down using only the LO version shown in Eq. (2.7). Notice that, even though at the scale $\mu = M_W$ the only modified Wilson coefficients are $C_1(M_W)$ and $C_2(M_W)$, the non diagonal nature of the evolution matrices propagates these effects to all the other Wilson coefficients undergoing mixing at $\mu = m_b$. Hence, when writing expressions for the different physical observables, it makes sense to consider NP effects in $C_i(m_b)$ even for $i \neq 1, 2$.

3.1 Statistical analysis

The values of $\Delta C_1(M_W)$ and $\Delta C_2(M_W)$ compatible with experimental data are evaluated using the program MyFitter [63]. The full statistical procedure is based on a likelihood ratio test. The basic ingredient is the χ^2 function

$$\chi^2(\vec{\omega}) = \sum_i \left(\frac{\tilde{O}_{i,\text{exp}} - \tilde{O}_{i,\text{theo}}(\vec{\omega})}{\sigma_{i,\text{exp}}} \right)^2, \quad (3.3)$$

where $\tilde{O}_{i,\text{exp}}$ and $\tilde{O}_{i,\text{theo}}$ are the experimental and theoretical values of the i -th observable respectively and $\sigma_{i,\text{exp}}$ is the corresponding experimental uncertainty. The vector $\vec{\omega}$ contains all the inputs necessary for the evaluation of $\tilde{O}_{i,\text{theo}}$ and will be written as

$$\vec{\omega} = \left(\Delta C_1(M_W), \Delta C_2(M_W), \vec{\lambda} \right). \quad (3.4)$$

In Eq. (3.4) we are making a distinction between $\{\Delta C_1(M_W), \Delta C_2(M_W)\}$ and the rest of the theoretical inputs, which have been included in the subvector $\vec{\lambda}$. Examples of the entries

inside $\vec{\lambda}$ are masses, decay constants, form-factors, etc. Notice that our main target is the determination of $\Delta C_1(M_W)$ and $\Delta C_2(M_W)$, however, the components entering $\vec{\lambda}$ are crucial in defining the uncertainty of our observables and hence in establishing the potential values of $\Delta C_1(M_W)$ and $\Delta C_2(M_W)$. In this respect, we will say that the elements inside $\vec{\lambda}$ are our nuisance parameters, and that the determination of the possible NP values compatible with data are obtained by profiling the likelihood with respect to $\{\Delta C_1(M_W), \Delta C_2(M_W)\}$. During our analysis the elements of $\{\Delta C_1(M_W), \Delta C_2(M_W)\}$ are assumed to be complex and, as indicated in the argument, the initial evaluation is done at the scale $\mu = M_W$. The statistical theory behind the χ^2 -fit software used, e.g. MyFitter [63], can be found in the documentation of the computer program. Here we only summarize the key steps involved in our analysis:

1. We first define the Confidence Level CL for the χ^2 -fit. Following the criteria established in [55, 57] for our study we take

$$CL = 90\%, \quad (3.5)$$

which is equivalent to 1.64 standard deviations approximately.

2. Then, we establish a sampling region on the plane defined by the real and the imaginary components of $\{\Delta C_1(M_W), \Delta C_2(M_W)\}$. The sampling region is observable dependent. In our case we opt for rectangular grids around the origin of the complex plane defined by $\Delta C_1(M_W)$ and $\Delta C_2(M_W)$. Notice that the origin of our complex plane corresponds to the SM value. The number of points in our test grid depends on three factors: the numerical stability of our algorithms, on the time required to compute a particular combination of observables and the size of the NP regions determined by them.
3. Each one of the points inside the sampling grid described in the previous step corresponds to a null-hypothesis for the components of $\Delta C_1(M_W)$ and $\Delta C_2(M_W)$. We test our null-hypothesis values using a likelihood ratio test considering the confidence level established in the first step. For a combination of multiple observables several nuisance parameters are involved and the full statistical procedure becomes time and resource consuming. Hence, the parallelization of our calculations using a computer cluster became necessary. We did our first numerical evaluations partially at the Institute for Particle Physics and Phenomenology (IPPP, Durham University). The results presented in this work were obtained in full using the computing facilities available at the Dutch National Institute for Subatomic Physics (Nikhef).

4 Individual Constraints

In this section we present the different observables considered during the analysis. From Sections 4.1 to 4.3 we focus exclusively on observables that constrain individual b decay channels, in our case: $b \rightarrow c\bar{u}d$, $b \rightarrow u\bar{u}d$, $b \rightarrow c\bar{c}s$ and $b \rightarrow c\bar{c}d$. In Section 4.5 we will study observables that affect multiple b decay channels. In what follows and unless stated

otherwise, the SM predictions as well as the experimental determinations are given at 1σ , i.e. 68% C.L.. However the allowed NP regions for C_1 and C_2 are presented at 1.64σ , i.e. 90% C.L..

Following the notation introduced in Eqs. (2.1) and (2.3) we will denote the NP effects in the Wilson coefficient of the operator $\hat{Q}_i^{q,pp'}$ as $\Delta C_i^{q,pp'}$ for $i = 1, 2$ and $q = d, s$. Then for example, $\{\Delta C_1^{d,cu}(M_W), \Delta C_2^{d,cu}(M_W)\}$ will quantify the potential deviations from the SM values in the coefficients of $\{\hat{Q}_1^{d,cu}, \hat{Q}_2^{d,cu}\}$ which describe the tree level process $b \rightarrow c\bar{u}d$.

In this work NP is supposed to be leading order in α_s and α only. Since all the vertex corrections V_i^M , penguins $P_i^{p,M}$ and hard scattering spectator interactions $H_i^{M_1M_2}$ inside Eq. (2.20) are already suppressed by factors of $\mathcal{O}(\alpha_s)$ and $\mathcal{O}(\alpha)$, we will consistently drop the extra contributions $\Delta C_1^{d,uu}(M_W)$ and $\Delta C_2^{d,uu}(M_W)$ affecting any of these terms for all observables that are described by QCDF.

4.1 Observables constraining $b \rightarrow c\bar{u}d$ transitions

We start with the dominant quark level decay $b \rightarrow c\bar{u}d$ and describe our analysis of the potential NP regions for $\Delta C_1^{d,cu}(M_W)$ and $\Delta C_2^{d,cu}(M_W)$. The decay $\bar{B}^0 \rightarrow D^{*+}\pi^-$ will exclude large positive values of $\Delta C_1^{d,cu}(M_W)$ and it will significantly constrain $\Delta C_2^{d,cu}(M_W)$.

4.1.1 $\bar{B}_d^0 \rightarrow D^{*+}\pi^-$

Our bounds will be established using the ratio between the decay width for the non-leptonic decay $\bar{B}_d^0 \rightarrow D^{*+}\pi^-$ and the differential rate for the semi-leptonic process $\bar{B}_d^0 \rightarrow D^{*+}l^-\bar{\nu}_l$ evaluated at $q^2 = m_\pi^2$ for $l = e, \mu$

$$R_{D^*\pi} = \frac{\Gamma(\bar{B}^0 \rightarrow D^{*+}\pi^-)}{d\Gamma(\bar{B}^0 \rightarrow D^{*+}l^-\bar{\nu}_l)/dq^2|_{q^2=m_\pi^2}} \simeq 6\pi^2 f_\pi^2 |V_{ud}|^2 |\alpha_2^{D^*\pi} + \beta_2^{D^*\pi}|^2. \quad (4.1)$$

This observable was proposed by Bjorken to test the factorization hypothesis [109], it is free from the uncertainties associated with the required form factor to describe the transition $B \rightarrow D^*$ and offers the possibility of comparing directly the coefficient $\alpha_2^{D^*\pi}$ calculated using QCDF against experimental observations. At NLO the TA $\alpha_2^{D^*\pi}$ [18] is given by

$$\alpha_2^{\text{NLO}, D^*\pi} = C_2^{d,cu}(\mu_b) + \frac{C_1^{d,cu}(\mu_b)}{3} + \frac{\alpha_s(\mu_b)}{4\pi} \frac{C_F}{N_c} C_1^{d,cu}(\mu_b) \left[-\tilde{B} - 6\ln \frac{\mu^2}{m_b^2} + \int_0^1 du F(u, -x_c) \Phi_\pi(u) \right] \approx 1.057 \pm 0.040, \quad (4.2)$$

where the term \tilde{B} inside the square bracket cancels the renormalisation scheme dependence of the Wilson coefficients $C_1^{d,cu}$ and $C_2^{d,cu}$, which in naive dimensional regularisation requires $\tilde{B} = 11$. The kernel $F(u, -x_c)$ includes QCD vertex corrections arising in the decay $b \rightarrow c\bar{u}d$ and has to be evaluated at $x_c = \bar{m}_c(\bar{m}_b)/\bar{m}_b$ before being convoluted with the light-cone distribution Φ_π associated with the π^- meson in the final state. For the explicit evaluation of Eq. (4.1) we use the updated determination of the TA $\alpha_2^{D^*\pi}$ at NNLO calculated in [110]

Parameter	Relative error
X_A	13.05%
μ	2.53%
f_π	1.23%
Λ_5^{QCD}	0.09%
$A_0^{B \rightarrow D^*}$	0.08%
f_B	0.02%
Total	13.35%

Table 1: Error budget for the observable $R_{D^*\pi}$.

$$|\alpha_2^{\text{NNLO}, D^*\pi}| = 1.071_{-0.014}^{+0.013}. \quad (4.3)$$

The annihilation topologies contributions are taken into account through

$$\beta_2^{D^*\pi} = \frac{C_F}{N_c^2} \frac{B_{D^*\pi}}{A_{D^*\pi}} C_2^{d, cu}(\mu_h) A_1^i(\mu_h) \approx 0.014 \pm 0.045, \quad (4.4)$$

where

$$\frac{B_{D^*\pi}}{A_{D^*\pi}} = \frac{f_B f_{D^*}}{m_B^2 A_0^{B \rightarrow D^*}(0)}, \quad (4.5)$$

and

$$A_1^i(\mu_h) \approx 6\pi\alpha_s(\mu_h) \left[3 \left(X_A - 4 + \frac{\pi^2}{3} \right) + r_\chi^{D^*}(\mu_h) r_\chi^\pi(\mu_h) (X_A^2 - 2X_A) \right], \quad (4.6)$$

with the parameters X_A are given in Eq. (2.25) and the factors r_χ^π and $r_\chi^{D^*}$ quoted in Eq. (B.1). Using the numerical inputs given in A we find

$$R_{D^*\pi}^{\text{SM}} = (1.12 \pm 0.15) \text{GeV}^2, \quad (4.7)$$

corresponding to $x_c = 0.225$, the partial contributions to the total error are shown in Table 1.

The SM result is dominated by the contribution of C_2 , thus we will get from $R_{D^*\pi}$ strong constraints on C_2 and relatively weak ones on C_1 . To compute the experimental result we use [110]

$$d\Gamma(\bar{B}_d^0 \rightarrow D^{*+} l^- \bar{\nu}_l) / dq^2 \Big|_{q^2=m_\pi^2} = (2.04 \pm 0.10) \cdot 10^{-3} \text{GeV}^{-2} \text{ps}^{-1}, \quad (4.8)$$

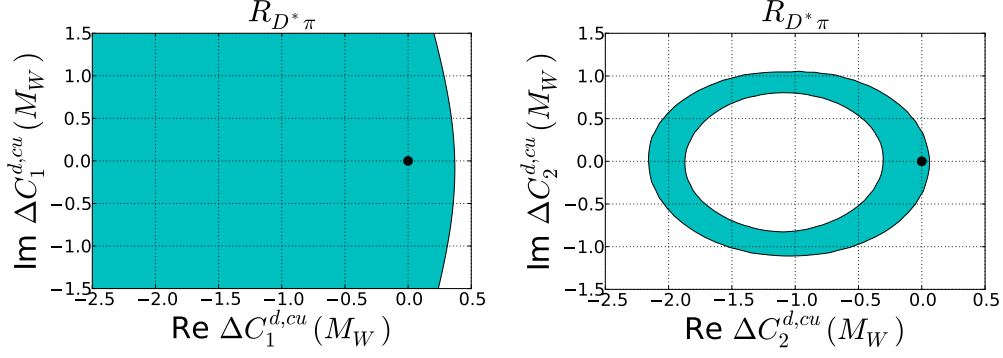


Figure 6: Potential regions for the NP contributions in $\Delta C_1^{d,cu}(M_W)$ and $\Delta C_2^{d,cu}(M_W)$ allowed by the observable $R_{D^*\pi}$ at 90% C.L.. The black point corresponds to the SM value. Since $R_{D^*\pi}$ is dominated by C_2 , we get strong constraints on C_2 and relatively weak ones on C_1 .

together with [111]

$$\mathcal{B}r(\bar{B}^0 \rightarrow D^{*+}\pi^-) = (2.84 \pm 0.15) \cdot 10^{-3}, \quad (4.9)$$

to obtain

$$R_{D^*\pi}^{\text{Exp}} = (0.92 \pm 0.07) \text{GeV}^2. \quad (4.10)$$

Our χ^2 -fit provides the 90 % confidence level regions allowed by $\Delta C_1^{d,cu}(M_W)$ and $\Delta C_2^{d,cu}(M_W)$ displayed in Fig. 6, which show that $\Delta C_1^{d,cu}(M_W)$ is quite unconstrained. On the other hand, there are stronger restrictions on the values that $\Delta C_2^{d,cu}(M_W)$ can assume. This is not surprising considering that $C_2^{d,cu}$ gives the leading contribution to $\alpha_2^{D^*\pi}$; this can be seen in the NLO version of the formula for this term in Eq. (4.2).

4.2 Observables constraining $b \rightarrow u\bar{u}d$ transitions

We proceed to describe the constraints to the NP contributions $\Delta C_{1,2}^{d,uu}(M_W)$ entering in the CKM suppressed quark level transition $b \rightarrow u\bar{u}d$. Our bounds are obtained taking into account both the branching ratios, but also the CP asymmetries of the decays $B \rightarrow \pi\pi, \rho\pi, \rho\rho$ and using again QCDF for the theoretical description. The combination of CP-conserving and CP-violating observables significantly shrinks the allowed region for $\Delta C_2^{d,uu}(M_W)$.

4.2.1 $R_{\pi\pi}$

Our first observable is the theoretical clean ratio [109]

$$R_{\pi\pi} = \frac{\Gamma(B^+ \rightarrow \pi^+\pi^0)}{d\Gamma(\bar{B}_d^0 \rightarrow \pi^+\ell^-\bar{\nu}_\ell)/dq^2|_{q^2=0}} \simeq 3\pi^2 f_\pi^2 |V_{ud}|^2 |\alpha_1^{\pi\pi} + \alpha_2^{\pi\pi}|^2, \quad (4.11)$$

where $\ell^- = \mu^-, e^-$ and $\alpha_1^{\pi\pi}, \alpha_2^{\pi\pi}$ are the TA associated with the decays $B \rightarrow \pi\pi$ which were introduced in a generic way in Eq. (2.20). The dependence of $R_{\pi\pi}$ is now symmetric

in C_1 and C_2 , so both Wilson coefficients will be constrained in an almost identical way. Notice that the denominator in Eq. (4.11) refers to the differential distribution $d\Gamma(\bar{B}_d^0 \rightarrow \pi^+ \ell^- \bar{\nu}_\ell)/dq^2$ evaluated at $q^2 = 0$, where q^2 is the four momentum transferred to the system composed by the ℓ^- and $\bar{\nu}_\ell$. In Eq. (4.11), our sensitivity to NP enters through the decay $B^+ \rightarrow \pi^+ \pi^0$ which is to a good degree of precision a pure tree level channel. We neglect hypothetical BSM effects in $\bar{B}_d^0 \rightarrow \pi^+ \ell^- \bar{\nu}_\ell$ for $\ell = e, \mu$, see e.g. [112] for a recent investigation of such a possibility. The observable $R_{\pi\pi}$ is theoretically clean since it does not depend on the CKM matrix element $|V_{ub}|$, which cancels in the ratio. Moreover, at leading order in α_s it is independent of the form factors $F_+^{B \rightarrow \pi}(0) = F_0^{B \rightarrow \pi}(0)$ which account for the hadronic transition $B \rightarrow \pi$. However, these parameters enter in the coefficients $\alpha_{1,2}^{\pi\pi}$ once the spectator interaction contributions $H_{\pi\pi}$ are taken into account. More precisely, they appear in the ratio $B_{\pi\pi}/A_{\pi\pi}$ inside $H_{\pi\pi}$, see Eqs. (B.1) and (B.14). Currently, the coefficients $\alpha_{1,2}^{\pi\pi}$ in Eq. (4.11) are available up to NNLO in QCDF [99, 113–115]. In order to optimize the computation time of our χ^2 -fit, we have accounted for the NNLO effects using the following formula

$$\frac{\alpha_{1,2}^{\pi\pi}}{\alpha_{1,2}^{\text{NNLO},\pi\pi}} = \frac{\alpha_{1,2}^{\text{NLO},\pi\pi}(\mu_0)}{\alpha_{1,2}^{(0)\text{NLO},\pi\pi}}. \quad (4.12)$$

Where in Eq. (4.12):

- $\alpha_{1,2}^{\text{NLO},\pi\pi}(\mu_0)$ corresponds to the fully programmed NLO expression for the amplitude $\alpha_{1,2}^{\pi\pi}$. For this term, the renormalization scale is kept fixed to the value $\mu_0 = m_b$ whereas the rest of the input parameters are allowed to float.
- $\alpha_{1,2}^{(0)\text{NLO},\pi\pi}$ are the NLO version of the amplitudes $\alpha_{1,2}^{\pi\pi}$ evaluated at the central value of all the input parameters and kept constant during the χ^2 -fit.
- $\alpha_{1,2}^{\text{NNLO},\pi\pi}$ are the NNLO version of the amplitude $\alpha_{1,2}^{\pi\pi}$. We are interested in the NNLO results because of the reduction in the renormalisation scale dependency with respect to the NLO determination. Therefore during the χ^2 -fit we have treated the coefficients $\alpha_{1,2}^{\text{NNLO},\pi\pi}$ as nuisance parameters given by [107]

$$\begin{aligned} \alpha_1^{\text{NNLO},\pi\pi} &= 0.195_{-0.025}^{+0.025} - \left(0.101_{-0.029}^{+0.021}\right)i, \\ \alpha_2^{\text{NNLO},\pi\pi} &= 1.013_{-0.011}^{+0.008} + \left(0.027_{-0.013}^{+0.020}\right)i, \end{aligned} \quad (4.13)$$

where the error indicated arises only from the renormalization scale uncertainty. Alternatively, we also tested the numerical values provided in [99] which give consistent results once the uncertainties arising by varying μ and μ_h ,⁴ are taken into account.

We predict the SM value of $R_{\pi\pi}$ to be

$$R_{\pi\pi}^{\text{SM}} = \left(0.70 \pm 0.14\right), \quad (4.14)$$

with the partial contributions to the total error shown in Table 2. To calculate the exper-

⁴T. Huber, private communication.

Parameter	Relative Error
X_H	16.86%
λ_B	8.85%
μ	4.42%
a_2^π	2.57%
$F_+^{B \rightarrow \pi}(0)$	1.77%
f_π	1.35%
m_s	0.68%
Λ_5^{QCD}	0.25%
f_B	0.14%
m_b	0.04%
V_{us}	0.01%
Total	19.86%

Table 2: Error budget for the observable $R_{\pi\pi}$. Here X_H accounts for the endpoint singularities from hard scattering spectator interactions. $F_+^{B \rightarrow \pi}(0)$ is the relevant form factor for the transitions $B \rightarrow \pi$. The parameter λ_B is the inverse moment of the LCDA of the B meson and a_2^π is the second Gegenbauer moment for the π meson.

imental result, we consider the following updated value for the branching fraction for the process $B^+ \rightarrow \pi^+ \pi^0$ [116]

$$\mathcal{B}r(B^+ \rightarrow \pi^+ \pi^0) = (5.5 \pm 0.4) \cdot 10^{-6}, \quad (4.15)$$

together with the product [117]

$$|V_{ub} F_+^{B \rightarrow \pi}(0)| = (9.25 \pm 0.31) \cdot 10^{-4}, \quad (4.16)$$

which was extracted via a fit to data including experimental results from BaBar, Belle and CLEO [118–122] under the assumption of the SM, neglecting the mass of the light leptons and keeping the mass of the B^* meson fixed. Using the inputs indicated in Eqs. (4.15) and (4.16) we obtain the following result for the experimental value of $R_{\pi\pi}$

$$R_{\pi\pi}^{\text{Exp}} = (0.83 \pm 0.08). \quad (4.17)$$

This determination is in agreement with the result given in [99], however, the uncertainty is reduced by nearly 50% due to the update on the product $|V_{ub} F_+^{B \rightarrow \pi}(0)|$ shown in Eq. (4.16). The allowed regions for $\Delta C_1^{d,uu}(M_W)$ and $\Delta C_2^{d,uu}(M_W)$ are shown in Fig. 7 - we note here rather stringent constraints on positive and real values of $\Delta C_1^{d,uu}(M_W)$ and $\Delta C_2^{d,uu}(M_W)$.

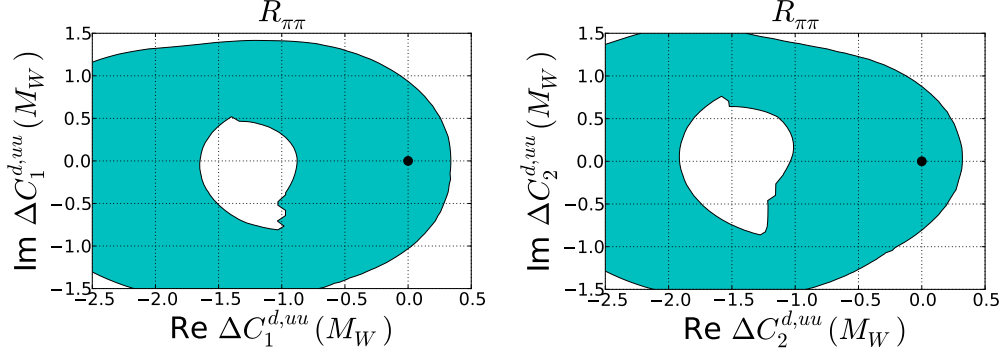


Figure 7: Potential regions for the NP contributions $\Delta C_1^{d,uu}(M_W)$ and $\Delta C_2^{d,uu}(M_W)$ allowed by the observable $R_{\pi\pi}$ at 90% C.L.. The black point corresponds to the SM value. The dependence of $R_{\pi\pi}$ is symmetric in C_1 and C_2 , therefore both Wilson coefficients are constrained in an almost identical way.

4.2.2 $S_{\pi\pi}$

Since our NP contributions are allowed to be complex, we are exploring the possibility of having new CP violating phases. We can constrain these effects through the time-dependent asymmetries

$$\begin{aligned} \mathcal{A}_f^{CP}(t) &= \frac{d\Gamma[\bar{B}_q^0 \rightarrow f](t)/dt - d\Gamma[B_q^0 \rightarrow f](t)/dt}{d\Gamma[\bar{B}_q^0 \rightarrow f](t)/dt + d\Gamma[B_q^0 \rightarrow f](t)/dt} \\ &\simeq S_f \sin \Delta M_q t - C_f \cos \Delta M_q t, \end{aligned} \quad (4.18)$$

where we have neglected the effects of the observable $\Delta\Gamma_q$ entering in the denominator - this is only justified for the case of B_d -mesons. The symbol f in Eq. (4.18) denotes a final state to which both, the B_q^0 and the \bar{B}_q^0 meson can decay, for $q = d, s$. The mixing induced (S_f) and direct CP asymmetries (C_f) are defined as

$$S_f \equiv \frac{2 \operatorname{Im}(\lambda_f^q)}{1 + |\lambda_f^q|^2}, \quad C_f \equiv \frac{1 - |\lambda_f^q|^2}{1 + |\lambda_f^q|^2}. \quad (4.19)$$

with the parameter λ_f^q given by

$$\lambda_f^q := \frac{q}{p} \Big|_{B_q} \frac{\bar{A}_f^q}{A_f^q}. \quad (4.20)$$

In Eq. (4.20) the amplitude for the process $B_q^0 \rightarrow f$ has been denoted as A_f^q and the one for $\bar{B}_q^0 \rightarrow f$ as \bar{A}_f^q . Finally,

$$\frac{q}{p} \Big|_{B_q} = \frac{M_{12}^{q*}}{|M_{12}^q|}, \quad (4.21)$$

where M_{12}^d is the contribution from virtual internal particles to the $B_q^0 - \bar{B}_q^0$ mixing diagrams. For instance in the case of B_d mesons we get

$$\frac{q}{p} \Big|_{B_d} = \left[\frac{V_{td} V_{tb}^*}{|V_{td} V_{tb}^*|} \right]^2. \quad (4.22)$$

Notice that the observable S_f , in Eq. (4.19), is particularly sensitive to the imaginary components of $\Delta C_1(M_W)$ and $\Delta C_2(M_W)$.

For the decays $\bar{B}_d^0 \rightarrow \pi^+\pi^-$ and $B_d^0 \rightarrow \pi^+\pi^-$ we get

$$S_{\pi\pi} = \frac{2 \operatorname{Im}(\lambda_{\pi\pi}^d)}{1 + |\lambda_{\pi\pi}^d|^2}, \quad \lambda_{\pi\pi}^d = \left[\frac{V_{td}V_{tb}^*}{|V_{td}V_{tb}^*|} \right]^2 \frac{\bar{\mathcal{A}}_{\pi^+\pi^-}}{\mathcal{A}_{\pi^+\pi^-}}. \quad (4.23)$$

Here $\bar{\mathcal{A}}_{\pi^+\pi^-}$ and $\mathcal{A}_{\pi^+\pi^-}$ denote the transition amplitudes for the processes $\bar{B}_d^0 \rightarrow \pi^+\pi^-$ and $B_d^0 \rightarrow \pi^+\pi^-$ respectively. They have been calculated in [20] using the QCDF formalism briefly described in Section 2.3. The explicit expression for $\bar{\mathcal{A}}_{\pi^+\pi^-}$ is

$$\begin{aligned} \bar{\mathcal{A}}_{\pi^+\pi^-} = A_{\pi\pi} & \left(\lambda_u^{(d)} \alpha_2^{\pi\pi} + \lambda_u^{(d)} \beta_2^{\pi\pi} + \sum_{p=u,c} \lambda_p^{(d)} \left[\tilde{\alpha}_4^{p,\pi\pi} + \tilde{\alpha}_{4,EW}^{p,\pi\pi} \right. \right. \\ & \left. \left. + \beta_3^{p,\pi\pi} - 1/2 \beta_{3,EW}^{p,\pi\pi} + 2\beta_4^{p,\pi\pi} + 1/2 \beta_{4,EW}^{p,\pi\pi} \right] \right). \end{aligned} \quad (4.24)$$

To determine the remaining amplitude $\mathcal{A}_{\pi^+\pi^-}$, the CP conjugate of the expression in Eq. (4.24) has to be obtained. The parameters $\lambda_{u,c}^{(d)}$ in Eq. (4.24) correspond to products of CKM matrix elements as defined in Eq. (2.2). Notice that our sensitivity towards NP in tree level enters mainly through $\alpha_2^{\pi\pi}$, which according to Eq. (2.20) has a leading dependency on $\Delta C_2^{d,uu}(M_W)$. Therefore, the observable $S_{\pi\pi}$ yields to strong constraints on $\Delta C_2^{d,uu}(M_W)$, while giving weak ones in $\Delta C_1^{d,uu}(M_W)$. Besides the TA $\alpha_2^{\pi\pi}$, which is introduced in our analysis at NNLO following the prescription shown in Eq. (4.12), there are now also contributions from QCD and electroweak penguins given by $\tilde{\alpha}_4^{p,\pi\pi}$ and $\tilde{\alpha}_{4,EW}^{p,\pi\pi}$ respectively. Finally $\beta_4^{p,\pi\pi}$ accounts for QCD penguin annihilation and $\beta_{4,EW}^{p,\pi\pi}$ for electroweak penguin annihilation. All the TA can be calculated using Eq. (2.20) together with the information presented in Appendix B. At leading order in α_s , the normalization factor $A_{\pi\pi}$ introduced in Eq. (B.1), which depends on the form factor $F_+^{B \rightarrow \pi}(0)$ and the decay constant f_π , cancels in the ratio given in Eq. (4.23). However it appears again once interactions with the spectator are taken into account. This leads to small effects in the error budget of $\mathcal{O}(1 \%)$ and $\mathcal{O}(0.1 \%)$ from $F_+^{B \rightarrow \pi}(0)$ and f_π respectively, see Table 3. Our theoretical prediction for the SM value of the asymmetry $S_{\pi\pi}$ is

$$S_{\pi\pi}^{\text{SM}} = -0.59 \pm 0.25. \quad (4.25)$$

For the corresponding experimental value we have [111]

$$S_{\pi\pi}^{\text{Exp}} = -0.63 \pm 0.04, \quad (4.26)$$

showing consistency with the SM estimation in Eq. (4.25). The relevant constraints on $\Delta C_2^{d,uu}(M_W)$ derived from $S_{\pi\pi}$ are presented in Fig. 8 - constraints on $\Delta C_1^{d,uu}(M_W)$ are very weak and will thus not be shown.

4.2.3 $S_{\rho\pi}$

We also included the mixing induced CP asymmetry associated with the decays $B_d, \bar{B}_d \rightarrow \rho\pi$. Our evaluation is based in the following definition

$$S_{\pi\rho} = \frac{1}{2} \left(\tilde{S}_{\pi\rho} + \tilde{S}_{\rho\pi} \right), \quad (4.27)$$

Parameter	Relative Error
X_A	41.76%
γ	6.24%
m_s	4.43%
$ V_{ub}/V_{cb} $	4.31%
X_H	3.08%
μ	2.79%
Λ_5^{QCD}	2.25%
λ_B	1.55%
$F_+^{B \rightarrow \pi}$	0.89%
m_b	0.76%
$ V_{us} $	0.13%
f_B	0.07%
m_c	0.06%
f_π	0.06%
a_2^π	0.03%
Total	42.98%

Table 3: Error budget for the observable $S_{\pi\pi}$. Most of the inputs coincide with those for $R_{\pi\pi}$ described in Table 2. Additionally the effects of annihilation topologies are accounted by X_A .

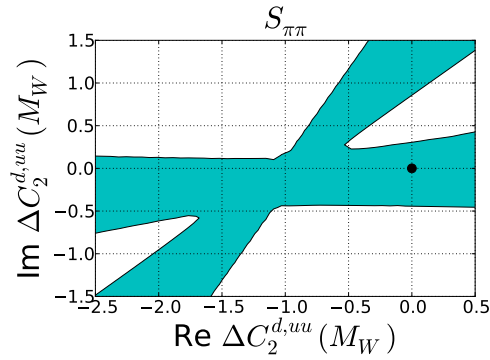


Figure 8: Potential regions for the NP contributions in $\Delta C_2^{d,uu}(M_W)$ allowed by the observable $S_{\pi\pi}$ at 90% C.L., the shift in the Wilson coefficient $\Delta C_1^{d,uu}(M_W)$ is only weakly constrained and therefore not shown. The black point corresponds to the SM value.

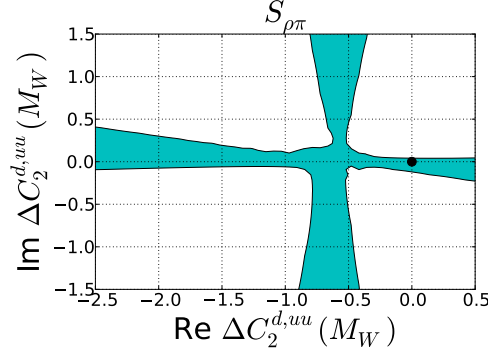


Figure 9: Potential regions for the NP contributions in $\Delta C_2^{d,uu}(M_W)$ allowed by the observable $S_{\rho\pi}$ at 90% C.L., the shift in the Wilson coefficient $\Delta C_1^{d,uu}(M_W)$ is only weakly constrained and therefore not shown. The black point corresponds to the SM value.

with the partial contributions given by

$$\tilde{S}_{\pi\rho} = \frac{2 \operatorname{Im}(\lambda_{\pi\rho}^d)}{1 + |\lambda_{\pi\rho}^d|^2}, \quad \tilde{S}_{\rho\pi} = \frac{2 \operatorname{Im}(\lambda_{\rho\pi}^d)}{1 + |\lambda_{\rho\pi}^d|^2}, \quad (4.28)$$

with

$$\lambda_{\pi\rho}^d = \left[\frac{V_{td}V_{tb}^*}{|V_{td}V_{tb}^*|} \right]^2 \frac{\bar{\mathcal{A}}_{\pi^+\rho^-}}{\mathcal{A}_{\rho^+\pi^-}}, \quad \lambda_{\rho\pi}^d = \left[\frac{V_{td}V_{tb}^*}{|V_{td}V_{tb}^*|} \right]^2 \frac{\bar{\mathcal{A}}_{\rho^+\pi^-}}{\mathcal{A}_{\pi^+\rho^-}}. \quad (4.29)$$

The individual amplitudes $\bar{\mathcal{A}}_{\pi^+\rho^-}$ and $\bar{\mathcal{A}}_{\rho^+\pi^-}$ for the processes $\bar{B}_d^0 \rightarrow \pi^+\rho^-$ and $\bar{B}_d^0 \rightarrow \rho^+\pi^-$ are respectively

$$\begin{aligned} \bar{\mathcal{A}}_{\pi^+\rho^-} &= A_{\pi\rho} \left(\lambda_u^{(d)} \alpha_2^{\pi\rho} + \sum_{p=u,c} \lambda_p^{(d)} \left[\tilde{\alpha}_4^{p,\pi\rho} + \tilde{\alpha}_{4,EW}^{p,\pi\rho} \right. \right. \\ &\quad \left. \left. + \beta_3^{p,\pi\rho} + \beta_4^{p,\pi\rho} - \frac{1}{2} \beta_{3,EW}^{p,\pi\rho} - \frac{1}{2} \beta_{4,EW}^{p,\pi\rho} \right] \right) \\ &\quad + A_{\rho\pi} \left(\lambda_u^{(d)} \beta_1^{\rho\pi} + \sum_{p=u,c} \lambda_p^{(d)} \left[\beta_4^{p,\rho\pi} + \beta_{4,EW}^{p,\rho\pi} \right] \right), \\ \bar{\mathcal{A}}_{\rho^+\pi^-} &= A_{\rho\pi} \left(\lambda_u^{(d)} \alpha_2^{\rho\pi} + \sum_{p=u,c} \lambda_p^{(d)} \left[\tilde{\alpha}_4^{p,\rho\pi} + \tilde{\alpha}_{4,EW}^{p,\rho\pi} + \beta_3^{p,\rho\pi} \right. \right. \\ &\quad \left. \left. + \beta_4^{p,\rho\pi} - \frac{1}{2} \beta_{3,EW}^{p,\rho\pi} - \frac{1}{2} \beta_{4,EW}^{p,\rho\pi} \right] \right) \\ &\quad + A_{\pi\rho} \left(\lambda_u^{(d)} \beta_1^{\pi\rho} + \sum_{p=u,c} \lambda_p^{(d)} \left[\beta_4^{p,\pi\rho} + \beta_{4,EW}^{p,\pi\rho} \right] \right), \end{aligned} \quad (4.30)$$

with $\lambda_{u,c}^{(d)}$ given by Eq. (2.2). In analogy with $S_{\pi\pi}$, there are also tree level amplitudes given by $\{\alpha_2^{\pi\rho}, \alpha_2^{\rho\pi}\}$, together with QCD and electroweak penguin contributions introduced through $\{\alpha_4^{\pi\rho}, \alpha_4^{\rho\pi}\}$ and $\{\tilde{\alpha}_4^{\pi\rho}, \tilde{\alpha}_4^{\rho\pi}\}$ respectively. Moreover, the coefficients $\{\beta_1^{p,\pi\rho}, \beta_1^{p,\rho\pi}\}$ correspond to current-current annihilation, $\{\beta_{3,4}^{p,\pi\rho}, \beta_{3,4}^{p,\rho\pi}\}$ to QCD penguin annihilation and $\{\beta_{4,EW}^{p,\pi\rho}, \beta_{4,EW}^{p,\rho\pi}\}$ to electroweak penguin annihilation. The TA can be obtained using

Parameter	Relative Error
γ	142.75%
X_A	96.41%
X_H	58.85%
$ V_{ub}/V_{cb} $	46.96%
m_s	37.31%
μ	20.58%
a_2^ρ	18.34%
Λ_5^{QCD}	13.16%
λ_B	8.27%
$A_0^{B \rightarrow \rho}$	7.06%
a_2^π	6.26%
m_b	5.22%
$F_+^{B \rightarrow \pi}$	2.19%
$ V_{us} $	1.38%
f_ρ	0.93%

Table 4: Error budget for the observable $S_{\pi\rho}$ (Part I). Here $A_0^{B \rightarrow \rho}$ is the form factor for the transition $B \rightarrow \rho$, a_2^ρ is the Gegenbauer moment for the leading twist LCDA for the ρ meson.

Eq. (2.20) and the information provided in Appendix B. Our SM determination of the mixing induced CP asymmetry reads

$$S_{\pi\rho}^{\text{SM}} = -0.04 \pm 0.08, \quad (4.31)$$

which is compatible with the current experimental average [111]

$$S_{\pi\rho}^{\text{Exp}} = 0.06 \pm 0.07. \quad (4.32)$$

The relative errors from each one of the inputs for $S_{\pi\rho}$ are presented in Tables 4 and 5, it can be seen that this observable is highly sensitive to the CKM input γ leading to a relative uncertainty of $\mathcal{O}(100\%)$. This is related to the fact that in the ratio $\lambda_{\rho\pi}$ given in Eq. (4.29) we have:

$$\text{Re} \left(\frac{\mathcal{A}_{\rho^+\pi^-}}{\mathcal{A}_{\pi^+\rho^-}} \right) \approx \text{Im} \left(\frac{\mathcal{A}_{\rho^+\pi^-}}{\mathcal{A}_{\pi^+\rho^-}} \right), \quad (4.33)$$

Parameter	Relative Error
f_π	0.51%
f_B	0.26%
f_ρ^\perp	0.23%
$ V_{cb} $	0.06%
m_c	0.02%
Total	194.57%

Table 5: Error budget for the observable $S_{\pi\rho}$ (Part II).

and

$$\text{Re} \left(\left[\frac{V_{td} V_{tb}^*}{|V_{td} V_{tb}^*|} \right]^2 \right) \approx -\text{Im} \left(\left[\frac{V_{td} V_{tb}^*}{|V_{td} V_{tb}^*|} \right]^2 \right), \quad (4.34)$$

which lead to a very strong cancellation on the resulting imaginary component. The allowed NP regions for $\Delta C_2^{d,uu}(M_W)$ are displayed in Fig. 9. Here we can see how, in spite of having an uncertainty of $\mathcal{O}(100\%)$, the observable $S_{\pi\rho}$ rules out large sections in the complex plane of $\Delta C_2^{d,uu}(M_W)$ and consequently deserves to be included in the analysis of $C_2^{d,uu}$. In contrast we find weak bounds for $\Delta C_1^{d,uu}(M_W)$ that are not strong enough to be taken into account. This is explained by the strong dependence of the amplitudes in Eqs. (4.30) on $C_2^{d,uu}(M_W)$, which enters through $\alpha_2^{\pi\rho}$ and $\alpha_2^{\rho\pi}$ as shown in Eq. (2.20).

4.2.4 $R_{\rho\rho}$

To obtain extra constraints on NP contributions to the tree level Wilson coefficients for the transition $b \rightarrow u\bar{u}d$ we include the ratio

$$R_{\rho\rho} = \frac{\mathcal{B}r(B^- \rightarrow \rho_L^- \rho_L^0)}{\mathcal{B}r(\bar{B}_d^0 \rightarrow \rho_L^+ \rho_L^-)} = \frac{|\mathcal{A}_{\rho^- \rho^0}|^2}{|\mathcal{A}_{\rho^+ \rho^-}|^2}, \quad (4.35)$$

where $\mathcal{A}_{\rho^- \rho^0}$ and $\mathcal{A}_{\rho^+ \rho^-}$ are the amplitudes for the processes $B^- \rightarrow \rho_L^- \rho_L^0$ and $\bar{B}_d^0 \rightarrow \rho_L^+ \rho_L^-$ respectively. In terms of TAs they can be written as [97, 98]

$$\begin{aligned} \mathcal{A}_{\rho^- \rho^0} &= \frac{A_{\rho\rho}}{\sqrt{2}} \left[\lambda_u^{(d)} (\alpha_1^{\rho\rho} + \alpha_2^{\rho\rho}) + \frac{3}{2} \sum_{p=u,c} \lambda_p^{(d)} (\alpha_7^{p,\rho\rho} + \alpha_9^{p,\rho\rho} + \alpha_{10}^{p,\rho\rho}) \right], \\ \mathcal{A}_{\rho^+ \rho^-} &= A_{\rho\rho} \left[\lambda_u^{(d)} (\alpha_2^{\rho\rho} + \beta_2^{\rho\rho}) + \sum_{p=u,c} \lambda_p^{(d)} (\alpha_4^{p,\rho\rho} + \alpha_{10}^{p,\rho\rho} \right. \\ &\quad \left. + \beta_3^{p,\rho\rho} + 2\beta_4^{p,\rho\rho} - \frac{1}{2}\beta_{3,EW}^{p,\rho\rho} + \frac{1}{2}\beta_{4,EW}^{p,\rho\rho}) \right]. \end{aligned} \quad (4.36)$$

Here we expect a stronger dependence on C_1 compared to C_2 . As indicated in Eq. (4.36), in addition to the tree level contributions $\alpha_{1,2}^{\rho\rho}$, we can also identify QCD $\alpha_4^{\rho\rho}$ and electroweak

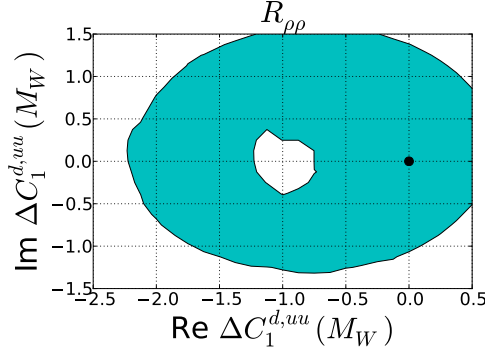


Figure 10: Potential regions for the NP contributions in $\Delta C_1^{d,uu}(M_W)$ allowed by the observable $R_{\rho\rho}$ at 90% C.L.. The bounds on $\Delta C_2^{d,uu}(M_W)$ are very weak and hence not shown. The black point corresponds to the SM value.

penguins $\alpha_{7,9,10}^{\rho\rho}$. Moreover QCD penguin annihilation topologies enter through $\beta_{3,4}^{p,\rho\rho}$. On the other hand electroweak penguin annihilation is given by $\beta_{3,4,EW}^{p,\rho\rho}$. The expressions for the topological amplitudes obey the structure indicated in Eq. (2.20) and can be calculated explicitly using the information provided in Appendix B. Currently $\alpha_{1,2}^{\rho\rho}$ are available up to NNLO, we introduce these effects following the same procedure used for the determination of $\alpha_{1,2}^{\pi\pi}$. Thus, we apply Eq. (4.12) under the replacements $\alpha_i^{\text{NNLO},\pi\pi} \rightarrow \alpha_i^{\text{NNLO},\rho_L\rho_L}$, $\alpha_i^{\text{NLO},\pi\pi} \rightarrow \alpha_i^{\text{NLO},\rho_L\rho_L}$ and $\alpha_i^{\text{NLO},\pi\pi} \rightarrow \alpha_{0,i}^{\text{NLO},\rho_L\rho_L}$, with $i = 1, 2$. For the corresponding NNLO components we use [107]

$$\begin{aligned}\alpha_1^{\text{NNLO},\rho_L\rho_L} &= 0.177_{-0.029}^{+0.025} - \left(0.097_{-0.029}^{+0.021}\right)i, \\ \alpha_2^{\text{NNLO},\rho_L\rho_L} &= 1.017_{-0.011}^{+0.010} + \left(0.025_{-0.013}^{+0.019}\right)i.\end{aligned}\tag{4.37}$$

The uncertainty shown in Eq. (4.37) has its origin in higher order perturbative corrections, we have taken this as the corresponding renormalization scale uncertainty when treating $\alpha_{1,2}^{\text{NNLO},\rho_L\rho_L}$ as nuisance parameters. Our SM determination for $R_{\rho\rho}$ is

$$R_{\rho\rho}^{\text{SM}} = \left(67.5 \pm 25.7\right) \cdot 10^{-2}.\tag{4.38}$$

The experimental result for $R_{\rho\rho}$ is obtained by calculating the ratio of $\mathcal{B}r(B^- \rightarrow \rho_L^- \rho_L^0)$ and $\mathcal{B}r(\bar{B}_d^0 \rightarrow \rho_L^+ \rho_L^-)$ weighted by the corresponding longitudinal polarization fractions f_L^{-0} and f_L^{+-} . Using the numerical values available in the PDG [116] we obtain

$$R_{\rho\rho}^{\text{Exp}} = \left(83.14 \pm 8.98\right) \cdot 10^{-2}.\tag{4.39}$$

The partial contributions to the error budget are presented in Table 6 and the constraints derived for $\Delta C_1^{d,uu}(M_W)$ in Fig. 10. We do not show the associated regions for $\Delta C_2^{d,uu}(M_W)$ because, for $R_{\rho\rho}$, the results are weaker than those derived from other observables in our study.

Parameter	Relative Error
X_A	26.40%
X_H	23.33%
λ_B	12.32%
μ	6.78%
$A_0^{B \rightarrow \rho}$	2.54%
a_2^ρ	2.24%
f_ρ	0.46%
Λ_5^{QCD}	0.45%
γ	0.38%
m_b	0.27%
f_B	0.15%
f_ρ^\perp	0.15%
m_c	0.12%
f_ρ^\perp	0.07%
$ V_{ub}/V_{cb} $	0.02%
Total	38.09%

Table 6: Error budget for the observable $R_{\rho\rho}$.

4.3 Observables constraining $b \rightarrow c\bar{c}s$ transitions

In this section we study bounds for $\Delta C_{1,2}^{s,cc}(M_W)$ stemming from $\mathcal{B}r(\bar{B} \rightarrow X_s \gamma)$, the mixing observable $\Delta\Gamma_s$, the CKM angle $\sin(2\beta_s)$ and the lifetime ratio τ_{B_s}/τ_{B_d} . These observables give very constrained regions for $\Delta C_{1,2}^{s,cc}(M_W)$.

4.3.1 $\bar{B} \rightarrow X_s \gamma$

The process $\bar{B} \rightarrow X_s \gamma$ is of mayor interest for BSM studies for several reasons. To begin with, within the SM it is generated mainly at the loop level (its branching fraction actually receives contributions below 0.4% from the tree-level CKM-suppressed transitions $b \rightarrow u\bar{u}s\gamma$ when the energy of the photon is within the phenomenologically relevant range $E_\gamma \geq 1.6$ GeV [123]). In the HQET, it corresponds to a flavour changing neutral current sensitive to new particles. Additionally, the experimental and theoretical precision achieved on its determination have an accuracy of the same order. Moreover, this transition is useful to constrain CKM elements involving the top quark.

The experimental world average for $\mathcal{B}r(\bar{B} \rightarrow X_s \gamma)$ up to date combines measurements from CLEO, Belle and BaBar leading to [111]

$$\mathcal{B}r^{\text{Exp}}(\bar{B} \rightarrow X_s \gamma) = (3.32 \pm 0.15) \cdot 10^{-4}. \quad (4.40)$$

On the theoretical side there has been a huge effort on the determination of this observable; the most precise results available are obtained at NNLO. Here we consider [124]

$$\mathcal{B}r^{\text{SM}}(\bar{B} \rightarrow X_s \gamma) = (3.36 \pm 0.22) \cdot 10^{-4}, \quad (4.41)$$

where the energy of the photon satisfies the cut

$$E_\gamma > E_0 = 1.6 \text{ GeV}. \quad (4.42)$$

The calculation of the branching ratio for the process $\bar{B} \rightarrow X_s \gamma$ can be written as [125]

$$\mathcal{B}r(\bar{B} \rightarrow X_s \gamma)_{E_\gamma > E_0} = \mathcal{B}r(\bar{B} \rightarrow X_c e \bar{\nu})_{\text{exp}} \left| \frac{V_{ts}^* V_{tb}}{V_{cb}} \right|^2 \frac{6\alpha_{\text{em}}}{\pi C} [P(E_0) + N(E_0)]. \quad (4.43)$$

In Eq. (4.43), $P(E_0)$ and $N(E_0)$ denote the perturbative and the non-perturbative contributions to the decay probability respectively. They depend on the lower cut for the energy of the photon in the Bremsstrahlung correction E_0 shown in Eq. (4.42). Using the parameterisation given in Ref. [126] we write $E_0 = m_b^{1S}/2(1 - \delta')$ and choose δ' such that the lower bound in Eq. (4.42) is saturated. The perturbative contribution $P(E_0)$ is given by [125]

$$P(E_0) = \sum_{i,j=1}^8 C_i^{\text{eff}}(\mu_b) C_j^{\text{eff}*}(\mu_b) K_{ij}(E_0, \mu_b) \quad (4.44)$$

with $K_{ij} = \delta_{i7}\delta_{j7} + \mathcal{O}(\alpha_s)$. The effective Wilson coefficients C_i^{eff} are expressed in terms of linear combinations of the coefficients for the operators \hat{Q}_i^s ($i = 1, \dots, 6$), $\hat{Q}_{7\gamma}^s$ and \hat{Q}_{8g}^s introduced in Section 2.1. For the denominator of Eq. (4.43) we have [125]

$$C = \left| \frac{V_{ub}}{V_{cb}} \right|^2 \frac{\Gamma(\bar{B} \rightarrow X_c e \bar{\nu})}{\Gamma(\bar{B} \rightarrow X_u e \bar{\nu})}. \quad (4.45)$$

In order to account for the NNLO result in Eq. (4.41) we write

$$\mathcal{B}r(\bar{B} \rightarrow X_s \gamma) = \mathcal{B}r^{\text{SM, NNLO}}(\bar{B} \rightarrow X_s \gamma) \cdot \frac{\mathcal{B}r^{\text{NLO}}(\bar{B} \rightarrow X_s \gamma)(\mu_0)}{\mathcal{B}r_0^{(0) \text{ SM, NLO}}(\bar{B} \rightarrow X_s \gamma)}. \quad (4.46)$$

Where

- $\mathcal{B}r^{\text{NLO}}(\bar{B} \rightarrow X_s \gamma)$ is the branching ratio for the process $\bar{B} \rightarrow X_s \gamma$ calculated at NLO including NP effects from $\Delta C_{1,2}^{s,cc}(M_W)$. All inputs are allowed to float except the renormalisation scale, which is fixed at $\mu_0 = m_b$. Our calculations are determined using the anomalous dimension matrices provided in [126]. NP contributions are introduced according to Eq. (3.1). They propagate to the rest of the Wilson coefficients C_i after applying the renormalisation group equations, described in Section 2 of Ref. [126].

Parameter	Relative error
$N(E_0)$	5.00%
μ	3.00%
$\mathcal{B}r(\bar{B} \rightarrow X_c e \bar{\nu}_e)$	2.68%
$m_c(m_c)$	1.10%
m_b^{1S}	0.61%
Λ_5^{QCD}	0.26%
γ	0.10%
$ V_{ub}/V_{cb} $	0.04%
$ V_{us} $	0.01%
Total	6.55%

Table 7: Error budget for the observable $\mathcal{B}r(\bar{B} \rightarrow X_s \gamma)$. Here $N(E_0)$ determines the uncertainty arising from non-perturbative contributions.

- $\mathcal{B}r_0^{\text{SM, NLO}}(\bar{B} \rightarrow X_s \gamma)$ is the SM branching ratio for the process $\bar{B} \rightarrow X_s \gamma$ calculated at NLO and evaluated at the central values of all the input parameters and then kept constant during the χ^2 -fit.
- $\mathcal{B}r^{\text{SM, NNLO}}(\bar{B} \rightarrow X_s \gamma)$ is the SM branching ratio for the process $\bar{B} \rightarrow X_s \gamma$ calculated at NNLO and allowed to float within the uncertainty associated with the renormalisation scale. In the case of the theoretical result given in Eq.(4.41) this corresponds to 3% of the central value [124]⁵.

The partial contributions to the final error are described in Table 7. The allowed regions for $\Delta C_1^{s,cc}(M_W)$ and $\Delta C_2^{s,cc}(M_W)$ are shown in Fig. 11, where it can be seen how this observable imposes strong constraints on $\Delta C_2^{s,cc}(M_W)$. The bounds in Fig. 11 are consistent with those reported in [60] once a 68% C.L. is taken into account.

4.3.2 $\Delta\Gamma_s$: Bounds and SM update

The decay rate differences $\Delta\Gamma_q$ and the semileptonic asymmetries a_{sl}^q arising from neutral B_q meson mixing are sensitive to the tree-level transitions $b \rightarrow u\bar{u}q$, $b \rightarrow u\bar{c}q$, $b \rightarrow c\bar{u}q$ and $b \rightarrow c\bar{c}q$ for $q = s, d$. We will, however, show below that for the decay rate difference of B_s -mesons our BSM study is completely dominated by the $b \rightarrow c\bar{c}s$ transition, yielding

⁵ In the NNLO determination in [124] two scales μ_b and μ_c are introduced. The 3% variation indicated in the error budget is derived from considering the variation $1.25 \text{ GeV} \leq \mu_{b,c} \leq 5 \text{ GeV}$ which accounts for about 2.4%. However a more conservative value is taken due to the lack of certainty on extra contributions to the perturbation series involved, see more details in [124].

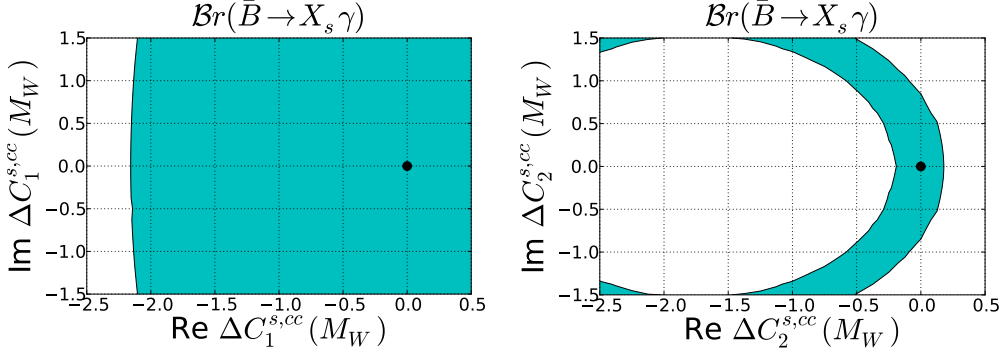


Figure 11: Potential regions for the NP contributions in $\Delta C_1^{s,cc}(M_W)$ and $\Delta C_2^{s,cc}(M_W)$ allowed by the observable $\mathcal{Br}(\bar{B} \rightarrow X_s \gamma)$ at 90% C.L.. The black point corresponds to the SM value.

therefore strong constraints to $\Delta C_1^{s,cc}(M_W)$ and $\Delta C_2^{s,cc}(M_W)$.

The definitions of the observables $\Delta\Gamma_q$ and a_{sl}^q in terms of Γ_{12}^q/M_{12}^q were introduced in Eqs. (2.16) and (2.17). Since, as explained in Section 2.2, the elements Γ_{12}^q are determined from the double insertion of $\hat{\mathcal{H}}_{eff}^{|\Delta B|=1}$ Hamiltonians, there are leading order contributions originating from the insertion of two current-current operators $\hat{Q}_j^{q,ab}$ for $ab = uu, uc, cc$ and $j = 1, 2$, see Eq. (2.3). Additionally, there are also double insertions from a single current-current $\hat{Q}_{1,2}^{q,ab}$ and a penguin operator $\hat{Q}_{3,4,5,6}^q$. In this section, we will only include NP effects to Γ_{12}^q , while we neglect tree level NP contributions to M_{12}^q (these contribution are discussed in Section 4.4.1 and they yield considerably weaker bounds for the observables $\Delta\Gamma_q$ and a_{sl}^q). To show the dominance of the $b \rightarrow c\bar{c}s$ contribution for B_s -mixing, we decompose Γ_{12}^q into partial contributions $\Gamma_{12}^{q,ab}$, where the indices $ab = uu, uc, cc$ indicate which “up” type quarks are included inside the corresponding effective fermionic loops. Thus, the expression for Γ_{12}^q/M_{12}^q becomes

$$\begin{aligned}
\frac{\Gamma_{12}^q}{M_{12}^q} &= - \frac{\left(\lambda_c^{(q)}\right)^2 \Gamma_{12}^{q,cc} + 2\lambda_u^{(q)} \lambda_c^{(q)} \Gamma_{12}^{q,uc} + \left(\lambda_u^{(q)}\right)^2 \Gamma_{12}^{q,uu}}{M_{12}^q} \\
&= - \frac{(\lambda_t^{(q)})^2 \Gamma_{12}^{q,cc} + 2\lambda_t^{(q)} \lambda_u^{(q)} \left[\Gamma_{12}^{q,cc} - \Gamma_{12}^{q,uc}\right] + (\lambda_u^{(q)})^2 \left[\Gamma_{12}^{q,cc} - 2\Gamma_{12}^{q,uc} + \Gamma_{12}^{q,uu}\right]}{(\lambda_t^{(q)})^2 \tilde{M}_{12}^q} \\
&= -10^{-4} \left[c^q + a^q \frac{\lambda_u^{(q)}}{\lambda_t^{(q)}} + b^q \left(\frac{\lambda_u^{(q)}}{\lambda_t^{(q)}} \right)^2 \right].
\end{aligned} \tag{4.47}$$

We have used here the unitarity of the CKM matrix: $\lambda_u^{(q)} + \lambda_c^{(q)} + \lambda_t^{(q)} = 0$ and we have split off the CKM dependence from M_{12}^q by introducing the quantity \tilde{M}_{12}^q . The GIM suppressed [127] terms a and b vanish in the limit $m_c \rightarrow m_u$ and the numerical values show a clear hierarchy

$$c^q \approx -48, \quad a^q \approx 11, \quad b^q \approx 0.23. \tag{4.48}$$

For the ratio of CKM elements we obtain

$$\frac{\lambda_u^{(q)}}{\lambda_t^{(q)}} \approx \begin{cases} 1.7 \cdot 10^{-2} - 4.2 \cdot 10^{-1} i & \text{for } q = d \\ -8.8 \cdot 10^{-3} + 1.8 \cdot 10^{-2} i & \text{for } q = s \end{cases} \quad (4.49)$$

$$\left(\frac{\lambda_u^{(q)}}{\lambda_t^{(q)}} \right)^2 = \begin{cases} -1.8 \cdot 10^{-1} - 1.5 \cdot 10^{-2} i & \text{for } q = d \\ -2.5 \cdot 10^{-4} - 3.2 \cdot 10^{-4} i & \text{for } q = s \end{cases} \quad (4.50)$$

Within the SM we find a very strong hierarchy of the three contributions in Eq. (4.47). The by far largest term is given by c^q and it is real. The second term proportional to a^q is GIM and CKM suppressed - slightly for the case of B_d mesons and more pronounced for B_s . Since $\lambda_u^{(q)}/\lambda_t^{(q)}$ is complex, this contribution gives rise to an imaginary part of Γ_{12}^q/M_{12}^q . Finally b^q is even further GIM suppressed and again slightly/strongly CKM suppressed for B_d/B_s mesons - this contribution has also both a real and an imaginary part. According to Eqs. (2.16) the decay rate difference $\Delta\Gamma_q$, given by the real part of Γ_{12}^q/M_{12}^q , is dominated by the coefficient c^q - stemming from $b \rightarrow c\bar{c}q$ transitions - and the coefficients a^q and b^q yield corrections of the order of 2 per mille. The semi-leptonic asymmetries are given by the imaginary part of Γ_{12}^q/M_{12}^q (c.f. Eq. (2.17)), which in turn is dominated by the coefficient a^q , with b^q giving sub-per mille corrections and no contributions from c^q . Allowing new, complex contributions to C_1 and C_2 for individual quark level contributions we get the following effects:

1. The numerically leading coefficient c^q can now also obtain an imaginary part.
2. The GIM cancellations in the coefficients a^q and b^q can be broken, if $b \rightarrow c\bar{c}q$, $b \rightarrow c\bar{u}q$, $b \rightarrow u\bar{c}q$ and $b \rightarrow u\bar{u}q$ are differently affected by NP. If there is a universal BSM contribution then the GIM cancellation will stay.
3. The CKM suppression will not be affected by our BSM modifications.

For the real part of Γ_{12}^s/M_{12}^s , we expect at most a correction of 2 per cent due to a^s and b^s , even if the corresponding GIM suppression is completely lifted - thus $\Delta\Gamma_s$ is even in our BSM approach, completely dominated by c^s and gives therefore only bounds on $b \rightarrow c\bar{c}s$. In the case of B_d mesons, the corrections due to a^d and b^d could be as large as 40 per cent - here all possible decay channels have to be taken into account - except we are considering universal BSM contributions to all decay channels. Since $\Delta\Gamma_d$ is not yet measured, we will revert our strategy and use the obtained bounds on the Wilson coefficients C_1 and C_2 to obtain potential enhancements or reductions of $\Delta\Gamma_d$ due to BSM effects in non-leptonic tree-level decays. Considering the imaginary part of Γ_{12}^s/M_{12}^s , we can get dramatically enhanced values for the semi-leptonic CP asymmetries, if C_1 or C_2 are complex, which will result in an imaginary part of the GIM-unsuppressed coefficient c^q . On the other hand new contributions to e.g. only $b \rightarrow c\bar{u}q$ or $b \rightarrow u\bar{c}q$ would have no effect on c^q , but they could lift the GIM suppression of the coefficient a^q and thus lead to also large effects. Therefore the semileptonic CP asymmetries are not completely dominated by the $b \rightarrow c\bar{c}q$ transitions. Next we explain in detail how to implement BSM contributions to C_1 and C_2 in the

theoretical description of Γ_{12}^q . Each one of the functions $\Gamma_{12}^{q,ab}$ in Eq. (4.47) are given by [87]

$$\Gamma_{12}^{q,ab} = \frac{G_F^2 m_b^2}{24\pi M_{B_q}} \left[\left(G^{q,ab} + \frac{1}{2} \alpha_2 G_S^{q,ab} \right) \langle B_q | \hat{Q}_1 | \bar{B}_q \rangle + \alpha_1 G_S^{q,ab} \langle B_q | \hat{Q}_3 | \bar{B}_q \rangle \right] + \tilde{\Gamma}_{12,1/m_b}^{q,ab}. \quad (4.51)$$

The coefficients α_1 and α_2 in Eq. (4.51) include NLO corrections and are written in the $\overline{\text{MS}}$ scheme as

$$\alpha_1 = 1 + \frac{\alpha_s(\mu)}{4\pi} C_F \left(12 \ln \frac{\mu}{m_b} + 6 \right), \quad \alpha_2 = 1 + \frac{\alpha_s(\mu)}{4\pi} C_F \left(12 \ln \frac{\mu}{m_b} + \frac{13}{2} \right). \quad (4.52)$$

Furthermore, the expressions for $G^{q,ab}$ and $G_S^{q,ab}$ in Eq. (4.51) are decomposed as

$$G^{q,ab} = F^{q,ab} + P^{q,ab}, \quad G_S^{q,ab} = -F_S^{q,ab} - P_S^{q,ab}, \quad (4.53)$$

with $F^{q,ab}$ and $F_S^{q,ab}$ encoding the perturbative contributions resulting from the double insertion of current-current operators. Finally, $P^{q,ab}$ and $P_S^{q,ab}$ contain the perturbative effects from the combined insertion of a current-current and a penguin operators. In terms of the tree-level Wilson coefficients $C_1^{q,ab}$ and $C_2^{q,ab}$, the equations for $F^{q,ab}$ and $F_S^{q,ab}$ have the following generic structure

$$F^{q,ab} = F_{11}^{q,ab} \left[C_1^{q,ab}(\mu) \right]^2 + F_{12}^{q,ab} C_1^{q,ab}(\mu) C_2^{q,ab}(\mu) + F_{22}^{q,ab} \left[C_2^{q,ab}(\mu) \right]^2, \quad (4.54)$$

where the individual factors $F_{11,12,22}^{q,ab}$ are available in the literature up to NLO

$$F_{ij}^{q,ab} = F_{ij}^{q,(0)} + \frac{\alpha_s(\mu)}{4\pi} F_{ij}^{q,(1)}. \quad (4.55)$$

To account for NP effects, the Wilson coefficients inside Eq. (4.54) should be determined using Eq. (3.1) and applying the renormalization group equations introduced in Sec. 2. Notice that Eq. (4.54) is sensitive to the different transitions $b \rightarrow c\bar{c}q$, $b \rightarrow u\bar{c}q$, $b \rightarrow c\bar{u}q$ and $b \rightarrow u\bar{u}q$. To be consistent with the inclusion of NP effects $\Delta C_1^{q,ab}(M_W)$ and $\Delta C_2^{q,ab}(M_W)$ at LO only, we omit all the terms involving products between $\alpha_s(\mu)$ and the NP factors $\Delta C_{1,2}^{q,ab}(M_W)$ inside Eq. (4.54). The penguin functions $P^{q,ab}$ and $P_S^{q,ab}$ also contain LO contributions from $C_{1,2}^{q,ab}$. For the purposes of illustration we will show the explicit expressions for the functions $P^{s,cc}$ and $P_S^{s,cc}$ corresponding to the $B_s^0 - \bar{B}_s^0$ system. At NLO we have [67]

$$\begin{aligned} P^{s,cc} &= \sqrt{1-4\bar{z}} \left[(1-\bar{z}) K_1'^{cc}(\mu) + \frac{1}{2} (1-4\bar{z}) K_2'^{cc}(\mu) + 3\bar{z} K_3'^{cc}(\mu) \right] \\ &\quad + \frac{\alpha_s(\mu)}{4\pi} F_p^{cc}(\bar{z}) \left[C_2^{s,cc}(\mu) \right]^2, \\ P_S^{s,cc} &= \sqrt{1-4\bar{z}} \left[1+2\bar{z} \right] \left[K_1'^{cc}(\mu) - K_2'^{cc}(\mu) \right] - \frac{\alpha_s(\mu)}{4\pi} 8F_p(\bar{z}) \left[C_2^{s,cc}(\mu) \right]^2. \end{aligned} \quad (4.56)$$

Where the following definition for the ratio of the masses of the bottom and charm quarks, evaluated in the $\overline{\text{MS}}$ scheme [87], has been used

$$\bar{z} = \left[\bar{m}_c(\bar{m}_b) / \bar{m}_b(\bar{m}_b) \right]^2. \quad (4.57)$$

The functions $K'_{1,2,3}{}^{cc}$ inside Eq. (4.56) are given by

$$\begin{aligned} K_1'^{cc}(\mu) &= 2 \left[3C_1^{s,cc}(\mu)C_3^s(\mu) + C_1^{s,cc}(\mu)C_4^s(\mu) + C_2^{s,cc}(\mu)C_3^s(\mu) \right], \\ K_2'^{cc}(\mu) &= 2C_2^{s,cc}(\mu)C_4^s(\mu), \\ K_3'^{cc}(\mu) &= 2 \left[3C_1^{s,cc}(\mu)C_5^s(\mu) + C_1^{s,cc}(\mu)C_6^s(\mu) + C_2^{s,cc}(\mu)C_5^s(\mu) + C_2^{s,cc}(\mu)C_6^s(\mu) \right], \end{aligned} \quad (4.58)$$

and the expression for the NLO correction function $F_p^{cc}(z)$ is

$$\begin{aligned} F_p^{cc}(z) &= -\frac{1}{9}\sqrt{1-4\bar{z}}(1+2\bar{z}) \left[2\ln\frac{\mu}{m_b} + \frac{2}{3} + 4\bar{z} - \ln\bar{z} \right. \\ &\quad \left. + \sqrt{1-4\bar{z}}(1+2\bar{z}) \ln\frac{1-\sqrt{1-4\bar{z}}}{1+\sqrt{1+4\bar{z}}} + \frac{3C_{8g}^s(\mu)}{C_2^{s,cc}(\mu)} \right]. \end{aligned} \quad (4.59)$$

The Wilson coefficients inside Eqs. (4.58) should be calculated by introducing NP deviations at the scale $\mu = M_W$ and then running down their corresponding values to the scale $\mu \sim m_b$ through the renormalization group equations, for details see the discussion in Sec. 2. In Appendix A, we provide details on the numerical inputs used. Since there was tremendous progress [64, 65] in the theoretical precision of the mixing observables we will present in this work numerical updates of all mixing observables: $\Delta\Gamma_q$ below, ΔM_q in Section 4.4.1 and the semi-leptonic CP asymmetries a_{sl}^q and ϕ_q in Section 4.5. For our numerical analysis we use results for $\Gamma_{12,3}^{q,(0)}$, $\Gamma_{12,3}^{q,(1)}$ and $\Gamma_{12,4}^{q,(0)}$, from [67, 80, 83–87] and for the hadronic matrix elements the averages presented in [65] based on [82, 90, 91] and [92–95], as well as the dimension seven matrix elements from [96]. The new SM determinations for $\Delta\Gamma_s$ and $\Delta\Gamma_d$ are

$$\Delta\Gamma_s^{\text{SM}} = (9.1 \pm 1.3) \cdot 10^{-2} \text{ ps}^{-1}, \quad (4.60)$$

$$\Delta\Gamma_d^{\text{SM}} = (2.6 \pm 0.4) \cdot 10^{-3} \text{ ps}^{-1}. \quad (4.61)$$

The error budgets of the mixing observables $\Delta\Gamma_s$ and $\Delta\Gamma_d$ are presented in Tabs. 8 and 9 respectively. Compared to the SM estimates for $\Delta\Gamma_s$ stemming from 2006 [87], 2011 [128] and 2015 [31] we find a huge improvement in the SM precision. Moreover, the value of $\Delta\Gamma_s$ in Eq. (4.60) is in good agreement with the corresponding result of $\Delta\Gamma_s = (9.2 \pm 1.4) \cdot 10^{-2} \text{ ps}^{-1}$ obtained in [96].

In addition, the current SM predictions are based for the first time on a non-perturbative determination [96] of the leading uncertainty due to dimension seven operators. All previous predictions had to rely on vacuum insertion approximation for the corresponding matrix elements. To further reduce the theory uncertainties, improvements in the lattice

$\Delta\Gamma_s^{\text{SM}}$	this work	ABL 2015	LN 2011	LN 2006
Central Value	0.091 ps ⁻¹	0.088 ps ⁻¹	0.087 ps ⁻¹	0.096 ps ⁻¹
$B_{R_2}^s$	10.9%	14.8%	17.2%	15.7%
μ	6.6%	8.4%	7.8%	13.7%
V_{cb}	3.4%	4.9%	3.4%	4.9%
$B_{R_0}^s$	3.2%	2.1%	3.4%	3.0%
$f_{B_s}\sqrt{B_1^s}$	3.1%	13.9%	13.5%	34.0%
B_3^s	2.2%	2.1%	4.8%	3.1%
\bar{z}	0.9%	1.1%	1.5%	1.9%
m_b	0.9%	0.8%	0.1%	1.0%
$B_{R_3}^s$	0.5%	0.2%	0.2%	— — —
$B_{\tilde{R}_3}^s$	-	0.6%	0.5%	— — — —
m_s	0.3%	0.1%	1.0%	1.0%
$B_{\tilde{R}_1}^s$	0.2%	0.7%	1.9%	— — —
Λ_5^{QCD}	0.1%	0.1%	0.4%	0.1%
γ	0.1%	0.1%	0.3%	1.0%
$B_{R_1}^s$	0.1%	0.5%	0.8%	— — —
$ V_{ub}/V_{cb} $	0.1%	0.1%	0.2%	0.5%
$\bar{m}_t(\bar{m}_t)$	0.0%	0.0%	0.0%	0.0%
Total	14.1%	22.8%	24.5%	40.5%

Table 8: List of the individual contributions to the theoretical error of the decay rate difference $\Delta\Gamma_s$ within the Standard Model and comparison with the values obtained in 2015 [31], in 2011 [128] and in 2006 [87]. We have used equations of motion in the current analysis to get rid of the operator \tilde{R}_3 .

$\Delta\Gamma_d^{\text{SM}}$	This work	ABL 2015
Central Value	$2.61 \cdot 10^{-3} \text{ ps}^{-1}$	$2.61 \cdot 10^{-3} \text{ ps}^{-1}$
$B_{R_2}^d$	11.1%	14.4%
$f_{B_d} \sqrt{B_1^d}$	3.6%	13.7%
μ	6.7%	7.9%
V_{cb}	3.4%	4.9%
B_3^d	2.4%	4.0%
$B_{R_0}^d$	3.3%	2.5%
\bar{z}	0.9%	1.1%
m_b	0.9%	0.8%
$\tilde{B}_{R_3}^d$	-	0.5%
$B_{R_3}^d$	0.5%	0.2%
γ	2.2%	2.5%
Λ_5^{QCD}	0.1%	0.1%
$ V_{ub}/V_{cb} $	0.0%	0.1%
$\bar{m}_t(\bar{m}_t)$	0.0%	0.0%
Total	14.7%	22.7%

Table 9: List of the individual contributions to the theoretical error of the mixing quantity $\Delta\Gamma_d$ and comparison with the values obtained in 2015 [31]. We have used equations of motion in the current analysis to get rid of the operator \tilde{R}_3 .

determination would be very welcome or a corresponding sum rule calculation. The next important uncertainty stems from the renormalisation scale dependence, to reduce this a NNLO calculation is necessary. First steps in that direction have been done in [129]. In the ratio $\Delta\Gamma_q/\Delta M_q$ uncertainties due to the matrix elements of dimension six are cancelling - so for a long time this ratio was considerably better known than the individual value of $\Delta\Gamma_s$. Due to the huge progress in determining precise values for these non-perturbative parameter, this advantage is now considerably less pronounced, see Table 10. For the corresponding experimental values we use the HFLAV averages

$$\begin{aligned}
\Delta\Gamma_s^{\text{Exp}} &= (8.8 \pm 0.6) \cdot 10^{-2} \text{ ps}^{-1}, [111] \\
\Delta\Gamma_d^{\text{Exp}} &= (-1.3 \pm 6.6) \cdot 10^{-3} \text{ ps}^{-1},
\end{aligned} \tag{4.62}$$

$\Delta\Gamma_s^{\text{SM}}/\Delta M_s^{\text{SM}}$	this work	ABL 2015	LN 2011	LN 2006
Central Value	$48.2 \cdot 10^{-4}$	$48.1 \cdot 10^{-4}$	$50.4 \cdot 10^{-4}$	$49.7 \cdot 10^{-4}$
$B_{R_2}^s$	10.9%	14.8%	17.2%	15.7%
μ	6.6%	8.4%	7.8%	9.1%
$B_{R_0}^s$	3.2%	2.1%	3.4%	3.0%
B_3^s	2.2%	2.1%	4.8%	3.1%
\bar{z}	0.9%	1.1%	1.5%	1.9%
m_b	0.9%	0.8%	1.4%	1.0%
$B_{R_3}^s$	0.5%	0.2%	0.2%	— — —
$B_{\tilde{R}_3}^s$	—	0.6%	0.5%	— — — —
$\bar{m}_t(\bar{m}_t)$	0.3%	0.7%	1.1%	1.8%
m_s	0.3%	0.1%	1.0%	0.1%
Λ_5^{QCD}	0.2%	0.2%	0.8%	0.1%
$B_{\tilde{R}_1}^s$	0.2%	0.7%	1.9%	— — —
$B_{R_1}^s$	0.1%	0.5%	0.8%	— — —
γ	$< 0.1\%$	0.0%	0.0%	0.1%
$ V_{ub}/V_{cb} $	$< 0.1\%$	0.0%	0.0%	0.1%
V_{cb}	$< 0.1\%$	0.0%	0.0%	0.0%
Total	13.4%	17.3%	20.1%	18.9%

Table 10: List of the individual contributions to the theoretical error of the ratio $\Delta\Gamma_s/\Delta M_s$ within the Standard Model and comparison with the values obtained in 2015 [31], in 2011 [128] and in 2006 [87]. We have used equations of motion in the current analysis to get rid of the operator \tilde{R}_3 .

where $\Delta\Gamma_d^{\text{Exp}}$ was obtained using [111]

$$\left(\Delta\Gamma_d/\Gamma_d\right)^{\text{Exp}} = -0.002 \pm 0.010, \quad \tau_{B_d^0}^{\text{Exp}} = \left(1.520 \pm 0.004\right) \text{ ps.} \quad (4.63)$$

The resulting regions for $\Delta C_1^{s,cc}(M_W)$ and $\Delta C_2^{s,cc}(M_W)$ allowed by $\Delta\Gamma_s$ are presented in Fig.12.

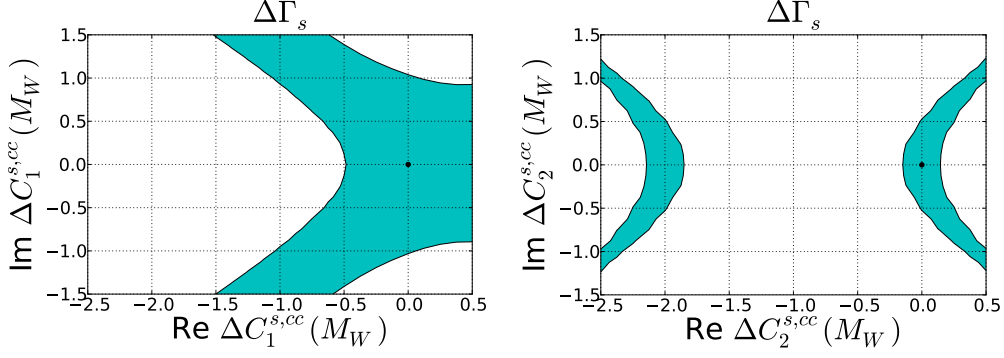


Figure 12: Potential regions for the NP contributions in $\Delta C_1^{s,cc}(M_W)$ and $\Delta C_2^{s,cc}(M_W)$ allowed by the observable $\Delta\Gamma_s$ at 90% C.L.. The black point corresponds to the SM value.

4.3.3 $S_{J/\psi\phi}$

The mixing induced CP asymmetry for the decay $\bar{B}_s \rightarrow J/\psi\phi$, given as

$$S_{J/\psi\phi} = \frac{2 \operatorname{Im}(\lambda_{J/\psi\phi}^s)}{1 + |\lambda_{J/\psi\phi}^s|^2} = \sin(2\beta_s), \quad (4.64)$$

can be used to constrain $\Delta C_1^{s,cc}(M_W)$. In Eq. (4.64), $\lambda_{J/\psi\phi}^s$ is determined according to Eq. (4.20) considering the amplitudes $\bar{\mathcal{A}}_{J/\psi\phi}$ and $\mathcal{A}_{J/\psi\phi}$ for the decays $\bar{B}_s^0 \rightarrow J/\psi\phi$ and $B_s^0 \rightarrow J/\psi\phi$ respectively. The required theoretical expressions have been calculated explicitly within the QCDF formalism in [130]. The equation for the decay amplitude obeys the structure

$$\mathcal{A}_{J/\psi\phi}^h \propto \alpha_1^{J/\psi\phi,h} + \alpha_3^{J/\psi\phi,h} + \alpha_5^{J/\psi\phi,h} + \alpha_7^{J/\psi\phi,h} + \alpha_9^{J/\psi\phi,h}, \quad (4.65)$$

where the proportionality constant has been omitted since it cancels in the ratio $\lambda_{J/\psi\phi}^s$. The amplitudes $\alpha_i^{J/\psi\phi}$ appearing in Eq. (4.65) obey the structure given in Eq. (2.20). The required expressions for the vertices and hard-scattering functions can be found in the appendix. The index $h = 0, \pm$ indicated in Eq. (4.65) makes reference to helicity of the particles in the final state. During our analysis we average over the different helicity contributions. Therefore we take

$$S_{J/\psi\phi} = \frac{S_{J/\psi\phi}^0 + S_{J/\psi\phi}^+ + S_{J/\psi\phi}^-}{3}, \quad (4.66)$$

where each one of the asymmetries $S_{J/\psi\phi}^h$, are determined individually considering the corresponding amplitude $\mathcal{A}_{J/\psi\phi}^h$ for $h = 0, \pm$.

Neglecting penguin contributions our theoretical evaluation leads to

$$\sin(2\beta_s^{\text{SM}}) = 0.037 \pm 0.001, \quad (4.67)$$

Parameter	Relative error
$ V_{ub}/V_{cb} $	2.44%
γ	1.39%
$ V_{us} $	0.07%
Total	2.81%

Table 11: Error budget for the observable $\sin(2\beta_s)$.

which numerically coincides with $2\beta_s^{\text{SM}}$ within the precision under consideration. The error budget is shown in Table 11. On the experimental side we use the average [111]

$$2\beta_s^{\text{Exp}} = 0.021 \pm 0.031. \quad (4.68)$$

The effect of $S_{J/\psi\phi}$ on the allowed values for $\Delta C_1^{s,cc}(M_W)$ is not as strong as the results derived from other observables. However we included it in our analysis for completeness. For this reason we do not show the individual constraints from $S_{J/\psi\phi}$ and present only its effect in the global χ^2 -fit described in Section 5.4.

4.3.4 τ_{B_s}/τ_{B_d}

The lifetime ratio τ_{B_s}/τ_{B_d} gives us sensitivity to $\Delta C_1^{s,cc}(M_W)$ and $\Delta C_2^{s,cc}(M_W)$ via the weak exchange diagram contributing to the B_s -lifetime as CKM leading part. We assumed here that no new effects are arising in the B_d -lifetime, where the CKM leading part is given by a $b \rightarrow c\bar{u}d$ transition. Allowing new effects in both $b \rightarrow c\bar{c}s$ and $b \rightarrow c\bar{u}d$ the individually large effects will hugely cancel. We also neglect the currently unknown contribution of the Darwin term ⁶.

Using the results presented in [58] we write

$$\frac{\tau_{B_s}}{\tau_{B_d}} = \left(\frac{\tau_{B_s}}{\tau_{B_d}} \right)^{\text{SM}} + \left(\frac{\tau_{B_s}}{\tau_{B_d}} \right)^{\text{NP}}, \quad (4.69)$$

for the SM value we take [82]

$$\left(\frac{\tau_{B_s}}{\tau_{B_d}} \right)^{\text{SM}} = 1.0006 \pm 0.0020. \quad (4.70)$$

The experimental result for the ratio is [111]

$$\left(\frac{\tau_{B_s}}{\tau_{B_d}} \right)^{\text{Exp}} = 0.994 \pm 0.004. \quad (4.71)$$

⁶Recently the Wilson coefficient of the Darwin operator was found to be large [131, 132] for B mesons. Due to the currently unknown size of the matrix element of this operator in between B_s states, the numerical effect of these new contributions on the lifetime ratio τ_{B_s}/τ_{B_d} - being proportional to $\langle B_s | \rho_D^3 | B_s \rangle - \langle B_d | \rho_D^3 | B_d \rangle$ - cannot yet be estimated.

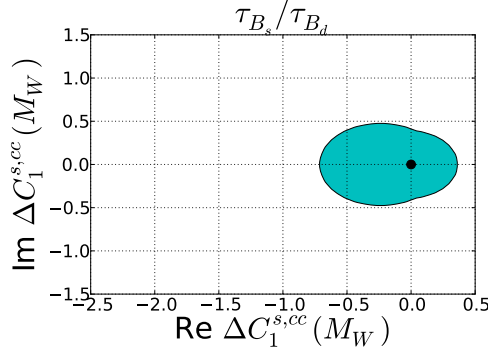


Figure 13: Potential regions for the NP contributions in $\Delta C_1^{s,cc}(M_W)$ and $\Delta C_2^{s,cc}(M_W)$ allowed by the life-time ratio τ_{B_s}/τ_{B_d} at 90% C.L.. Here we assumed only BSM contributions to the decay channel $b \rightarrow c\bar{c}s$, but none to $b \rightarrow c\bar{u}d$. The black point corresponds to the SM value.

To estimate the NP contribution $(\tau_{B_s}/\tau_{B_d})^{\text{NP}}$ we consider the following function [58]

$$F_{\tau_{B_s}/\tau_{B_d}}(C_1, C_2) = G_F^2 |V_{cb} V_{cs}|^2 m_b^2 M_{B_s} f_{B_s}^2 \tau_{B_s} \frac{\sqrt{1-4x_c^2}}{144\pi} \left\{ (1-x_c^2) \left[4|C'|^2 B_1 + 24|C_2|^2 \epsilon_1 \right] - \frac{M_{B_s}^2 (1+2x_c^2)}{(m_b + m_s)^2} \left[4|C'|^2 B_2 + 24|C_2|^2 \epsilon_2 \right] \right\}, \quad (4.72)$$

where $x_c = m_c/m_b$ and C' denotes the following combination of tree-level Wilson coefficients

$$C' \equiv 3C_1 + C_2. \quad (4.73)$$

The non-perturbative matrix elements of the arising four-quark $\Delta B = 0$ operators are parameterised in terms of the decay constant f_{B_s} and the bag parameter B_1 , B_2 , ϵ_1 and ϵ_2 , which we take from the recent evaluation in [82]. The numerical values used are listed in Appendix A. The NP contribution to the lifetime ratio can be written as

$$\left(\frac{\tau_{B_s}}{\tau_{B_d}} \right)^{\text{NP}} = F_{\tau_{B_s}/\tau_{B_d}}(C_1^{s,cc}(\mu), C_2^{s,cc}(\mu)) - F_{\tau_{B_s}/\tau_{B_d}}(C_1^{s,cc}(\mu), C_2^{s,cc}(\mu)) \Big|_{\text{SM}}, \quad (4.74)$$

where in the second term in Eq. (4.74) we have dropped the NP contributions $\Delta C_1^{s,cc}(\mu)$ and $\Delta C_2^{s,cc}(\mu)$. Our bounds for $\Delta C_1^{s,cc}(M_W)$ are shown in Fig. 13, the corresponding results for $\Delta C_2^{s,cc}(M_W)$ turn out to be weak and therefore we do not display them. We would like to highlight the consistency between our regions and those presented in [60] which were calculated at the 68% C. L..

4.4 Observables constraining $b \rightarrow c\bar{c}d$ transitions

We devote this section to the derivation of bounds on $\Delta C_1^{d,cc}(M_W)$ and $\Delta C_2^{d,cc}(M_W)$ from $\sin(2\beta_d)$ and $B \rightarrow X_d\gamma$. In our final analysis we also included contributions from a_{sl}^d which will be described in more detail in Section 4.5.

4.4.1 $\sin(2\beta_d)$ and SM update of ΔM_q

In our BSM framework mixing induced CP asymmetries can be modified by changes in the tree-level decay or by changes to the neutral B -meson mixing. The first effect was studied in Section for the case of $B_s \rightarrow J/\Psi\phi$ and found to give very weak bounds. Thus we will not consider them here. The second effect is also expected to give relatively weak bounds, but since the lack of strong bounds on new contributions to $b \rightarrow c\bar{c}d$ we will consider it here - in the $b \rightarrow c\bar{c}s$ we neglected it, because of much stronger constraints from other observables.

We can constrain $\Delta C_2^{d,cc}(M_W)$ with the observable

$$\sin(2\beta_d) = -S_{J/\psi K_S} \quad (4.75)$$

which can be evaluated by applying the generic definition of the CP asymmetry shown in Eq. (4.19) and using

$$\lambda_{J/\psi K_S}^d = \frac{q}{p} \Big|_{B_d} \frac{\bar{\mathcal{A}}_{J/\psi K_S}}{\mathcal{A}_{J/\psi K_S}}. \quad (4.76)$$

Where in Eq. (4.76), $\mathcal{A}_{J/\psi K_S}$ and $\bar{\mathcal{A}}_{J/\psi K_S}$ correspond to the amplitudes for the processes $B^0 \rightarrow J/\psi K_S$ and $\bar{B}^0 \rightarrow J/\psi K_S$ respectively.

We study here modifications of $q/p|_{B_d}$, while we neglect the change of the amplitudes $\mathcal{A}_{J/\psi K_S}$ and $\bar{\mathcal{A}}_{J/\psi K_S}$ - since an exploratory study found much weaker bounds. The definition of $q/p|_{B_d}$ in terms of the B_d matrix element M_{12}^d is given in Eq. (4.21).

In the SM we have

$$M_{12}^{d,\text{SM}} = \frac{\langle B_d^0 | \hat{\mathcal{H}}_d^{|\Delta B|=2,\text{SM}} | \bar{B}_d^0 \rangle}{2M_{B_d^0}}, \quad (4.77)$$

with

$$\hat{\mathcal{H}}_d^{|\Delta B|=2,\text{SM}} = \frac{G_F^2}{16\pi^2} (\lambda_t^{(d)})^2 C^{|\Delta B|=2}(m_t, M_W, \mu) \hat{Q}_1^d + h.c.. \quad (4.78)$$

The dimension six effective $|\Delta B| = 2$ operator Q_1^d in Eq. (4.78) is given by

$$\hat{Q}_1^d = \left(\bar{d}\hat{b} \right)_{V-A} \left(\bar{d}\hat{b} \right)_{V-A}, \quad (4.79)$$

and the Wilson coefficient $C^{|\Delta B|=2}(m_t, M_W, \mu)$ corresponds to

$$C^{|\Delta B|=2}(m_t, M_W, \mu) = \tilde{\eta} M_W^2 S_0(x_t), \quad (4.80)$$

ΔM_s^{SM}	This work	ABL 2015	LN 2011	LN 2006
Central Value	18.77 ps^{-1}	18.3 ps^{-1}	17.3 ps^{-1}	19.3 ps^{-1}
$f_{B_s} \sqrt{B_1^s}$	3.1%	13.9%	13.5%	34.1%
V_{cb}	3.4%	4.9%	3.4%	4.9%
$\bar{m}_t(\bar{m}_t)$	0.3%	0.7%	1.1%	1.8%
Λ_5^{QCD}	0.2%	0.1%	0.4%	2.0%
γ	0.1%	0.1%	0.3%	1.0%
$ V_{ub}/V_{cb} $	$< 0.1\%$	0.1%	0.2%	0.5%
\bar{m}_b	$< 0.1\%$	$< 0.1\%$	0.1%	— — —
Total	4.6%	14.8%	14.0%	34.6%

Table 12: List of the individual contributions to the theoretical error of the mass difference ΔM_s within the Standard Model and comparison with the values obtained in 2015 [31], in 2011 [128] and in 2006 [87].

where the factor $\tilde{\eta}$ accounts for the renormalization group evolution from the scale m_t down to the renormalization scale $\mu \sim m_b$ [89] and $S_0(x_t)$ is the Inami-Lim function [88]

$$S_0(x_t) = \frac{x_t}{(1-x_t)^2} \left(1 - \frac{11}{4}x_t + \frac{x_t^2}{4} - \frac{3x_t^2 \ln x_t}{(1-x_t)} \right). \quad (4.81)$$

Using the new averages presented in [65] for the hadronic matrix elements (based on the non-perturbative calculations in [82, 90, 91] and [92–95]) we get the new updated SM results

$$\Delta M_s^{\text{SM}} = (18.77 \pm 0.86) \text{ ps}^{-1}, \quad (4.82)$$

$$\Delta M_d^{\text{SM}} = (0.543 \pm 0.029) \text{ ps}^{-1}, \quad (4.83)$$

where we observe a huge reduction of the theoretical uncertainty, see Tables 12 and 13. Our numbers agree with the ones quoted in [65] - a tiny difference stems from a different treatment of the top quark mass, the CKM input and the symmetrisation of the error we have performed here.

HFLAV [111] gives for the experimental values

$$\Delta M_s^{\text{Exp}} = (17.757 \pm 0.021) \text{ ps}^{-1}, \quad (4.84)$$

$$\Delta M_d^{\text{exp}} = (0.5064 \pm 0.0019) \text{ ps}^{-1}. \quad (4.85)$$

We introduce BSM effects to Eq. (4.77) by adding to the SM expression in Eq. (4.78) the double insertion of the effective Hamiltonian

$$\hat{\mathcal{H}}_{eff}^{|\Delta B|=1} = \frac{G_F}{\sqrt{2}} \left(\sum_{p,p'=u,c} \lambda_{pp'}^{(d)} C_2^{d,pp'} \hat{Q}_2^{d,pp'} + h.c. \right). \quad (4.86)$$

ΔM_d^{SM}	This work	ABL 2015
Central Value	0.543 ps ⁻¹	0.528 ps ⁻¹
$f_{B_d}\sqrt{B_1^d}$	3.6%	13.7%
V_{cb}	3.4%	4.9%
m_b	0.1%	0.1%
γ	0.2%	0.2%
Λ_5^{QCD}	0.2%	0.1%
$ V_{ub}/V_{cb} $	0.1%	0.1%
$\bar{m}_t(\bar{m}_t)$	0.3%	0.1%
Total	5.3%	14.8%

Table 13: List of the individual contributions to the theoretical error of the mixing quantity ΔM_d and comparison with the values obtained in 2015 [31].

Following [133] we evaluate the full combination at the scale $\mu_c = m_c$, where the extra contribution to the SM $|\Delta B| = 2$ Hamiltonian in Eq. (4.78) is given by

$$\begin{aligned} \hat{\mathcal{H}}_{extra}^{|\Delta B|=2} \approx & \frac{G_F^2}{16\pi^2} \left\{ C'_1(\mu_c) \hat{P}_1 + C'_2(\mu_c) \hat{P}_2 \right. \\ & \left. + \left[\left(2\lambda_c^{(d)} \lambda_t^{(d)} \tilde{C}_3(x_t^2) + (\lambda_c^{(d)})^2 \right) + C'_3(\mu_c) \right] \hat{P}_3 \right\}, \end{aligned} \quad (4.87)$$

with

$$\begin{aligned} C'_1(\mu_c) = & -\frac{2}{3} \ln \left[\frac{\mu_c^2}{M_W^2} \right] \left\{ \frac{(\lambda_c^{(d)})^2}{2} \left(C_2^{d,cc} \right)^2 - (\lambda_c^{(d)})^2 C_2^{d,cu} C_2^{d,uc} - \lambda_c^{(d)} \lambda_t^{(d)} C_2^{d,cu} C_2^{d,uc} \right. \\ & \left. + \frac{(\lambda_c^{(d)})^2}{2} \left(C_2^{d,uu} \right)^2 + \lambda_c^{(d)} \lambda_t^{(d)} \left(C_2^{d,uu} \right)^2 + \frac{(\lambda_t^{(d)})^2}{2} \left(C_2^{d,uu} \right)^2 \right\}, \\ C'_2(\mu_c) = & \frac{2}{3} \ln \left[\frac{\mu_c^2}{M_W^2} \right] \left\{ (\lambda_c^{(d)})^2 \left(C_2^{d,cc} \right)^2 - 2(\lambda_c^{(d)})^2 C_2^{d,cu} C_2^{d,uc} - 2\lambda_c^{(d)} \lambda_t^{(d)} C_2^{d,cu} C_2^{d,uc} \right. \\ & \left. + (\lambda_c^{(d)})^2 \left(C_2^{d,uu} \right)^2 + 2\lambda_c \lambda_t^{(d)} \left(C_2^{d,uu} \right)^2 + (\lambda_t^{(d)})^2 \left(C_2^{d,uu} \right)^2 \right\}, \\ C'_3(\mu_c) = & \frac{2}{3} \ln \left[\frac{\mu_c^2}{M_W^2} \right] \left\{ 3(\lambda_c^{(d)})^2 \left(C_2^{d,cc} \right)^2 - 3(\lambda_c^{(d)})^2 C_2^{d,cu} C_2^{d,uc} - 3\lambda_c^{(d)} \lambda_t^{(d)} C_2^{d,cu} C_2^{d,uc} \right\}. \end{aligned} \quad (4.88)$$

and

$$\tilde{C}_3(x_t) = \ln x_t - \frac{3x_t}{4(1-x_t)} - \frac{3x_t^2 \ln x_t}{4(1-x_t)^2}. \quad (4.89)$$

The set of HQET operators required in Eq. (4.87) are

$$\begin{aligned} \hat{P}_0 &= (\bar{h}^{(+)} \hat{d})_{V-A} (\bar{h}^{(-)} \hat{d})_{V-A}, \quad \hat{P}_1 = m_b^2 \hat{P}_0, \\ \hat{P}_2 &= m_b^2 \left(\bar{h}_v^{(+)} [1 - \gamma_5] \hat{d} \right) \left(\bar{h}_v^{(-)} [1 - \gamma_5] \hat{d} \right), \quad \hat{P}_3 = m_c^2 \hat{P}_0. \end{aligned} \quad (4.90)$$

Thus, our full determination of M_{12}^d is given by

$$M_{12}^d = \frac{\langle B_d^0 | \hat{\mathcal{H}}_d^{|\Delta B|=2, SM} + \hat{\mathcal{H}}_{extra}^{|\Delta B|=2} | \bar{B}_d^0 \rangle}{2M_{B_d^0}}, \quad (4.91)$$

where the $|\Delta B| = 2$ operator \hat{Q}_1^d is matched at the scale $\mu_c = m_c$ into \hat{P}_0 [133]. The required matrix elements for the numerical evaluations are [82]

$$\begin{aligned} \langle B_d^0 | \hat{P}_0 | \bar{B}_d^0 \rangle &= \frac{8}{3} f_{B_d}^2 M_{B_d}^2 B_1^d(\mu_c), \\ \langle B_d^0 | \hat{P}_2 | \bar{B}_d^0 \rangle &= -\frac{5}{3} m_b^2 \left(\frac{M_{B_d}}{m_b + m_d} \right)^2 f_{B_d}^2 M_{B_d}^2 B_2^d(\mu_c), \end{aligned} \quad (4.92)$$

with the values for the Bag parameters as indicated in Appendix A. Our theoretical result - neglecting contributions from penguins - is

$$\sin(2\beta_d^{\text{SM}}) = 0.707 \pm 0.030, \quad (4.93)$$

the full error budget in the SM can be found in Table 14. Notice that, the contributions from double insertions of the $|\Delta B| = 1$ effective Hamiltonian are relevant only when $\Delta C_2^{d,cc}(M_W) \neq 0$, hence they do not appear in Table 14. On the experimental side we use the average from direct measurements [111]

$$\sin(2\beta_d^{\text{Exp}}) = 0.699 \pm 0.017, \quad (4.94)$$

our results for the allowed regions on $\Delta C_2^{d,cc}(M_W)$ are shown in Fig. 14.

4.4.2 $\bar{B} \rightarrow X_d \gamma$

The branching ratio of the process $\bar{B} \rightarrow X_d \gamma$ allows us to impose further constraints on the NP contribution $\Delta C_2^{d,cc}(M_W)$. For the theoretical determination, we used the NNLO branching ratio for the transition $\bar{B} \rightarrow X_d \gamma$ given in [134]

$$\mathcal{B}_r^{\text{NNLO}}(\bar{B} \rightarrow X_d \gamma) = (1.73_{-0.22}^{+0.12}) \cdot 10^{-5} \quad \text{for } E_\gamma > 1.6 \text{ GeV}. \quad (4.95)$$

On the experimental side we consider [135–137]

$$\mathcal{B}_r^{\text{Exp}}(\bar{B} \rightarrow X_d \gamma) = (1.41 \pm 0.57) \cdot 10^{-5}. \quad (4.96)$$

The NP regions on $\Delta C_1^{cc,d}(M_W)$ derived from $\mathcal{B}_r^{\text{NNLO}}(\bar{B} \rightarrow X_d \gamma)$ are shown in Fig. 15. Our treatment for $\bar{B} \rightarrow X_d \gamma$ is analogous to the one of $\bar{B} \rightarrow X_s \gamma$, therefore our discussion here is rather short and we refer the reader to the details provided in Section 4.3.1.

Parameter	Relative error
$ V_{ub}/V_{cb} $	4.22%
$ V_{us} $	0.20%
γ	0.04%
μ_c	0.02%
$ V_{cb} $	0.01%
Total	4.22%

Table 14: Error budget for the observable $\sin(2\beta_d)$.

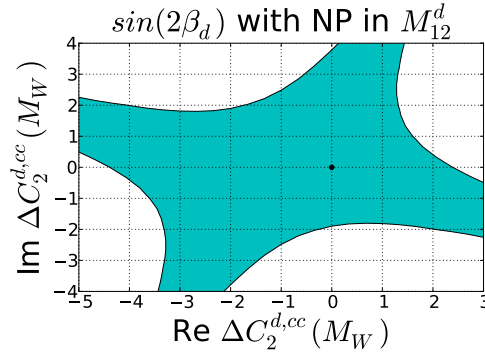


Figure 14: Potential regions for the NP contributions in $\Delta C_2^{d,cc}(M_W)$ allowed by the observable $\sin(2\beta_d)$ from modifications in M_{12}^d through double insertions of the $\Delta B = 1$ effective Hamiltonian at 90% C.L.. Due to the weakness of the current bounds, penguin pollution has been neglected in the analysis. The black point corresponds to the SM value.

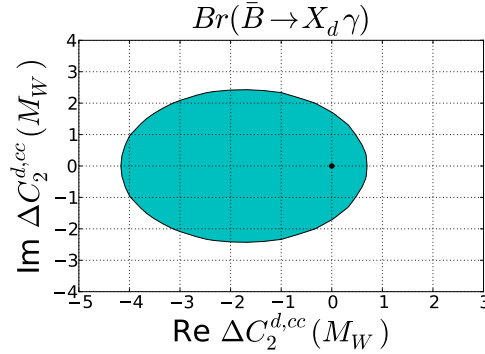


Figure 15: Potential regions for the NP contributions in $\Delta C_2^{d,cc}(M_W)$ allowed by the observable $\mathcal{B}r(\bar{B} \rightarrow X_d \gamma)$ at 90% C.L.. The black point corresponds to the SM value.

4.5 Observables constraining multiple channels

Several observables like $\Delta\Gamma_q$, $\tau(B_s)/\tau(B_d)$ and the semi-leptonic CP asymmetries are affected by different decay channels. We have shown that $\Delta\Gamma_s$ is by far dominated by the $b \rightarrow c\bar{c}s$ transition, $\Delta\Gamma_d$ has not yet been measured. In $\tau(B_s)/\tau(B_d)$ a new effect in the $b \rightarrow c\bar{c}s$ transition roughly cancels a similar size effect in a $b \rightarrow c\bar{u}d$ transition, thus we have assumed for this observable only BSM effects in the $b \rightarrow c\bar{c}s$ transition. Below we will study constraints stemming from a_{sl}^q , which is affected by the decay channels $b \rightarrow c\bar{c}q$, $b \rightarrow c\bar{u}q$, $b \rightarrow u\bar{c}q$ and $b \rightarrow u\bar{u}q$.

4.5.1 a_{sl}^s and a_{sl}^d : Bounds and SM update

The theoretical description of the semi-leptonic CP asymmetries was already presented in detail in Section 4.3.2. Our SM predictions for the semileptonic asymmetries a_{sl}^s and a_{sl}^d are

$$a_{sl}^{s,\text{SM}} = (2.06 \pm 0.18) \cdot 10^{-5}, \quad (4.97)$$

$$a_{sl}^{d,\text{SM}} = (-4.73 \pm 0.42) \cdot 10^{-4}. \quad (4.98)$$

The error budgets of the mixing observables a_{sl}^s and a_{sl}^d within the SM are presented in Tabs. 15 and 16 respectively.

The current experimental bounds [111] are far above the SM predictions

$$\begin{aligned} a_{sl}^{s,\text{Exp}} &= (60 \pm 280) \cdot 10^{-5}, \\ a_{sl}^{d,\text{Exp}} &= (-21 \pm 17) \cdot 10^{-4}. \end{aligned} \quad (4.99)$$

Nevertheless, these observables yield already, with the current experimental precision, strong bounds on C_1 and C_2 due to the pronounced sensitivity of $\text{Im}(\Gamma_{12}^q/M_{12}^q)$ on the imaginary components of the $\Delta B = 1$ Wilson coefficients. The regions for $\Delta C_1(M_W)$ and $\Delta C_2(M_W)$ allowed by the observables a_{sl}^s and a_{sl}^d are presented in Figs. 16 and 17 respectively where for simplicity we have assumed the universal behaviour

$$\Delta C_j^{q,uu}(M_W) = \Delta C_j^{q,uc}(M_W) = \Delta C_j^{q,cc}(M_W), \quad (4.100)$$

for $j = 1, 2$. As discussed in Section 4.3.2 different BSM effects in individual decay channels could lift the severe GIM suppression and lead to large effects, while the scenario given in Eq.(4.100) is dominated by $b \rightarrow c\bar{c}q$ transitions. However, in Secs. 5.1, 5.2 and 4.4 we will also study the effects of a_{sl}^d on the different b -quark decay channels $b \rightarrow u\bar{u}d$, $b \rightarrow c\bar{u}d$, and $b \rightarrow c\bar{c}d$ independently.

5 Global χ^2 -fit results

So far, we have limited our discussion to constraints derived from individual observables. In this section, we present, as the main result of this work, the resulting regions for $\Delta C_1(M_W)$ and $\Delta C_2(M_W)$ obtained after combining observables for the different exclusive b quark transitions. We will investigate three consequences of BSM effects in non-leptonic tree-level decays.

$a_{sl}^{s,SM}$	this work	ABL 2015	LN 2011	LN 2006
Central Value	$2.06 \cdot 10^{-5}$	$2.22 \cdot 10^{-5}$	$1.90 \cdot 10^{-5}$	$2.06 \cdot 10^{-5}$
μ	6.7%	9.5%	8.9%	12.7%
\bar{z}	4.0%	4.6%	7.9%	9.3%
$ V_{ub}/V_{cb} $	2.6%	5.0%	11.6%	19.5%
$B_{R_3}^s$	2.3%	1.1%	1.2%	1.1%
$B_{\tilde{R}_3}^s$	-	2.6%	2.8%	2.5%
m_b	1.3%	1.0%	2.0%	3.7%
γ	1.1%	1.3%	3.1%	11.3%
$B_{R_2}^s$	0.8%	0.1%	0.1%	— — —
Λ_5^{QCD}	0.6%	0.5%	1.8%	0.7%
$\bar{m}_t(\bar{m}_t)$	0.3%	0.7%	1.1%	1.8%
B_3^s	0.3%	0.3%	0.6%	0.4%
$B_{R_0}^s$	0.3%	0.2%	0.3%	— — —
m_s	$< 0.1\%$	0.1%	0.1%	0.1%
$B_{\tilde{R}_1}^s$	$< 0.1\%$	0.5%	0.2%	— — —
$B_{R_1}^s$	$< 0.1\%$	$< 0.1\%$	0.0%	— — —
V_{cb}	$< 0.1\%$	0.0%	0.0%	0.0%
Total	8.8%	12.2%	17.3%	27.9%

Table 15: List of the individual contributions to the theoretical error of the semileptonic CP asymmetries a_{sl}^s within the Standard Model and comparison with the values obtained in 2015 [31], in 2011 [128] and in 2006 [87]. We have used equations of motion in the current analysis to get rid of the operator \tilde{R}_3 .

1. The allowed size of BSM contributions to the Wilson coefficients C_1 and C_2 , governing the leading tree-level decays.
2. The impact of these new effects on the possible size of the observable $\Delta\Gamma_d$, which has not been measured yet. Notice that, if one sigma deviations are considered, the current experimental uncertainty associated with $\Delta\Gamma_d$, see Eq. (4.62), allows enhancement factors within the interval

$$-3.40 < \Delta\Gamma_d^{\text{Exp}}/\Delta\Gamma_d^{\text{SM}} < 2.27. \quad (5.1)$$

$a_{sl}^{d,SM}$	This work	ABL 2015
Central Value	$-4.7 \cdot 10^{-4}$	$-4.7 \cdot 10^{-4}$
$B_{R_2}^d$	0.8%	0.1%
μ	6.7%	9.4%
V_{cb}	0.0%	0.0%
B_3^d	0.4%	0.6%
$B_{R_0}^d$	0.3%	0.2%
\bar{z}	4.1%	4.9%
m_b	1.3%	1.3%
$B_{\tilde{R}_3}^d$	—%	2.7%
$B_{R_3}^d$	2.3%	1.2%
γ	1.0%	1.1%
Λ_5^{QCD}	0.8%	0.5%
$ V_{ub}/V_{cb} $	2.7%	5.2%
$\bar{m}_t(\bar{m}_t)$	0.3%	0.7%
Total	8.8%	12.3%

Table 16: List of the individual contributions to the theoretical error of the mixing quantity $a_{sl}^{d,SM}$ in the B^0 -sector and comparison with the values obtained in 2015 [31]. We have used equations of motion in the current analysis to get rid of the operator \tilde{R}_3 .

On the other hand, if the confidence interval is increased up to 1.65 sigmas, i.e. 90% C.L., then the potential effects in $\Delta\Gamma_d$ become

$$-5.97 < \Delta\Gamma_d^{\text{Exp}}/\Delta\Gamma_d^{\text{SM}} < 4.67. \quad (5.2)$$

The measured value of the dimuon asymmetry by the D0-collaboration [33–36] seems to be in conflict with the current experimental bounds on a_{sl}^d and a_{sl}^s , see e.g. the discussion in [138]. An enhanced value of $\Delta\Gamma_d$ could solve this experimental discrepancy [139], at the expense of introducing new physics in $\Delta\Gamma_d$ and potentially also in a_{sl}^s and a_{sl}^d . If all BSM effects in the dimuon asymmetry are due to $\Delta\Gamma_d$, then an enhancement factor of 6 with respect to its SM value is required. On the other hand, if there are also BSM contributions in a_{sl}^s and a_{sl}^d , then the BSM enhancement factor in $\Delta\Gamma_d$ can be smaller.

3. The impact of these new effects on the determination of the CKM angle γ . Within the

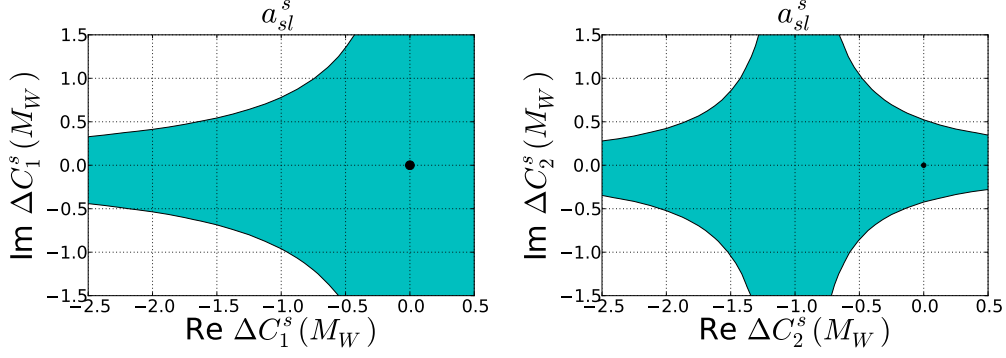


Figure 16: Potential regions for the NP contributions in $\Delta C_1^s(M_W)$ and $\Delta C_2^s(M_W)$ allowed by the semileptonic asymmetry a_{sl}^s at 90% C.L.. The black point corresponds to the SM value. For the purposes of illustration we have made the universality assumptions: $\Delta C_1^{s,uu}(M_W) = \Delta C_1^{s,cu}(M_W) = \Delta C_1^{s,uc}(M_W) = \Delta C_1^{s,cc}(M_W) = \Delta C_1^s(M_W)$ and similarly for $\Delta C_2^s(M_W)$.

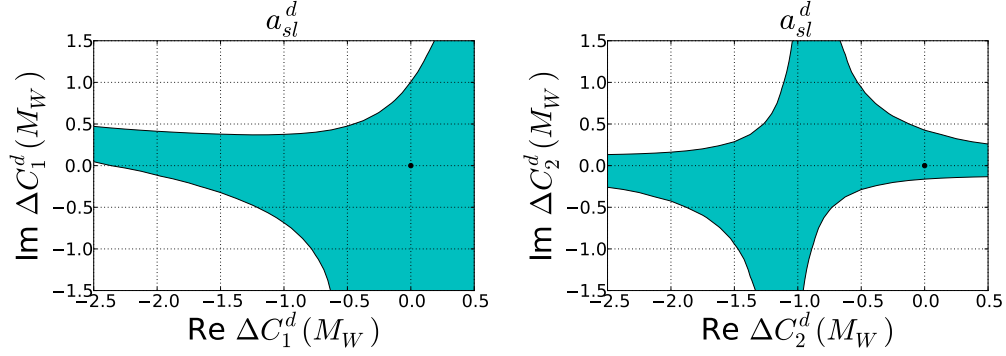


Figure 17: Potential regions for the NP contributions in $\Delta C_1^d(M_W)$ and $\Delta C_2^d(M_W)$ allowed by the semileptonic asymmetry a_{sl}^d at 90% C.L.. The black point corresponds to the SM value. For the purposes of illustration we have made the universality assumptions: $\Delta C_1^{d,uu}(M_W) = \Delta C_1^{d,cu}(M_W) = \Delta C_1^{d,uc}(M_W) = \Delta C_1^{d,cc}(M_W) = \Delta C_1^d(M_W)$ and similarly for $\Delta C_2^d(M_W)$.

SM, this quantity can be extracted with negligible uncertainties from $B \rightarrow DK$ tree-level decays [140–145]. This quantity is currently extensively tested by experiments, see e.g.[146, 147] and future measurements will dramatically improve its precision to the one degree level [148]. This observable is particular interesting since direct measurements, e.g. LHCb [146], seem to be larger than bounds from B-mixing [64]⁷.

$$\gamma^{\text{LHCb}} = (74.0^{+5.0}_{-5.8})^\circ, \quad (5.3)$$

$$\gamma^{\text{B-mixing}} \leq 66.9^\circ. \quad (5.4)$$

Therefore, in Sections 5.1 to 5.3 we combine our bounds from the $b \rightarrow u\bar{u}d$, $b \rightarrow c\bar{c}d$

⁷Similar observations were made in e.g.[149, 150].

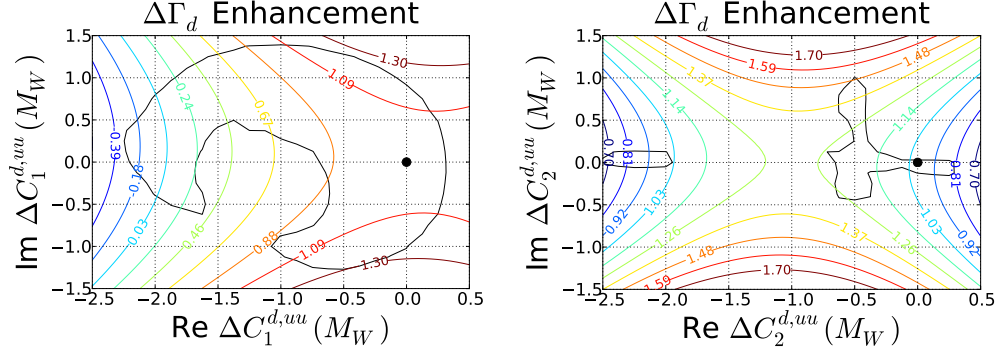


Figure 18: Global χ^2 -fit including observables constraining the inclusive transition $b \rightarrow u\bar{u}d$. The 90% C.L. allowed regions correspond to the areas contained within the black contours. The colored curves indicate the possible enhancements on $\Delta\Gamma_d$ with respect to the SM value. The black dot corresponds to the SM result.

and $b \rightarrow c\bar{c}d$ transitions, and evaluate the corresponding potential enhancement in $\Delta\Gamma_d$. We do not present the allowed regions for the NP contributions related to the channel $b \rightarrow u\bar{c}d$, since the bounds are expected to be rather weak considering that our only bound will arise from a_{sl}^d . In Section 5.4 we report the maximal bounds on $\Delta C_1(M_W)$ and $\Delta C_2(M_W)$, assuming universal BSM contributions to all different quark level decays. Hence, we combine all our possible bounds regardless of the quark level transition and asses the implications on the measurement of the CKM angle γ . The target of this part of analysis, is to update the investigations reported in [57] in the light of a far more detailed study of BSM effects in non-leptonic tree-level decays. In particular we account here for uncertainties neglected in the former study and we also make a very careful choice of reliable observables.

5.1 χ^2 -fit for the $b \rightarrow u\bar{u}d$ channel and bounds on $\Delta\Gamma_d$

We perform a combined χ^2 -fit including $R_{\pi\pi}$, $S_{\pi\pi}$, $S_{\rho\pi}$, $R_{\rho\rho}$ and a_{sl}^d with the aim of constraining $\Delta C_1^{d,uu}(M_W)$ and $\Delta C_2^{d,uu}(M_W)$. The resulting regions are shown in Fig. 18. $\Delta C_2^{d,uu}(M_W)$ is considerably stronger constrained than $\Delta C_1^{d,uu}(M_W)$, but sizeable deviations can still not be excluded. Due to the irregularity of the regions for $\Delta C_1^{d,uu}(M_W)$ and $\Delta C_2^{d,uu}(M_W)$, expressing the possible NP values for the tree level contributions in terms of simple inequalities is not possible. Instead, we limit ourselves to quote the minimum and maximum bounds for the real and the imaginary components of our NP regions. For $\Delta C_1^{d,uu}(M_W)$ we have

$$\begin{aligned} \left. \text{Re} \left[\Delta C_1^{d,uu}(M_W) \right] \right|_{\min} &= -2.23, \quad \left. \text{Im} \left[\Delta C_1^{d,uu}(M_W) \right] \right|_{\min} = -1.27, \\ \left. \text{Re} \left[\Delta C_1^{d,uu}(M_W) \right] \right|_{\max} &= 0.32, \quad \left. \text{Im} \left[\Delta C_1^{d,uu}(M_W) \right] \right|_{\max} = 1.40. \end{aligned} \tag{5.5}$$

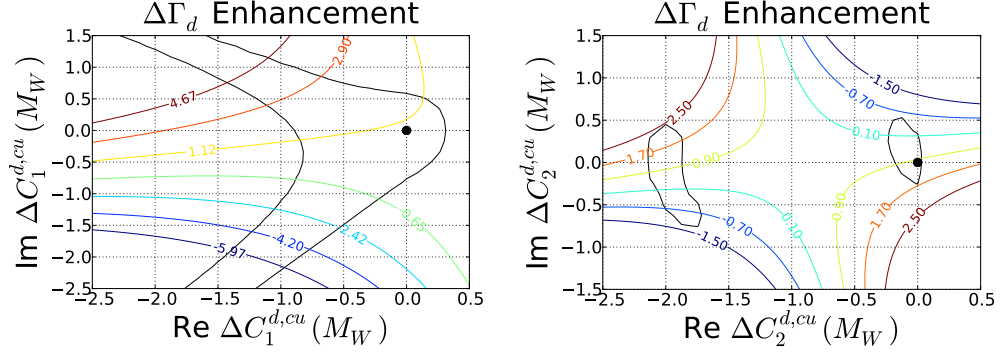


Figure 19: Global χ^2 -fit including observables constraining the inclusive transition $b \rightarrow c\bar{u}d$. The 90% C.L. allowed regions correspond to the areas contained within the black contours. The colored curves indicate the possible enhancements on $\Delta\Gamma_d$ with respect to the SM value. The black dot corresponds to the SM result.

On the other hand for $\Delta C_2^{d,uu}(M_W)$ we get

$$\begin{aligned} \text{Re} \left[\Delta C_2^{d,uu}(M_W) \right] \Big|_{\min} &= -2.5, \quad \text{Im} \left[\Delta C_2^{d,uu}(M_W) \right] \Big|_{\min} = -0.44, \\ \text{Re} \left[\Delta C_2^{d,uu}(M_W) \right] \Big|_{\max} &= 0.28, \quad \text{Im} \left[\Delta C_2^{d,uu}(M_W) \right] \Big|_{\max} = 1.00. \end{aligned} \quad (5.6)$$

We have also included the contour lines showing the potential enhancement of the observable $\Delta\Gamma_d$. Accounting for the uncertainties in theory and experiment we find the following 90% C.L. intervals for $\Delta\Gamma_d$ due to NP at tree level:

$$\begin{aligned} \text{for } \Delta C_1^{d,uu}(M_W): \quad & -0.39 < \Delta\Gamma_d/\Delta\Gamma_d^{\text{SM}} < 1.30, \\ \text{for } \Delta C_2^{d,uu}(M_W): \quad & 0.70 < \Delta\Gamma_d/\Delta\Gamma_d^{\text{SM}} < 1.48. \end{aligned} \quad (5.7)$$

Thus only moderate enhancements of $\Delta\Gamma_d$ seem to be possible, while a reduction to up to -39% of its SM values is still possible. This scenario could thus not be a solution for the dimuon asymmetry.

5.2 χ^2 -fit for the $b \rightarrow c\bar{u}d$ channel and bounds on $\Delta\Gamma_d$

To establish constraints on $\Delta C_1^{d,cu}(M_W)$ and $\Delta C_2^{d,cu}(M_W)$ we combine $R_{D^*\pi}$ together with a_{sl}^d . Our results are presented in Fig. 19. At the 90% C.L. we find the possibility of huge enhancements/reductions of $\Delta\Gamma_d$:

$$\begin{aligned} \text{for } \Delta C_1^{d,cu}(M_W): \quad & -5.97 < \Delta\Gamma_d/\Delta\Gamma_d^{\text{SM}} < 4.67, \\ \text{for } \Delta C_2^{d,cu}(M_W): \quad & -1.5 < \Delta\Gamma_d/\Delta\Gamma_d^{\text{SM}} < 2.50. \end{aligned} \quad (5.8)$$

Based on the bounds shown in Eq. (5.8), we find that this scenario could solve the dimuon asymmetry. Since the experimental bounds for $\Delta\Gamma_d$ are saturated in the case

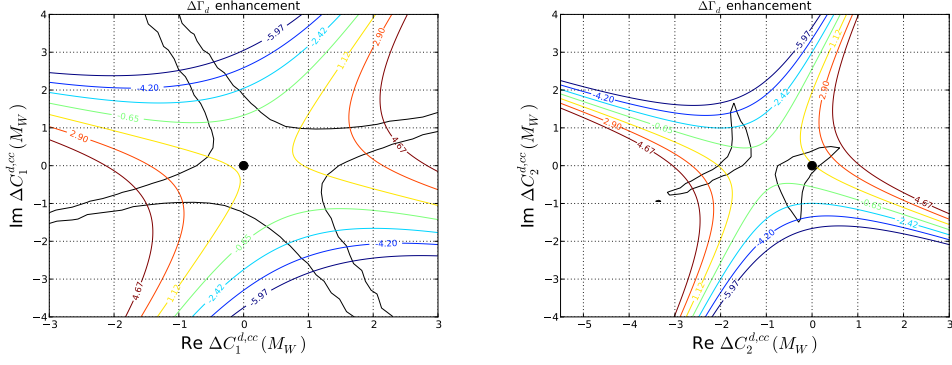


Figure 20: Global χ^2 -fit including observables constraining the inclusive transition $b \rightarrow c\bar{c}d$. The 90% C.L. allowed regions correspond to the areas contained within the black contours. The colored curves indicate the possible enhancements on $\Delta\Gamma_d$ with respect to the SM value. The black dot corresponds to the SM result.

of $\Delta C_1^{d,cu}(M_W)$ in Eq. (5.8), it turns out that $\Delta\Gamma_d$ acts as a constraint in itself. Using this additional information we establish the following bounds for $\Delta C_1^{d,cu}(M_W)$

$$\begin{aligned} \left. \text{Re} \left[\Delta C_1^{d,cu}(M_W) \right] \right|_{\min} &= -1.40, \quad \left. \text{Im} \left[\Delta C_1^{d,cu}(M_W) \right] \right|_{\min} = -2.17, \\ \left. \text{Re} \left[\Delta C_1^{d,cu}(M_W) \right] \right|_{\max} &= 0.32, \quad \left. \text{Im} \left[\Delta C_1^{d,cu}(M_W) \right] \right|_{\max} = 1.15. \end{aligned} \quad (5.9)$$

The corresponding bounds for $\Delta C_2^{d,cu}(M_W)$ read

$$\begin{aligned} \left. \text{Re} \left[\Delta C_2^{d,cu}(M_W) \right] \right|_{\min} &= -2.14, \quad \left. \text{Im} \left[\Delta C_2^{d,cu}(M_W) \right] \right|_{\min} = -0.75, \\ \left. \text{Re} \left[\Delta C_2^{d,cu}(M_W) \right] \right|_{\max} &= 0.04, \quad \left. \text{Im} \left[\Delta C_2^{d,cu}(M_W) \right] \right|_{\max} = 0.53. \end{aligned} \quad (5.10)$$

5.3 χ^2 -fit for the $b \rightarrow c\bar{c}d$ channel and bounds on $\Delta\Gamma_d$

Next we perform a χ^2 -fit including $\mathcal{B}r(B \rightarrow X_d \gamma)$, a_{sl}^d and $\sin(2\beta_d)$. These observables give strong constraints for $\Delta C_2^{d,cc}(M_W)$ (see Fig. 20), which turn out to saturate the current experimental bounds on $\Delta\Gamma_d$. At the 90% C.L. we find

$$\text{for } \Delta C_1^{d,cc}(M_W) \text{ and } \Delta C_2^{d,cc}(M_W): \quad -5.97 < \Delta\Gamma_d / \Delta\Gamma_d^{\text{SM}} < 4.67. \quad (5.11)$$

We find again that this scenario could solve the tension between theory and experiment found in the measurement of the dimuon asymmetry. Considering the results shown in

Fig. 20 we see that $\Delta\Gamma_d$ is indeed a powerful constraint for $\Delta C_1^{d,cc}(M_W)$ and $\Delta C_2^{d,cc}(M_W)$, which together with $\mathcal{B}r(B \rightarrow X_d\gamma)$, a_{sl}^d and $\sin(2\beta_d)$ defines the following limits

$$\begin{aligned} \left. \text{Re} \left[\Delta C_1^{d,cc}(M_W) \right] \right|_{\min} &= -1.66, \quad \left. \text{Im} \left[\Delta C_1^{d,cc}(M_W) \right] \right|_{\min} = -2.80, \\ \left. \text{Re} \left[\Delta C_1^{d,cc}(M_W) \right] \right|_{\max} &= 2.36, \quad \left. \text{Im} \left[\Delta C_1^{d,cc}(M_W) \right] \right|_{\max} = 2.74, \end{aligned} \quad (5.12)$$

and

$$\begin{aligned} \left. \text{Re} \left[\Delta C_2^{d,cc}(M_W) \right] \right|_{\min} &= -2.70, \quad \left. \text{Im} \left[\Delta C_2^{d,cc}(M_W) \right] \right|_{\min} = -1.46, \\ \left. \text{Re} \left[\Delta C_2^{d,cc}(M_W) \right] \right|_{\max} &= 0.58, \quad \left. \text{Im} \left[\Delta C_2^{d,cc}(M_W) \right] \right|_{\max} = 1.65. \end{aligned} \quad (5.13)$$

As can be seen on the l.h.s. of Fig. 20 $\Delta C_1^{d,cc}(M_W)$ is only weakly constrained by the semi-leptonic CP asymmetries, here additional information stemming from $\Delta\Gamma_d$ will be important to shrink the allowed regions.

5.4 Universal fit on $\Delta C_1(M_W)$ and $\Delta C_2(M_W)$

In this section we work under the assumptions

$$\Delta C_1^{s,ab}(M_W) = \Delta C_1^{d,ab}(M_W) = \Delta C_1(M_W) \quad (5.14)$$

$$\Delta C_2^{s,ab}(M_W) = \Delta C_2^{d,ab}(M_W) = \Delta C_2(M_W) \quad (5.15)$$

for $a = u, d$ and $b = u, d$. This procedure allows us to obtain the maximal constraints for our NP contributions. Making a combined χ^2 -fit is time and resource consuming, consequently we select the set of observables that give the strongest possible bounds. For $\Delta C_1(M_W)$ this includes: $R_{D^*\pi}$, $S_{\rho\pi}$, $\Delta\Gamma_s$, $\mathcal{B}r(\bar{B} \rightarrow X_s\gamma)$ and a_{sl}^d and for $\Delta C_2(M_W)$ we use: $R_{D^*\pi}$, $R_{\pi\pi}$, $\Delta\Gamma_s$, $S_{J/\psi\phi}$ and τ_{B_s}/τ_{B_d} . We show in Fig. 21 our resulting regions from which we extract

$$\begin{aligned} \left. \text{Re} \left[\Delta C_1(M_W) \right] \right|_{\min} &= -0.36, \quad \left. \text{Im} \left[\Delta C_1(M_W) \right] \right|_{\min} = -0.47, \\ \left. \text{Re} \left[\Delta C_1(M_W) \right] \right|_{\max} &= 0.26, \quad \left. \text{Im} \left[\Delta C_1(M_W) \right] \right|_{\max} = 0.45, \end{aligned} \quad (5.16)$$

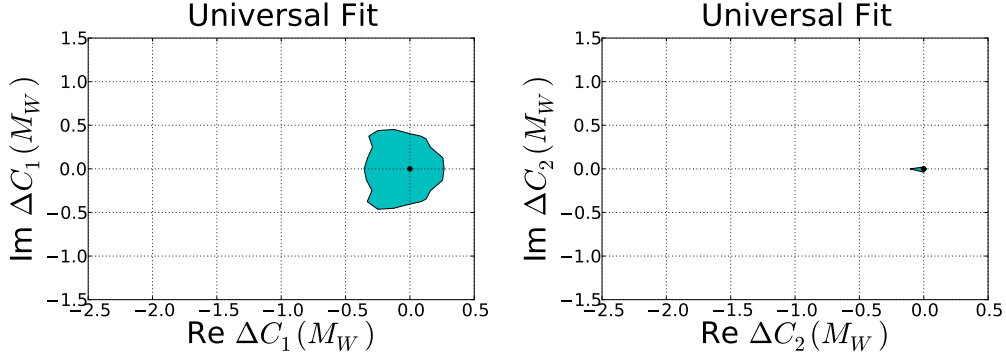


Figure 21: Potential regions for the NP contributions $\Delta C_1(M_W)$ and $\Delta C_2(M_W)$ allowed by the observables used in our analysis at 90% C.L. assuming universal NP contributions. The black dot corresponds to the SM result.

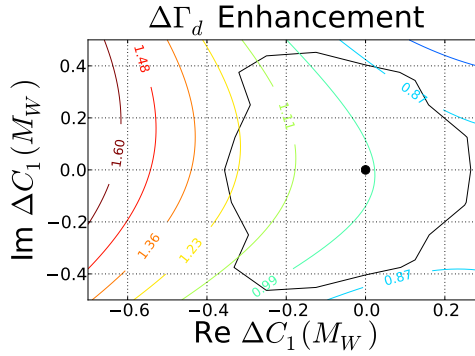


Figure 22: Enhancements on $\Delta\Gamma_d$ when assuming universal NP effects in $C_1(M_W)$. The black dot corresponds to the SM result.

and

$$\begin{aligned}
 \left. \text{Re} [\Delta C_2(M_W)] \right|_{\min} &= -0.11, \quad \left. \text{Im} [\Delta C_2(M_W)] \right|_{\min} = -0.04, \\
 \left. \text{Re} [\Delta C_2(M_W)] \right|_{\max} &= 0.02, \quad \left. \text{Im} [\Delta C_2(M_W)] \right|_{\max} = 0.02.
 \end{aligned} \tag{5.17}$$

We can see from Eqs. (5.16) and (5.17) how severely constrained is $\Delta C_2(M_W)$ allowing deviations with respect to the SM point of a few percent at most. This behaviour is clearly in contrast with the results obtained for $\Delta C_1(M_W)$, where effects of almost up to ± 0.5 are still possible. For completeness we present the implications of universal NP in $\Delta C_1(M_W)$ on $\Delta\Gamma_d$ in Fig. 22. We find that at 90% C.L. only $\mathcal{O}(20\%)$ deviations on $\Delta\Gamma_d$ with respect to its SM value can be induced, which is in a similar ballpark as the SM uncertainties of $\Delta\Gamma_d$ and can clearly not explain the D0 measurement of the dimuon asymmetry.

5.5 NP in non-leptonic tree-level decays and its interplay with the CKM angle γ

As is well known [140–145] the CKM phase γ can be determined from the interference of the transition amplitudes associated with the quark tree level decays $b \rightarrow c\bar{u}s$ and $b \rightarrow u\bar{c}s$ with negligible theory uncertainty within the SM [151]⁸. At the exclusive level, this can be done with the decay channels $B^- \rightarrow D^0 K^-$ and $B^- \rightarrow \bar{D}^0 K^-$. The ratio of the two corresponding decay amplitudes can be written as

$$r_B e^{i(\delta_B - \gamma)} = \frac{\mathcal{A}(B^- \rightarrow \bar{D}^0 K^-)}{\mathcal{A}(B^- \rightarrow D^0 K^-)}, \quad (5.18)$$

where the r_B stands for the ratio of the modulus of the relevant amplitudes. The resulting phase has a strong component, denoted as δ_B , and a weak one, which is precisely CKM γ . New effects in C_1 and C_2 can lead to huge shifts in γ . To study this possibility we follow [152] and assume universal NP in C_1 and C_2 . Thus $\Delta C_1^{s,uc} = \Delta C_1^{s,cu}$ and $\Delta C_2^{s,uc} = \Delta C_2^{s,cu}$. Then, the left side of Eq. (5.18) will be modified according to [57]

$$r_B e^{i(\delta_B - \gamma)} \rightarrow r_B e^{i(\delta_B - \gamma)} \cdot \left[\frac{C_2 + \Delta C_2 + r_{A'}(C_1 + \Delta C_1)}{C_2 + r_{A'} C_1} \cdot \frac{C_2 + r_A C_1}{C_2 + \Delta C_2 + r_A(C_1 + \Delta C_1)} \right], \quad (5.19)$$

where

$$r_{A'} = \frac{\langle \bar{D}^0 K^- | Q_1^{\bar{u}cs} | B^- \rangle}{\langle \bar{D}^0 K^- | Q_2^{\bar{u}cs} | B^- \rangle}, \quad r_A = \frac{\langle D^0 K^- | Q_1^{\bar{c}us} | B^- \rangle}{\langle D^0 K^- | Q_2^{\bar{c}us} | B^- \rangle}. \quad (5.20)$$

The ratios of matrix elements in Eq. (5.20) have not been determined from first principles, to provide an estimation we use naive factorization arguments and colour counting to obtain [57],[152]

$$r_A = 0.4, \quad r_A - r_{A'} = -0.6. \quad (5.21)$$

Eq.(5.19) gives a particularly strong dependence of the shift in γ on the imaginary part of C_1 ; approximately we get [57]

$$\delta\gamma = (r_A - r_{A'}) \frac{\text{Im}[\Delta C_1]}{C_2}. \quad (5.22)$$

We are now ready to update the study presented in [57] on the effects of NP in C_1 and C_2 on the precision for the determination of the CKM angle γ , our results are presented graphically in Fig. 23. On the left hand side of Fig. 23 we can see how for the values

⁸Due to the absence of penguins and the fact that the relevant hadronic matrix elements cancel, the extraction of CKM γ is extremely clean. The irreducible theoretical uncertainty is due to higher-order electroweak corrections and has been found to be negligible. For instance, when the modes $B \rightarrow DK$ are used the correction effect is $|\delta\gamma/\gamma| < \mathcal{O}(10^{-7})$ [151]. On the other hand, if CKM γ is obtained using $B \rightarrow D\pi$ decays instead, then $|\delta\gamma/\gamma| < \mathcal{O}(10^{-4})$ [152].

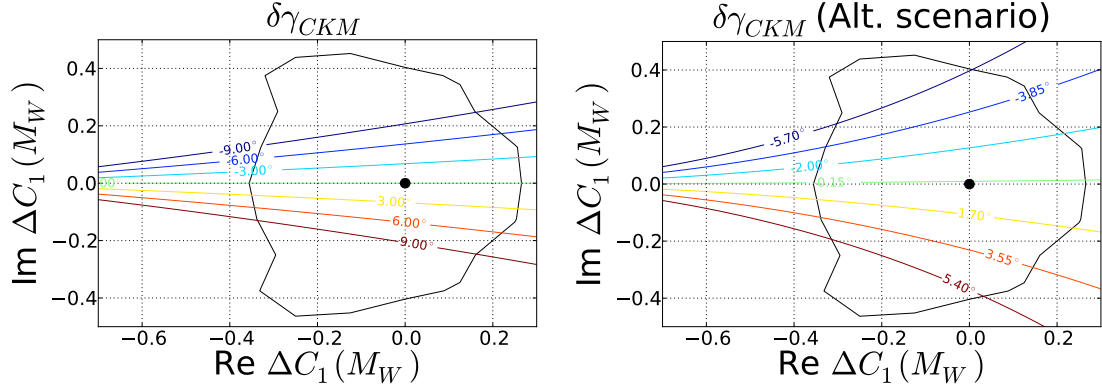


Figure 23: Possible deviations on the CKM phase γ due to NP at tree level in $C_1(M_W)$ assuming $r_A = 0.4$ (left) and $r_A = 0.8$ (right). In both cases we have considered $r'_A = 1$. The black dot corresponds to the SM result.

of r_A and r'_A shown in Eq. (5.21), the current uncertainties in our knowledge of C_1 seem to indicate an uncertainty in the extraction of the CKM angle γ of considerably more than 10° . This is much higher than the current experimental uncertainty of around five degrees [146, 147]. Interestingly direct measurements give typically larger values than the ones obtained by CKM fits [153, 154] or extracted from B-mixing [64]. Even more interestingly, future measurements will dramatically improve the precision of γ to the one degree level [148] and our BSM approach would offer a possibility of explaining large deviations in the extraction of the CKM angle γ . We would like, however, to add some words of cautions: for a quantitative reliable relation between the deviations of C_1 and the shifts in the CKM angle γ , the non-perturbative parameter r_A and $r_{A'}$ have to be known more precisely. The values proposed in Eq. (5.21) correspond to an educated ansatz. We can explore the effects of modifying these values on CKM- γ . For instance, consider an alternative scenario where r_A is twice the value presented in Eq. (5.21), while r'_A remains fixed. This is equivalent to assigning an uncertainty of 100% to r_A and taking the upper limit. The results for this new scenario are presented on the right hand side of Fig. 23, where the shifts $\delta\gamma_{CKM}$ have been halved with respect to those found on the left hand side of the same figure, however the absolute numerical values of about $\pm 5^\circ$, still represent huge effects on the CKM angle γ itself.

Here clearly more theoretical work leading to a more precise understanding of r_A and $r_{A'}$ is highly desirable.

6 Future prospects

In this section we will present projections for observables, that are particularly promising to further shrink the allowed regions of NP contributions to non-leptonic tree-level decays. We have already studied the impact of BSM effects in non-leptonic tree-level decays on the observables $\Delta\Gamma_d$ and the CKM angle γ in detail. More precise experimental data on $\Delta\Gamma_d$

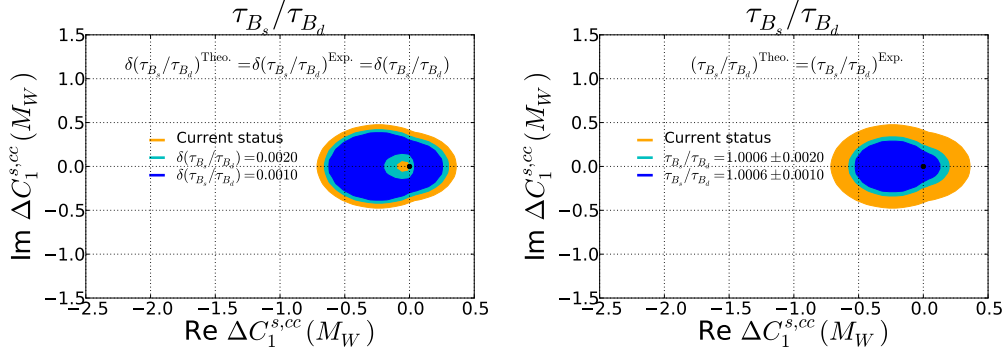


Figure 24: Future scenarios concerning the behaviour of τ_{B_s}/τ_{B_d} . In the left panel the central experimental value of the lifetime ratio is assumed to remain unchanged in the future whereas the uncertainties will be reduced. In the right panel, the theoretical and experimental values for the lifetime ratio are supposed to become equal. The black dot corresponds to the SM result.

will immediately lead to stronger bounds on the $\Delta B = 1$ Wilson coefficients, it could also exclude the possibility of solving the D0 dimuon asymmetry with an enlarged value of $\Delta\Gamma_d$. Alternatively, if the measured values of $\Delta\Gamma_d$ will not be SM-like, we could get an intriguing hint for BSM physics. In order to make use of the extreme sensitivity of the CKM angle γ on an imaginary part of C_1 more theory work is required to make this relation quantitatively reliable. If this is available, then already the current experimental uncertainty on γ will exclude a large part of the allowed region on ΔC_1 - or it will indicate the existence of NP effects. Below we will show projections for improved experimental values on the lifetime ratio τ_{B_s}/τ_{B_d} and the semi-leptonic CP asymmetries, as well as commenting on consequences of our BSM approach to the recently observed flavour anomalies.

6.1 τ_{B_s}/τ_{B_d}

As already explained, the lifetime ratio τ_{B_s}/τ_{B_d} can pose very strong constraints on the Wilson coefficients C_1 and C_2 , if we e.g. assume that BSM effects are only acting in the $b \rightarrow c\bar{c}s$ channel. In Fig. 24 we show future projections, assuming the errors will go down to 2 per mille or even one per mille. On the l.h.s. of Fig. 24 we assume that the current experiment value will stay - in this case a tension between the SM value and the experimental measurement will emerge. On the r.h.s. of Fig. 24 we assume that the future experimental value perfectly agrees with the SM prediction.

6.2 Semi-leptonic CP asymmetries

The experimental precision for the semi-leptonic CP asymmetries is still much larger than the tiny SM values for these quantities. Nevertheless already at this stage a_{sl}^q provide important bounds on possible BSM effects in the Wilson coefficients. The experimental precision in the semi-leptonic CP-asymmetries will rise considerable in the near future, see

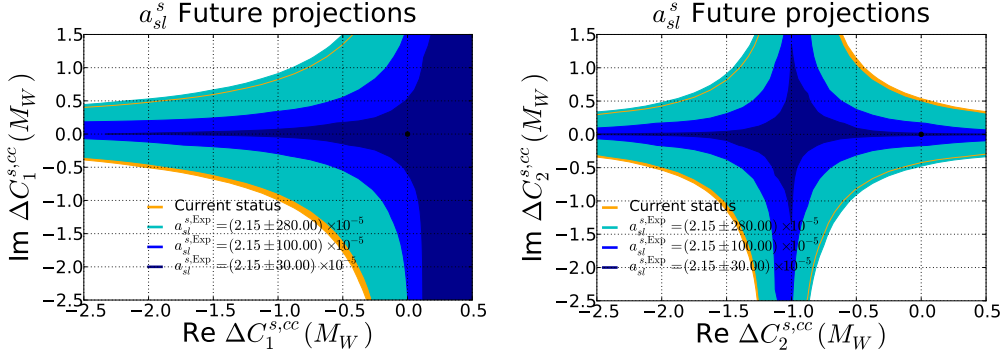


Figure 25: Future scenarios for the precision in the observable a_{sl}^s and resulting constraints on ΔC_1 and ΔC_2 . The current uncertainty is expected to be reduced down to 1 per mille and later even to 0.3 per mille.

e.g. Table 1 of [155] from where we take:

$$\delta(a_{sl}^s) = 1 \cdot 10^{-3} \quad \text{LHCb 2025} \quad (6.1)$$

$$\delta(a_{sl}^s) = 3 \cdot 10^{-4} \quad \text{Upgrade II} \quad (6.2)$$

We show the dramatic impact of these future projections on the BSM bounds on the Wilson coefficients in Fig. 25.

6.3 Rare decays

As discussed in [58, 60] NP effects in the $b \rightarrow c\bar{c}s$ transitions can induce shifts in the Wilson coefficient of the operator

$$\hat{Q}_{9V} = \frac{\alpha}{4\pi} (\bar{s}_L \gamma_\mu \hat{b}_L) (\bar{\ell} \gamma^\mu \hat{\ell}), \quad (6.3)$$

leading to

$$\Delta C_9^{\text{eff}} \Big|_{\mu=m_b} = \left[8.48 \Delta C_1 + 1.96 \Delta C_2 \right] \Big|_{\mu=M_W}. \quad (6.4)$$

This result offers an interesting link with the anomalous deviations in observables associated with the decay $B \rightarrow K^{(*)} \mu^+ \mu^-$, where model independent explanations with physics only in C_9 require $\Delta C_9^{\text{eff}} \Big|_{\mu=m_b} = -\mathcal{O}(1)$. In order to account for NP phases we use the results presented in [156] where ΔC_9 is allowed to take complex values leading to the constraints shown in Fig. 26. Here both C_1 and C_2 get a shift towards negative values. BSM in effects in non-leptonic tree-level can in principle explain the deviations seen in lepton-flavour universal observables, like the branching ratios or P_5' ; they can, however, not explain the anomalous values of lepton flavour universality violating observables like R_K . Future measurements will show, whether the bounds, obtained in Fig. 26 should be included in our full fit.

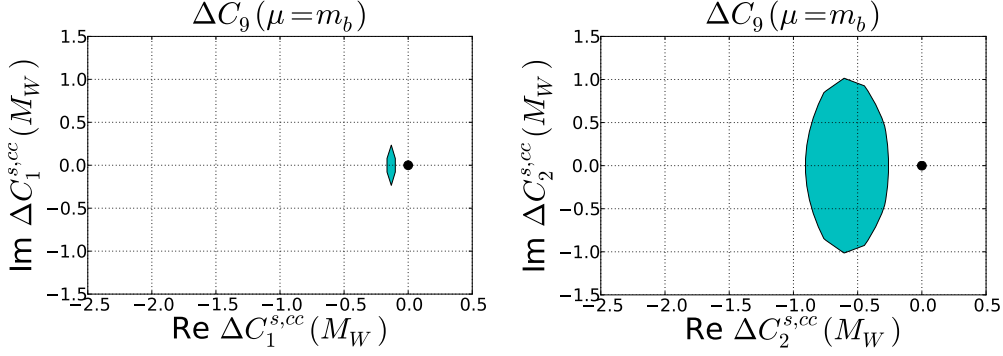


Figure 26: Regions for NP, at 90% C. L., in the $\text{Re } \Delta C_1^{s,cc}$ - $\text{Im } \Delta C_1^{s,cc}$ (left) and $\text{Re } \Delta C_2^{s,cc}$ - $\text{Im } \Delta C_2^{s,cc}$ (right) planes allowed by the B physics anomalies related with the decay $B \rightarrow K^{(*)}\mu^+\mu^-$. The black dot corresponds to the SM result.

7 Conclusions and outlook

In this work we have questioned the well accepted assumption of having no NP in tree level decays, in particular we explored for possible deviations with respect to the SM values in the dimension six current-current operators \hat{Q}_1 (colour suppressed) and \hat{Q}_2 (colour allowed) associated with the quark level transitions $b \rightarrow q\bar{q}'s$ and $b \rightarrow q\bar{q}'d$ ($q, q' = u, c$). We evaluated the size of the NP effects by modifying the corresponding Wilson coefficients according to $C_1 \rightarrow C_1 + \Delta C_1$, $C_2 \rightarrow C_2 + \Delta C_2$, for $\Delta C_{1,2} \in \mathcal{C}$; we found that sizeable deviations in $\Delta C_{1,2}$ are not ruled out by the recent experimental data.

Our analysis was based on a χ^2 -fit where we included different B-physics observables involving the decay processes: $\bar{B}_d^0 \rightarrow D^*\pi$, $\bar{B}_d^0 \rightarrow \pi\pi$, $\bar{B}_d^0 \rightarrow \pi\rho$, $\bar{B}_d^0 \rightarrow \rho\rho$, $\bar{B} \rightarrow X_s\gamma$, $\bar{B}_s \rightarrow J/\psi\phi$ and $\bar{B} \rightarrow X_d\gamma$. We also considered neutral B mixing observables: the semi-leptonic asymmetries a_{sl}^s and a_{sl}^d as well as the decay width difference $\Delta\Gamma_s$ of B_s^0 oscillations and the lifetime ratio of B_s and B_d mesons. Finally we also studied the CKM angles β , β_s and γ . For the amplitudes of the hadronic transitions $\bar{B}_d^0 \rightarrow D^*\pi$, $\bar{B}_d^0 \rightarrow \pi\pi$, $\bar{B}_d^0 \rightarrow \pi\rho$ and $\bar{B}_d^0 \rightarrow \rho\rho$ and $\bar{B}_s \rightarrow J/\psi\phi$ we used the formulas calculated within the QCD factorization framework. We have identified a high sensitivity on $\Delta C_{1,2}$ with respect to the power corrections arising in the annihilation topologies and in some cases in those for the hard-spectator scattering as well. It is also important to mention that the uncertainty in the parameter λ_B used to describe the inverse moment of the light cone distribution for the neutral B mesons is of special importance in defining the size of ΔC_1 and ΔC_2 . For the mixing observables and the lifetime ratios we have benefited from the enormous progress achieved in the precision of the hadronic input parameters, thus we have also updated the corresponding SM predictions:

$$\begin{aligned} \Delta M_s &= (18.77 \pm 0.86) \text{ ps}^{-1}, \quad \Delta M_d = (0.543 \pm 0.029) \text{ ps}^{-1}, \\ \Delta\Gamma_s &= (9.1 \pm 1.3) \cdot 10^{-2} \text{ ps}^{-1}, \quad \Delta\Gamma_d = (2.6 \pm 0.4) \cdot 10^{-3} \text{ ps}^{-1}, \\ a_{sl}^s &= (2.06 \pm 0.18) \cdot 10^{-5}, \quad a_{sl}^d = (-4.73 \pm 0.42) \cdot 10^{-4}. \end{aligned} \quad (7.1)$$

We have made a channel by channel study by combining different constraints for the decay chains $b \rightarrow u\bar{u}d$, $b \rightarrow c\bar{u}d$, $b \rightarrow c\bar{c}s$ and $b \rightarrow c\bar{c}d$; we also performed a universal χ^2 -fit where we have included observables mediated by $b \rightarrow qq's$ decays as well. The universal χ^2 -fit provides the strongest bounds on the NP deviations, we found that

$$|\text{Re}(\Delta C_1)| \leq \mathcal{O}(0.4), \quad |\text{Re}(\Delta C_2)| \leq \mathcal{O}(0.1), \quad (7.2)$$

$$|\text{Im}(\Delta C_1)| \leq \mathcal{O}(0.5), \quad |\text{Im}(\Delta C_2)| \leq \mathcal{O}(0.04), \quad (7.3)$$

whereas for the independent channel analyses the corresponding deviations can much larger. We have analysed the implications of having NP in tree level b quark transitions on the decay width difference of neutral B_d^0 mixing $\Delta\Gamma_d$ - note, that the most recent experimental average is still consistent with zero. We found that enhancements in $\Delta\Gamma_d$ with respect to its SM value of up to a factor of five are consistent with the current experimental data. Such a huge enhancement could solve the tension between experiment and theory in the $D0$ measurement for the dimuon asymmetry. Thus we strongly encourage further experimental efforts to measure $\Delta\Gamma_d$, see also [157].

Next we evaluated the impact of our allowed NP regions for ΔC_1 and ΔC_2 on the determination of the CKM phase γ , where the absence of penguins leads in principle to an exceptional theoretical cleanness. We found that γ is highly sensitive to the imaginary components of ΔC_1 and ΔC_2 and our BSM effects could lead to deviations in this quantity by up to 10° . It has to be stressed, however, that for quantitative statements about the size of the shift $\delta\gamma$ the ratios of the matrix elements $\langle \bar{D}^0 K^- | Q_1^{\bar{u}cs} | B^- \rangle / \langle \bar{D}^0 K^- | Q_2^{\bar{u}cs} | B^- \rangle$ and $\langle D^0 K^- | Q_1^{\bar{c}us} | B^- \rangle / \langle D^0 K^- | Q_2^{\bar{c}us} | B^- \rangle$ have to be determined in future with more reliable methods. So far only naive estimates are available for these ratios.

Finally we studied future projections for observables that will shrink the allowed region for NP effects - or identify a BSM region - in non-leptonic tree-level decays. Here $\tau(B_s)/\tau(B_d)$ and the semi-leptonic CP asymmetries seem to be very promising.

Acknowledgements

We would like to thank Martin Wiebusch for collaborating at early stages of the project. This work benefited from physics discussions with Christoph Bobeth, Tobias Huber, Joachim Brod, Leonardo Vernazza, Michael Spannowsky, Marco Gersabeck, Thomas Rauh, Marcel Merk, Niels Tuning, Patrick Koppenburg and Laurent Dufour. We acknowledge Luiz Vale for his help with CKM-Fitter Live. We thank to Bert Schellekens for his help and support in accessing the Nikhef computing cluster “Stoomboot” during the development of this project and to Patrick Koppenburg for supporting the access in the final stages of the project as well. GTX acknowledges support from the NWO program 156, “Higgs as Probe and Portal” and by the Deutsche Forschungsgemeinschaft (DFG, German Research Foundation) under grant 396021762 - TRR 257. The work of AL was supported by STFC via the IPPP grant.

A Numerical Inputs

In this section we collect the numerical values of the input parameter used in this work.

Parameter	Value	Unit	Ref.	Parameter	Value	Unit	Ref.
Lepton masses, gauge boson masses and couplings							
m_μ	$0.1056583745(24)$	GeV	[116]	G_F	$1.1663787(6) \cdot 10^{-5}$	GeV^{-2}	[116]
m_τ	$1.77686(12)$	GeV	[116]	$\alpha_s(M_Z)$	0.1181 ± 0.0011		[116]
M_Z	$91.1876(21)$	GeV	[116]	α	$7.2973525664(17) \cdot 10^{-3}$		[116]
M_W	$80.379(12)$	GeV	[116]	Λ_5^{QCD}	0.210 ± 0.014	GeV	[116]
				\hbar	$6.582119514(40) \cdot 10^{-25}$	GeV s	[116]
CKM							
$ V_{us} $	$0.224746^{+0.000253}_{-0.000058}$			γ	$(65.17^{+0.26}_{-3.05})^\circ$		
$ V_{cb} $	$0.04243^{+0.00036}_{-0.00088}$			$\sin(2\beta)_{dir.}$	0.699 ± 0.017		[111]
$ V_{ub}/V_{cb} $	0.08833 ± 0.00218			$\sin(2\beta)_{indir.}$	0.732 ± 0.029		
Quark masses							
m_d	$0.00467^{+0.00048}_{-0.00017}$	GeV	[116]	m_b^{1S}	4.65 ± 0.03	GeV	[116]
$m_s(2 \text{ GeV})$	$0.093^{+0.011}_{-0.005}$	GeV	[116]	m_t^{pole}	173.1 ± 0.9	GeV	[116, 158]
$\bar{m}_c(\bar{m}_c)$	1.27 ± 0.02	GeV	[116]	$\bar{m}_t(\bar{m}_t)$	163.3 ± 0.9	GeV	
$\bar{m}_c(\bar{m}_b)$	0.96 ± 0.02	GeV		$m_t(m_W)$	172.6 ± 1.0	GeV	
$\bar{m}_b(\bar{m}_b)$	$4.214^{+0.042}_{-0.043}$	GeV	[159]				
m_b^{pole}	4.61 ± 0.05	GeV					

Table 17: Values of the input parameters used for our numerical evaluations.

Using the PDG value for the strong coupling

$$\alpha_s(M_Z) = 0.1181 \pm 0.0011 \quad (\text{A.1})$$

we derive with $M_Z = 91.1876 \pm 0.0021 \text{ GeV}$ at NLO-QCD

$$\Lambda_{QCD}^{(5)} = 228 \pm 14 \text{ MeV} , \quad (\text{A.2})$$

while PDG gives

$$\Lambda_{QCD}^{(5)} = 210 \pm 14 \text{ MeV} , \quad (\text{A.3})$$

using 4-loop running, 3-loop matching. We decided to use the latter value, the effects on $\alpha_s(m_b)$ are very small.

For quark masses we use the PDG values in the $\overline{\text{MS}}$ definition, except for the b-quark, where we use a more conservative determination. The PDG value reads for comparison

$$m_b(m_b) = 4.18^{+0.04}_{-0.03} \text{ GeV} \quad (\text{A.4})$$

The PDG value for $m_c(m_c)$ correspond to $m_c(m_b) = 0.947514$, which will be used ⁹ for the analysis of the mixing quantities $\Delta\Gamma_q$ and a_{sl}^q .

For the top quark pole mass we use the result obtained from cross-section measurements given in [116]

$$m_t^{\text{Pole}} = 173.1 \pm 0.9 \text{ GeV} \quad (\text{A.5})$$

⁹Actually $\bar{z} := m_c^2(m_b)/m_b^2(m_b) = 0.0505571$ is used.

Parameter	Value	Unit	Ref.	Parameter	Value	Unit	Ref.
<i>B</i>- and light meson properties (cont.)							
m_{B^+}	5279.33(13)	MeV	[116]	a_1^π	0.0		[160, 161]
m_{B_d}	5279.64(13)	MeV	[116]	a_2^π	0.17 ± 0.10		[161]
m_{B_s}	5366.88(17)	MeV	[116]	a_1^ρ	0.0		[162]
m_{π^+}	139.57061(24)	MeV	[116]	$a_{1\perp}^\rho$	0.0		[162]
m_{π^0}	134.9770(5)	MeV	[116]	a_2^ρ	0.1 ± 0.3		[20]
m_{ρ^+}	775.11 ± 0.34	MeV	[116]	$a_{2\perp}^\rho$	0.11 ± 0.05		[162, 163]
m_ω	782.65 ± 0.12	MeV	[116]	$a_{1 }^\phi$	0		[164]
$m_{D^{*+}}$	2010.26 ± 0.05	MeV	[116]	$a_{2 }^\phi$	0 ± 0.1		[164]
m_{K^0}	497.611 ± 0.013	MeV	[116]	B_3^s/B_1^s	1.006 ± 0.066		
$f_{B_{u,d}}$	190.0 ± 1.3	MeV	[165]	$B_{R_0}^s/B_1^s$	0.377 ± 0.154		
$f_{B_d}^2 B_1^d$	(0.0305 ± 0.0011)	GeV ²		$B_{R_1}^s/B_1^s$	1.193 ± 0.052		
$f_{B_s}^2 B_1^s$	(0.0452 ± 0.0014)	GeV ²		$B_{R_2}^s/B_1^s$	0.318 ± 0.118		
f_π	130.2 ± 0.8	MeV	[165]	$B_{R_3}^s/B_1^s$	0.389 ± 0.130		
f_ρ	216 ± 3	MeV	[107, 166]	$B_{R_1}^s/B_1^s$	1.130 ± 0.047		
f_ρ^\perp (1 GeV)	165 ± 9	MeV	[162, 166]				
f_ω	195 ± 3	MeV	[167]	B_3^d/B_1^d	0.928 ± 0.072		
f_{D^*}	223.5 ± 8.4	MeV	[168]	$B_{R_0}^d/B_1^d$	0.383 ± 0.156		
$F_+^{B \rightarrow \pi}(0)$	0.261 ± 0.023		[117, 169]	$B_{R_1}^d/B_1^d$	1.190 ± 0.060		
$A_0^{B \rightarrow \rho}(0)$	0.36 ± 0.04		[170]	$B_{R_2}^d/B_1^d$	0.323 ± 0.120		
$A_0^{B \rightarrow D^*}$	0.66 ± 0.02		[171, 172]	$B_{R_3}^d/B_1^d$	0.395 ± 0.132		
$A_0^{B \rightarrow \phi}(m_{J/\psi}^2)$	0.68 ± 0.07		[170]	$B_{R_1}^d/B_1^d$	1.190 ± 0.060		
$A_1^{B \rightarrow \phi}(m_{J/\psi}^2)$	0.37 ± 0.04		[170]				
$A_2^{B \rightarrow \phi}(m_{J/\psi}^2)$	0.40 ± 0.14		[170]	$\tau(B_s^0)$	1.509 ± 0.004	ps	[111]
$V_2^{B \rightarrow \phi}(m_{J/\psi}^2)$	0.70 ± 0.06		[170]	$\tau(B_d^0)$	1.520 ± 0.004	ps	[111]
Λ_h	500	MeV	[20]	Γ_ω	8.49 ± 0.08	MeV	[116]
λ_B	400 ± 150	MeV	[107]	Γ_ρ	149.5 ± 1.3	MeV	[116]

Table 18: Values of the input parameters used for our numerical evaluations (cont.).

which is an average including measurements from D0, ATLAS and CMS. Entering Eq. A.5 in the version 3 of the software RunDec [173] we obtain

$$\bar{m}_t(\bar{m}_t) = 163.3 \pm 0.9 \text{ GeV}, \quad (\text{A.6})$$

and

$$m_t(M_W) = 172.6 \pm 1.0 \text{ GeV}. \quad (\text{A.7})$$

We use the averages of the B mixing bag parameters obtained in [65] based on the HQET

sum rule calculations in [82, 90, 91, 174] and the corresponding lattice studies in [175–179]:

$$\begin{aligned}
B_1^s(\mu_b) &= 0.849 \pm 0.023, & B_1^d(\mu_b) &= 0.835 \pm 0.028, \\
B_2^s(\mu_b) &= 0.835 \pm 0.032, & B_2^d(\mu_b) &= 0.791 \pm 0.034, \\
B_3^s(\mu_b) &= 0.854 \pm 0.051, & B_3^d(\mu_b) &= 0.775 \pm 0.054, \\
B_4^s(\mu_b) &= 1.031 \pm 0.035, & B_4^d(\mu_b) &= 1.063 \pm 0.041, \\
B_5^s(\mu_b) &= 0.959 \pm 0.031, & B_5^d(\mu_b) &= 0.994 \pm 0.037,
\end{aligned}$$

at the scale $\mu_b = \bar{m}_b(\bar{m}_b)$. For the first time we do not have to rely on vacuum insertion approximation for the dimension seven operators, instead we can now use the values obtained in [96, 179]

$$\begin{aligned}
B_{R_0}^q &= 0.32 \pm 0.13, \\
B_{R_1}^q &= 1.031 \pm 0.035, \\
B_{\bar{R}_1}^q &= 0.959 \pm 0.031, \\
B_{R_2}^q &= 0.27 \pm 0.10, \\
B_{R_3}^q &= 0.33 \pm 0.11.
\end{aligned} \tag{A.8}$$

Note that our notation for the dimension seven Bag parameter $B_{R_2}^q$ and $B_{R_3}^q$ corresponds to the primed bag parameter of [96]. For the remaining two operators we are using equations of motion [83]

$$\begin{aligned}
B_{\bar{R}_2}^q &= -B_{R_2}^q \\
B_{\bar{R}_3}^q &= \frac{7}{5}B_{R_3}^q - \frac{2}{5}B_{R_2}^q.
\end{aligned} \tag{A.9}$$

For the determination of the uncertainties of the ratios of Bag parameter, we first symmetrized the errors of the individual bag parameter. Based on the updated value for the bag parameter B_1^q given above and the lattice average ($N_f = 2 + 1 + 1$) for f_{B_q} presented in [165] - based on [92–95]

$$\begin{aligned}
f_{B_s} &= (230.3 \pm 1.3) \text{ MeV}, \\
f_{B_d} &= (190.0 \pm 1.3) \text{ MeV},
\end{aligned} \tag{A.10}$$

we obtain after symmetrizing the uncertainties

$$\begin{aligned}
f_{B_s}^2 B_1^s &= (0.0452 \pm 0.0014) \text{ GeV}^2, \\
f_{B_d}^2 B_1^d &= (0.0305 \pm 0.0011) \text{ GeV}^2.
\end{aligned} \tag{A.11}$$

Additionally, for the determination of the contributions of the double insertion of the $\Delta B = 1$ effective Hamiltonians to M_{12}^d we require the following Bag parameters at the scale $\mu_c = 1.5 \text{ GeV}$ (see [82])

$$B_1^d(1.5 \text{ GeV}) = 0.910_{-0.031}^{+0.023}, \quad B_2^d(1.5 \text{ GeV}) = 0.923_{-0.035}^{+0.029}. \tag{A.12}$$

To calculate the CKM-elements in Eq. (A.20) we require the renormalization group invariant bag parameter \hat{B}_1^s which in the $\overline{\text{MS}}$ -NDR scheme relates with B_1^s , via (see e.g. [66])

$$\hat{B}_1^s = \alpha_s(\mu)^{-\gamma_0/(2\beta_0)} \left[1 + \frac{\alpha_s(\mu)}{4\pi} \left(\frac{\beta_1\gamma_0 - \beta_0\gamma_1}{2\beta_0^2} \right) \right] B_1^s \quad (\text{A.13})$$

$$= \alpha_s(\mu)^{-\frac{6}{23}} \left[1 + \frac{\alpha_s(\mu)}{4\pi} \frac{5165}{3174} \right] B_1^s = 1.52734 B_1^s, \quad (\text{A.14})$$

where we have used

$$C_F = \frac{N_c^2 - 1}{2N_c}, \quad (\text{A.15})$$

$$\beta_0 = \frac{11N_c - 2n_f}{3}, \quad \beta_1 = \frac{34}{3}N_c^2 - \frac{10}{3}N_cn_f - 2C_Fn_f, \quad (\text{A.16})$$

$$\gamma_0 = 6\frac{N_c - 1}{N_c}, \quad \gamma_1 = \frac{N_c - 1}{2N_c} \left(-21 + \frac{57}{N_c} - \frac{19}{3}N_c + \frac{4}{3}n_f \right). \quad (\text{A.17})$$

Finally we take the lifetime bag parameter from the recent HQET sum rule evaluation in [82] - here no corresponding up to date lattice evaluation exists

$$\begin{aligned} B_1(\mu = m_b) &= 1.028_{-0.056}^{+0.064}, & B_2(\mu = m_b) &= 0.988_{-0.079}^{+0.087}, \\ \epsilon_1(\mu = m_b) &= -0.107_{-0.029}^{+0.028}, & \epsilon_2(\mu = m_b) &= -0.033_{-0.021}^{+0.021}. \end{aligned} \quad (\text{A.18})$$

Using CKMfitter-Live [153] online, we perform a fit to the CKM elements $|V_{us}|$, $|V_{ub}|$, $|V_{cb}|$ and the CKM angle γ excluding in all the cases the direct determination of the CKM angle γ itself. Our inputs coincide mostly with the CKMfitter-Summer 2018 analysis, however in order to be consistent with our main study we modify the following entries $\bar{m}_t(\bar{m}_t)$, $\bar{m}_c(\bar{m}_c)$, \hat{B}_1^s and the ratios

$$\frac{\hat{B}_1^s}{\hat{B}_1^d} = 0.987 \pm 0.008 [91], \quad \frac{f_{B_s}}{f_{B_d}} = 1.212 \pm 0.011. \quad (\text{A.19})$$

Our results are

$$\begin{aligned} |V_{us}| &= 0.224746_{-0.000058}^{+0.000253}, & |V_{ub}| &= 0.003741_{-0.000061}^{+0.000082} \\ |V_{cb}| &= 0.04243_{-0.00088}^{+0.00036}, & \gamma &= (65.17_{-3.05}^{+0.26})^\circ, \end{aligned} \quad (\text{A.20})$$

from which we obtain

$$\frac{|V_{ub}|}{|V_{cb}|} = 0.08833 \pm 0.00218. \quad (\text{A.21})$$

The full set of CKM matrix elements is then calculated under the assumption of the unitarity of the 3×3 CKM matrix.

B QCD-Factorization formulas

B.1 Generic parameters

$$\begin{aligned}
f_V^\perp(\mu) &= f_V^\perp(\mu_0) \left(\frac{\alpha_s(\mu)}{\alpha_s(\mu_0)} \right)^{\frac{C_F}{\beta_0}}, \quad r_\chi^\pi(\mu) = \frac{2m_\pi^2}{m_b(\mu)2m_q(\mu)}, \\
r_\chi^\rho(\mu) &= \frac{2m_\rho}{m_b(\mu)} \frac{f_\rho^\perp(\mu)}{f_\rho}, \quad r_\chi^{D^*}(\mu) = \frac{2m_{D^*}}{m_b(\mu)} \frac{f_{D^*}^\perp(\mu)}{f_{D^*}}, \\
r_\chi^K(\mu) &= \frac{2m_K^2}{m_b(\mu)(m_q(\mu) + m_s(\mu))}, \quad A_{\pi\pi} = i \frac{G_F}{\sqrt{2}} m_B^2 F_0^{B \rightarrow \pi}(0) f_\pi, \\
A_{\pi\rho} &= -i \frac{G_F}{\sqrt{2}} m_B^2 F_0^{B \rightarrow \pi}(0) f_\rho, \quad A_{\rho\pi} = -i \frac{G_F}{\sqrt{2}} m_B^2 A_0^{B \rightarrow \rho}(0) f_\pi, \\
A_{\rho\rho} &= i \frac{G_F}{\sqrt{2}} m_B^2 A_0^{B \rightarrow \rho}(0) f_\rho, \quad B_{\pi\pi} = i \frac{G_F}{\sqrt{2}} f_B f_\pi f_\pi, \\
B_{\pi\rho} &= B_{\rho\pi} = -i \frac{G_F}{\sqrt{2}} f_B f_\pi f_\rho, \quad B_{\rho\rho} = i \frac{G_F}{\sqrt{2}} f_B f_\rho f_\rho, \\
\tilde{\alpha}_4^{p,\pi\pi/\pi\rho} &= \alpha_4^{p,\pi\pi/\pi\rho} + r_\chi^{\pi/\rho} \alpha_6^{p,\pi\pi/\pi\rho}, \quad \tilde{\alpha}_4^{p,\rho\pi} = \alpha_4^{p,\rho\pi} - r_\chi^\pi \alpha_6^{p,\rho\pi}, \\
\tilde{\alpha}_{4,EW}^{\pi\pi/\pi\rho} &= \alpha_{10}^{p,\pi\pi/\pi\rho} + r_\chi^{\pi/\rho} \alpha_8^{p,\pi\pi/\pi\rho}, \quad \tilde{\alpha}_{4,EW}^{\rho\pi} = \alpha_{10}^{p,\rho\pi} - r_\chi^\pi \alpha_8^{p,\rho\pi}.
\end{aligned} \tag{B.1}$$

Following [19, 20] we take

$$m_q(\mu) = \frac{m_\pi^2}{(2m_K^2 - m_\pi^2)} m_s(\mu), \tag{B.2}$$

which leads to the condition $r_\chi^\pi(\mu) = r_\chi^K(\mu)$.

B.1.1 Vertices for the $B \rightarrow \pi\pi, \rho\pi, \pi\rho, \rho\rho$ decays

$$\begin{aligned}
V_{1,2,4,10}^\pi &= 12\ln\frac{m_b}{\mu} - 18 + \left[-\frac{1}{2} - 3i\pi + \left(\frac{11}{2} - 3i\pi\right)a_1^\pi - \frac{21}{20}a_2^\pi\right], \\
V_{6,8}^\pi &= -6, \\
V_{1,2,3,9}^\rho &= V^\rho = 12\ln\frac{m_b}{\mu} - 18 + \left[-\frac{1}{2} - 3i\pi + \left(\frac{11}{2} - 3i\pi\right)a_1^\rho - \frac{21}{20}a_2^\rho\right], \\
V_4^\rho &= \begin{cases} V^\rho & \text{for } \bar{B}^0 \rightarrow \pi^+\rho^-, \\ V^\rho - \frac{C_5}{C_3}r_\chi^\rho V_\perp^\rho & \text{for } B \rightarrow \rho\rho, \end{cases} \\
V_\perp^\rho &= 9 - 6i\pi + \left(\frac{19}{6} - i\pi\right)a_{2,\perp}^\rho, \\
V_7^\rho &= -12\ln\frac{m_b}{\mu} + 6 - \left[-\frac{1}{2} - 3i\pi - \left(\frac{11}{2} - 3i\pi\right)a_1^\rho - \frac{21}{20}a_2^\rho\right], \\
V_{6,8}^\rho &= 9 - 6i\pi + \left(\frac{19}{6} - i\pi\right)a_{2,\perp}^\rho, \\
V_{10}^\rho &= \begin{cases} V^\rho & \text{for } \bar{B}^0 \rightarrow \pi^+\rho^-, \\ V^\rho - \frac{C_7}{C_9}r_\chi^\rho V_\perp^\rho & \text{for } B \rightarrow \rho\rho. \end{cases}
\end{aligned} \tag{B.3}$$

B.1.2 Vertices for the $B \rightarrow J/\psi\phi$ decay.

$$V_{J/\psi\phi}^i = \begin{cases} -18 - 12\ln\frac{\mu}{m_b} + f_I^h & \text{for } i = 1, 3, 9 \\ -6 - 12\ln\frac{\mu}{m_b} + f_I^h & \text{for } i = 5, 7 \end{cases} \tag{B.4}$$

$$f_I^h = \begin{cases} f_I + g_I \cdot (1 - \tilde{z}) \frac{A_0^{BK*}}{A_3^{BK*}} & \text{for } h = 0 \\ f_I & \text{for } h = \pm \end{cases} \tag{B.5}$$

$$\begin{aligned}
f_I = & \int_0^1 d\xi \Phi_{\parallel}^{J/\psi}(\xi) \left\{ \frac{2\tilde{z}\xi}{1-\tilde{z}(1-\xi)} + (3-2\xi) \frac{\ln \xi}{1-\xi} \right. \\
& + \left(-\frac{3}{1-\tilde{z}\xi} + \frac{1}{1-\tilde{z}(1-\xi)} - \frac{2\tilde{z}\xi}{[1-\tilde{z}(1-\xi)]^2} \right) \times \tilde{z}\xi \ln[\tilde{z}\xi] \\
& + \left(3(1-\tilde{z}) + 2\tilde{z}\xi + \frac{2\tilde{z}^2\xi^2}{1-\tilde{z}(1-\xi)} \right) \times \frac{\ln(1-\tilde{z}) - i\pi}{1-\tilde{z}(1-\xi)} \Big\} \\
& + \int_0^1 d\xi \Phi_{\perp}^{J/\psi}(\xi) \left\{ -4r \frac{\ln \xi}{1-\xi} + \frac{4\tilde{z}r \ln[\tilde{z}\xi]}{1-\tilde{z}(1-\xi)} \right. \\
& \left. - 4\tilde{z}r \frac{\ln(1-\tilde{z}) - i\pi}{1-\tilde{z}(1-\xi)} \right\}
\end{aligned} \tag{B.6}$$

$$\begin{aligned}
g_I = & \int_0^1 d\xi \Phi_{\parallel}^{J/\Psi}(\xi) \left\{ \frac{-4\xi}{(1-\tilde{z})(1-\xi)} \ln \xi + \frac{\tilde{z}\xi}{(1-\tilde{z}(1-\xi))^2} \ln(1-\tilde{z}) \right. \\
& + \left(\frac{1}{(1-\tilde{z}\xi)^2} - \frac{1}{(1-\tilde{z}(1-\xi))^2} + \frac{2(1+\tilde{z}-2\tilde{z}\xi)}{(1-\tilde{z})(1-\tilde{z}\xi)^2} \right) \times \tilde{z}\xi \ln[\tilde{z}\xi] \\
& \left. - i\pi \frac{\tilde{z}\xi}{(1-\tilde{z}(1-\xi))^2} \right\} + \int_0^1 d\xi \Phi_{\perp}^{J/\Psi}(\xi) \left\{ \frac{4r}{(1-\tilde{z})(1-\xi)} \ln \xi \right. \\
& \left. - \frac{4r\tilde{z}}{(1-\tilde{z})(1-\tilde{z}\xi)} \ln[\tilde{z}\xi] \right\}
\end{aligned} \tag{B.7}$$

for

$$\tilde{z} = \frac{m_{J/\Psi}^2}{m_B^2}, \quad r = 2 \cdot \left(\frac{m_c}{m_{J/\Psi}} \right)^2. \tag{B.8}$$

B.1.3 Penguin functions

To simplify the following equations we have denoted $M = \pi, \rho$ when the corresponding expressions apply to both π and ρ mesons. In addition we have used

$$s_p = \left(\frac{m_p}{m_b} \right)^2, \tag{B.9}$$

for $p = u, c$, although in practice we consider $s_u = 0$. Notice that in the following equations the symbol “hat” does not denote an operator and is used to distinguish the different kind of functions under consideration.

$$\begin{aligned}
P_{1,2,3}^{p,M} &= P_{1,2,3}^M = 0, \\
P_4^{p,\pi} &= \frac{C_F \alpha_s}{4\pi N_c} \left\{ C_2 \left[\frac{4}{3} \ln \frac{m_b}{\mu} + \frac{2}{3} - G_\pi(s_p) \right] + C_3 \left[\frac{8}{3} \ln \frac{m_b}{\mu} + \frac{4}{3} - G_\pi(0) - G_\pi(1) \right] \right. \\
&\quad + \left(C_4 + C_6 \right) \left[\frac{4n_f}{3} \ln \frac{m_b}{\mu} - (n_f - 2)G_\pi(0) - G_\pi(s_c) - G_\pi(1) \right] \\
&\quad \left. - 6C_{8g}^{eff} \left(1 + \alpha_1^\pi + \alpha_2^\pi \right) \right\}, \\
P_6^{p,M} &= \frac{C_F \alpha_s}{4\pi N_c} \left\{ C_2 \left[\frac{4}{3} \ln \frac{m_b}{\mu} + \frac{2}{3} - \hat{G}_M(s_p) \right] + C_3 \left[\frac{8}{3} \ln \frac{m_b}{\mu} + \frac{4}{3} - \hat{G}_M(0) - \hat{G}_M(1) \right] \right. \\
&\quad + \left(C_4 + C_6 \right) \left[\frac{4n_f}{3} \ln \frac{m_b}{\mu} - (n_f - 2)\hat{G}_M(0) - \hat{G}_M(s_c) - \hat{G}_M(1) \right] - 2C_{8g}^{eff} \left. \right\}, \\
P_8^{p,\pi} &= \frac{\alpha}{9\pi N_c} \left\{ \left(N_c C_1 + C_2 \right) \left[\frac{4}{3} \ln \frac{m_b}{\mu} + \frac{2}{3} - \hat{G}_\pi(s_p) \right] - 3C_7^{eff} \right\}, \\
P_{10}^{p,M} &= \frac{\alpha}{9\pi N_c} \left\{ \left(N_c C_1 + C_2 \right) \left[\frac{4}{3} \ln \frac{m_b}{\mu} + \frac{2}{3} - G_M(s_p) \right] - 9C_7^{eff} \left(1 + \alpha_1^M + \alpha_2^M \right) \right\}, \\
P_4^{p,\rho} &= \begin{cases} P_4'^{p,\rho} & \text{for } \bar{B}^0 \rightarrow \pi^+ \rho^-, \\ P_4'^{p,\rho} - r_\chi^\rho P_4''^{p,\rho} & \text{for } B \rightarrow \rho \rho, \end{cases} \\
P_4'^{p,\rho} &= \frac{C_F \alpha_s}{4\pi N_c} \left\{ C_2 \left[\frac{4}{3} \ln \frac{m_b}{\mu} + \frac{2}{3} - G_\rho(s_p) \right] + C_3 \left[\frac{8}{3} \ln \frac{m_b}{\mu} + \frac{4}{3} - G_\rho(0) - G_\rho(1) \right] \right. \\
&\quad + \left(C_4 + C_6 \right) \left[\frac{4n_f}{3} \ln \frac{m_b}{\mu} - (n_f - 2)G_\rho(0) - G_\rho(s_c) - G_\rho(1) \right] \\
&\quad \left. - 6C_{8g}^{eff} \left(1 + \alpha_1^\rho + \alpha_2^\rho \right) \right\}, \\
P_4''^{p,\rho} &= - \left[C_2 \hat{G}_\rho(s_p) + C_3 \left(\hat{G}_\rho(0) + \hat{G}_\rho(1) \right) \right. \\
&\quad \left. + \left(C_4 + C_6 \right) \left(3\hat{G}_\rho(0) + \hat{G}_\rho(s_p) + \hat{G}_\rho(1) \right) \right], \\
P_{7,9}^{u,\rho} &= \frac{\alpha}{9\pi} \left\{ \left(N_c C_1 + C_2 \right) \left[\frac{4}{3} \frac{m_b}{\mu} - \frac{10}{9} + \frac{4\pi^2}{3} \sum_{r=\rho,\omega} \frac{f_r^2}{m_\rho^2 - m_r^2 + im_r \Gamma_r} \right. \right. \\
&\quad \left. \left. - \frac{2\pi}{3} \frac{m_\rho^2}{t_c} i + \frac{2}{3} \ln \frac{m_\rho^2}{m_b^2} + \frac{2}{3} \frac{t_c - m_\rho^2}{t_c} \ln \frac{t_c - m_\rho^2}{m_\rho^2} \right] - 3C_{7,\gamma}^{eff} \right\}, \\
P_{7,9}^{c,\rho} &= \frac{\alpha}{9\pi} \left\{ \left(N_c C_1 + C_2 \right) \left[\frac{4}{3} \ln \frac{m_b}{\mu} + \frac{2}{3} + \frac{4}{3} \ln \frac{m_c}{m_b} \right] - 3C_\gamma^{eff} \right\}, \\
P_8^{p,\rho} &= - \frac{\alpha}{9\pi N_c} \left(N_c C_1 + C_2 \right) \hat{G}_\rho(s_p), \\
P_{10}^{p,\rho} &= \frac{\alpha}{9\pi N_c} \left(P_{10}'^{p,\rho} + r_\chi^\rho P_{10}''^{p,\rho} \right), \\
P_{10}'^{p,\rho} &= \left(N_c C_1 + C_2 \right) \left[\frac{4}{3} \ln \frac{m_b}{\mu} + \frac{2}{3} - G_\rho(s_p) \right] - 9C_{7,\gamma}^{eff} \left(1 + \alpha_1^\rho + \alpha_2^\rho \right), \\
P_{10}''^{p,\rho} &= \left(N_c C_1 + C_2 \right) \hat{G}_\rho(s_p). \tag{B.10}
\end{aligned}$$

For the calculation of $P_{7,9}^{u,\rho}$ above the symbol t_c denotes

$$t_c = 4\pi^2(f_\rho^2 + f_\omega^2). \quad (\text{B.11})$$

Extra functions required for the evaluation of the penguin contributions

$$\begin{aligned} G_M(s_c) &= \frac{5}{3} - \frac{2}{3}\ln(s_c) + \frac{\alpha_1^M}{2} + \frac{\alpha_2^M}{5} + \frac{4}{3}(8 + 9\alpha_1^M + 9\alpha_2^M)s_c \\ &\quad + 2(8 + 63\alpha_1^M + 214\alpha_2^M)s_c^2 - 24(9\alpha_1^M + 80\alpha_2^M)s_c^3 \\ &\quad + 2880\alpha_2^M s_c^4 - \frac{2}{3}\sqrt{1-4s_c}(2\operatorname{arctanh}\sqrt{1-4s_c} - i\pi) \left[1 + 2s_c \right. \\ &\quad \left. + 6(4 + 27\alpha_1^M + 78\alpha_2^M)s_c^2 - 36(9\alpha_1^M + 70\alpha_2^M)s_c^3 + 4320\alpha_2^M s_c^4 \right] \\ &\quad + 12s_c^2(2\operatorname{arctanh}\sqrt{1-4s_c} - i\pi)^2 \left[1 + 3\alpha_1^M + 6\alpha_2^M - \frac{4}{3}(1 + 9\alpha_1^\rho \right. \\ &\quad \left. + 36\alpha_2^M)s_c + 18(\alpha_1^M + 10\alpha_2^M)s_c^2 - 240\alpha_2^M s_c^3 \right], \\ G_M(0) &= \frac{5}{3} + \frac{2i\pi}{3} + \frac{\alpha_1^M}{2} + \frac{\alpha_2^M}{5}, \\ G_M(1) &= \frac{85}{3} - 6\sqrt{3}\pi + \frac{4\pi^2}{9} - \left(\frac{155}{2} - 36\sqrt{3}\pi + 12\pi^2\right)\alpha_1^M + \left(\frac{7001}{5} \right. \\ &\quad \left. - 504\sqrt{3}\pi + 136\pi^2\right)\alpha_2^M, \\ \hat{G}_\pi^p(s_c) &= \frac{16}{9}(1 - 3s_c) - \frac{2}{3}[\ln(s_c) + (1 - 4s_c)^{3/2}(2\operatorname{arctan}\sqrt{1-4s_c} - i\pi)], \end{aligned} \quad (\text{B.12})$$

$$\begin{aligned} \hat{G}_\pi^p(0) &= \frac{16}{9} + \frac{2\pi i}{3}, \\ \hat{G}_\pi^p(1) &= \frac{2\pi}{\sqrt{3}} - \frac{32}{9}, \\ \hat{G}_\rho(s_c) &= 1 + \frac{\alpha_{1,\perp}^\rho}{3} + \frac{\alpha_{2,\perp}^\rho}{6} - 4s_c(9 + 12\alpha_{1,\perp}^\rho + 14\alpha_{2,\perp}^\rho) - 6s_c^2(8\alpha_{1,\perp}^\rho \\ &\quad + 35\alpha_{2,\perp}^\rho) + 360s_c^3\alpha_{2,\perp}^\rho + 12s_c\sqrt{1-4s_c}(1 + [1 + 4s_c]\alpha_{1,\perp}^\rho \\ &\quad + [1 + 15s_c - 30s_c^2]\alpha_{2,\perp}^\rho)(2\operatorname{arctanh}\sqrt{1-4s_c} - i\pi) \\ &\quad - 12s_c^2(1 + [3 - 4s_c]\alpha_{1,\perp}^\rho + 2[3 - 10s_c + 15s_c^2]\alpha_{2,\perp}^\rho) \\ &\quad \times (2\operatorname{arctanh}\sqrt{1-4s_c} - i\pi)^2, \\ \hat{G}_\rho(0) &= 1 + \frac{1}{3}\alpha_{1,\perp}^\rho + \frac{1}{6}\alpha_{2,\perp}^\rho, \\ \hat{G}_\rho(1) &= -35 + 4\sqrt{3}\pi + \frac{4\pi^2}{3} + \left(-\frac{287}{3} + 20\sqrt{3}\pi - \frac{4\pi^2}{3}\right)\alpha_{1,\perp}^\rho \\ &\quad + \left(\frac{565}{6} - 56\sqrt{3}\pi + \frac{64\pi^2}{3}\right)\alpha_{2,\perp}^\rho. \end{aligned} \quad (\text{B.13})$$

B.1.4 Hard Scattering functions for the $B \rightarrow \pi\pi, \rho\pi, \pi\rho, \rho\rho$ decays.

$$\begin{aligned}
H_{1,2,4,10}^{\pi\pi}(\mu) &= \frac{B_{\pi\pi}}{A_{\pi\pi}} \frac{m_B}{\lambda_B} \left(9 \left[1 + a_1^\pi + a_2^\pi \right]^2 + 3r_\chi^\pi(\mu) \left[1 - a_1^\pi + a_2^\pi \right] X_H \right), \\
H_{6,8}^{\pi\pi}(\mu) &= 0, \\
H_{2,4,10}^{\pi\rho}(\mu) &= \frac{B_{\pi\rho}}{A_{\pi\rho}} \frac{m_B}{\lambda_B} \left(9 \left[1 + a_1^\pi + a_2^\pi \right] \left[1 + a_1^\rho + a_2^\rho \right] + 3r_\chi^\pi(\mu) \left[1 - a_1^\rho + a_2^\rho \right] X_H \right), \\
H_{6,8}^{\pi\rho}(\mu) &= 0, \\
H_{2,4,10}^{\rho\pi} &= \frac{B_{\rho\pi}}{A_{\rho\pi}} \frac{m_B}{\lambda_B} \left(9 \left[1 + a_1^\pi + a_2^\pi \right] \left[1 + a_1^\rho + a_2^\rho \right] + 3r_\chi^\rho(\mu) \left[1 - a_1^\pi + a_2^\pi \right] \right. \\
&\quad \left. + a_2^\rho \right] X_H \Big), \\
H_{6,8}^{\rho\pi}(\mu) &= 0, \\
H_{2,4,10}^{\rho\rho} &= \frac{B_{\rho\rho}}{A_{\rho\rho}} \frac{m_B}{\lambda_B} \left(9 \left[1 + a_1^\pi + a_2^\pi \right] \left[1 + a_1^\rho + a_2^\rho \right] + 3r_\chi^\rho(\mu) \left[1 - a_1^\pi + a_2^\pi \right] \right. \\
&\quad \left. + a_2^\rho \right] \left[3(1 + a_{1,\perp}^\rho + a_{2,\perp}^\rho) X_H - (6 + 9a_{1,\perp}^\rho + 11a_{2,\perp}^\rho) \right] \Big), \\
H_{6,8}^{\rho\pi}(\mu) &= 0, \\
H_{1,2,4,9,10}^{\rho\rho}(\mu) &= \frac{B_{\rho\rho}}{A_{\rho\rho}} \left[\frac{m_{B_d}}{\lambda_B} \right] \left[9 \left(1 + a_1^\rho + a_2^\rho \right)^2 + 9r_\chi^\rho(\mu) \left(1 - a_1^\rho + a_2^\rho \right) \right. \\
&\quad \left. \times (X_H - 2) \right], \\
H_7^{\rho\rho}(\mu) &= -\frac{B_{\rho\rho}}{A_{\rho\rho}} \left[\frac{m_{B_d}}{\lambda_B} \right] \left[9 \left(1 + a_1^\rho + a_2^\rho \right) \left(1 - a_1^\rho + a_2^\rho \right) + 9r_\chi^\rho(\mu) \right. \\
&\quad \left. \times (1 + a_1^\rho + a_2^\rho) (X_H - 2) \right]. \tag{B.14}
\end{aligned}$$

B.1.5 Hard scattering function for the $B \rightarrow J/\psi\phi$

For the amplitudes of the decay $B \rightarrow J/\psi\phi$, the spectator interaction functions depend on the polarization of the final states, for $h = 0, \pm$ we have

$$\begin{aligned}
H_{1,3,9}^{J/\psi\phi,0} &= \frac{f_B f_{J/\psi} f_\phi}{\tilde{h}^0} \int_0^1 d\xi \frac{\Phi_1^B(\xi)}{\xi} \int_0^1 d\tilde{\xi} \frac{\Phi^{J/\Psi}(\tilde{\xi})}{\tilde{\xi}} \int_0^1 d\bar{\eta} \frac{\Phi^\phi(\bar{\eta})}{\bar{\eta}}, \\
H_{1,3,9}^{J/\psi\phi,\pm} &= \frac{2f_B f_{J/\Psi} f_\phi m_{J/\Psi} m_\phi}{m_B^2 \tilde{h}^\pm (1 - \tilde{z})} \int_0^1 d\xi \frac{\Phi_1^B(\xi)}{\xi} \int_0^1 d\tilde{\xi} \frac{\Phi^{J/\Psi}(\tilde{\xi})}{\tilde{\xi}} \cdot \\
&\quad \int_0^1 d\bar{\eta} \left[\frac{\Phi_\perp^{\phi,v}(\bar{\eta})}{\bar{\eta}} \pm \frac{\Phi_\perp^{\phi,a}(\bar{\eta})}{4\bar{\eta}^2} \right], \\
H_{5,7}^{J/\psi\phi,h} &= -H_{1,3,9}^{J/\psi\phi,h}. \tag{B.15}
\end{aligned}$$

The helicity functions in the denominators of Eqs. (B.15) are

$$\begin{aligned}
\tilde{h}^0 &= \frac{f_{J/\psi}}{2m_\phi} \left[\left(m_B^2 - m_{J/\Psi}^2 - m_\phi^2 \right) \left(m_B + m_\phi \right) A_1^{B \rightarrow \phi}(m_{J/\psi}^2) - \frac{4m_B^2 p_c^2}{m_B + m_\phi} A_2^{B \rightarrow \phi}(m_{J/\psi}^2) \right], \\
\tilde{h}^\pm &= m_{J/\psi} f_{J/\psi} \left[\left(m_B + m_\phi \right) A_1^{B \rightarrow \phi}(m_{J/\psi}^2) \pm \frac{2m_B p_c}{m_B + m_\phi} V^{B \rightarrow \phi}(m_{J/\psi}^2) \right], \tag{B.16}
\end{aligned}$$

with

$$p_c = \frac{\sqrt{\left(m_\phi^2 - m_{J/\psi}^2\right)^2 + m_B^2 \left(m_B^2 - 2\left[m_{J/\psi} + m_\phi^2\right]\right)}}{2m_B}. \quad (\text{B.17})$$

The form factors $A_{1,2}^{B \rightarrow \phi}(m_{J/\psi}^2)$ and $V^{B \rightarrow \phi}(m_{J/\psi}^2)$ used for the evaluation of the functions \tilde{h}^0 and \tilde{h}^\pm were calculated based on [169], the corresponding numerical values can be found in Appendix A.

The twist-3 distribution amplitudes of the ϕ meson in Eqs. (B.15) have been denoted by $\Phi_\perp^{\phi,a}(x)$ and $\Phi_\perp^{\phi,v}(x)$, they are given explicitly by

$$\begin{aligned} \Phi_\perp^{\phi,a}(x) = & 6x(1-x) \left[1 + a_1^\parallel [2x-1] + \left\{ \frac{1}{4}a_2^\parallel + \frac{5}{3}\zeta_3 \left(1 - \frac{3}{16}\omega_3^{A,\phi} \right. \right. \right. \\ & \left. \left. \left. + \frac{9}{16}\omega_3^{V,\phi} \right) \right\} \left(5[2x-1]^2 - 1 \right) + 6\delta_+ \left\{ 3x(1-x) \right. \right. \\ & \left. \left. + (1-x)\ln(1-x) + x\ln x \right\} + 6\delta_- \left\{ (1-x)\ln(1-x) - x\ln x \right\} \right], \\ \Phi_\perp^{\phi,v}(x) = & \frac{3}{4} \left\{ 1 + [2x-1]^2 \right\} + \frac{3}{2}a_1^\parallel [2x-1]^3 + \left\{ \frac{3}{7}a_2^\parallel + 5\zeta_3 \right\} \left\{ 3[2x-1]^2 - 1 \right\} \\ & + \left\{ \frac{9}{112}a_2^\parallel + \frac{15}{64}\zeta_3 \left[3\omega_3^V - \omega_3^A \right] \right\} \left\{ 3 - 30[2x-1]^2 + 35[2x-1]^4 \right\} \\ & + \frac{3}{2}\delta_+ \left\{ 2 + \ln x + \ln[1-x] \right\} + \frac{3}{2}\delta_- \left\{ 2[2x-1] + \ln(1-x) - \ln x \right\}. \end{aligned} \quad (\text{B.18})$$

For the rest of the LCD amplitudes of the vector mesons J/ψ and ϕ in Eqs. (B.6), (B.7) and (B.15) we use the leading term in the Gegenbauer expansion

$$\Phi^V(\xi) = 6\xi(1-\xi). \quad (\text{B.19})$$

For different hadronic parameters required for the numerical evaluation of Eq. (B.18) we use [164]

$$\zeta_3 = 0.023, \quad \omega_3^A = 0, \quad \omega_3^V = 3.7, \quad \delta_+ = 0.41, \quad \delta_- = 0. \quad (\text{B.20})$$

The divergences encountered when integrating the twist-3 distribution amplitudes in Eqs. (B.15) are parameterized following the model in Eq. (2.23).

B.2 Annihilation coefficients

$$\begin{aligned}
\beta_i^{p,M_1 M_2} &= \frac{B_{M_1 M_2}}{A_{M_1 M_2}} b_i^{p,M_1 M_2} \\
b_1^{M_1 M_2} &= \frac{C_F}{N_c^2} C_1 A_1^{i,M_1 M_2} \\
b_2^{M_1 M_2} &= \frac{C_F}{N_c^2} C_2 A_1^{i,M_1 M_2} \\
b_3^{p,M_1 M_2} &= \frac{C_F}{N_c^2} \left[C_3 A_1^{i,M_1 M_2} + C_5 \left(A_3^{i,M_1 M_2} + A_3^{f,M_1 M_2} \right) + N_c C_6 A_3^{f,M_1 M_2} \right] \\
b_4^{p,M_1 M_2} &= \frac{C_F}{N_c^2} \left[C_4 A_1^{i,M_1 M_2} + C_6 A_2^{i,M_1 M_2} \right] \\
b_{3,EW}^{p,M_1 M_2} &= \frac{C_F}{N_c^2} \left[C_9 A_1^{i,M_1 M_2} + C_7 \left(A_3^{i,M_1 M_2} + A_3^{f,M_1 M_2} \right) + N_c C_8 A_3^{f,M_1 M_2} \right] \\
b_{4,EW}^{p,M_1 M_2} &= \frac{C_F}{N_c^2} \left[C_{10} A_1^{i,M_1 M_2} + C_8 A_2^{i,M_1 M_2} \right]
\end{aligned} \tag{B.21}$$

B.3 Annihilation kernels

$$\begin{aligned}
A_1^{i,\pi\pi} &\approx A_2^{i,\pi\pi} \approx 2\pi\alpha_s(\mu_h) \left[9 \left(X_A - 4 + \frac{\pi^2}{3} \right) + r_\chi^\pi r_\chi^\pi X_A^2 \right] \\
A_1^{i,\pi\rho} &= A_1^{i,\rho\pi} \approx 6\pi\alpha_s \left[3 \left(X_A - 4 + \frac{\pi^2}{3} \right) + r_\chi^\rho r_\chi^\pi (X_A^2 - X_A) \right] \\
A_2^{i,\pi\rho} &= A_2^{i,\rho\pi} \approx -A_1^{i,\pi\rho} \\
A_3^{i,\pi\pi} &\approx 0 \\
A_3^{i,\pi\rho} &= A_3^{i,\rho\pi} \approx 6\pi\alpha_s \left[-3r_\chi^\rho \left(X_A^2 - 2X_A - \frac{\pi^2}{3} + 4 \right) + r_\chi^\pi \left(X_A^2 - 2X_A + \frac{\pi^2}{3} \right) \right] \\
A_1^{f,\pi\rho} &= A_2^{f,\pi\rho} = A_1^{f,\rho\pi} = A_2^{f,\rho\pi} = 0 \\
A_3^{f,\pi\pi} &\approx 12\pi\alpha_s r_\chi^\pi (2X_A^2 - X_A) \\
A_3^{f,\pi\rho} &\approx -6\pi\alpha_s \left[3r_\chi^\pi (2X_A - 1) (X_A - 2) + r_\chi^\rho (2X_A^2 - X_A) \right] \\
A_3^{f,\rho\pi} &= -A_3^{f,\pi\rho} \approx 6\pi\alpha_s \left[3r_\chi^\rho (2X_A - 1) (2 - X_A) - r_\chi^\pi (2X_A^2 - X_A) \right] \\
A_1^{i,\rho\rho} &= A_2^{i,\rho\rho} \approx 18\pi\alpha_s \left[\left(X_A - 4 + \frac{\pi^2}{3} \right) + (r_\chi^\rho)^2 (X_A - 2)^2 \right] \\
A_3^{i,\rho\rho} &= 0 \\
A_3^{f,\rho\rho} &\approx -36\pi\alpha_s r_\chi^\rho (2X_A^2 - 5X_A + 2)
\end{aligned} \tag{B.22}$$

References

- [1] N. Cabibbo, “Unitary Symmetry and Leptonic Decays,” *Phys. Rev. Lett.* **10** (1963) 531–533. [648(1963)].
- [2] M. Kobayashi and T. Maskawa, “CP Violation in the Renormalizable Theory of Weak Interaction,” *Prog. Theor. Phys.* **49** (1973) 652–657.

- [3] J. H. Christenson, J. W. Cronin, V. L. Fitch, and R. Turlay, “Evidence for the 2π Decay of the K_2^0 Meson,” *Phys. Rev. Lett.* **13** (1964) 138–140.
- [4] **BaBar** Collaboration, B. Aubert *et al.*, “Measurement of the CP-violating asymmetry amplitude $\sin 2\beta$,” *Phys. Rev. Lett.* **89** (2002) 201802, [arXiv:hep-ex/0207042 \[hep-ex\]](#).
- [5] **Belle** Collaboration, K. Abe *et al.*, “An Improved measurement of mixing induced CP violation in the neutral B meson system,” *Phys. Rev.* **D66** (2002) 071102, [arXiv:hep-ex/0208025 \[hep-ex\]](#).
- [6] **LHCb** Collaboration, R. Aaij *et al.*, “Observation of CP Violation in Charm Decays,” *Phys. Rev. Lett.* **122** no. 21, (2019) 211803, [arXiv:1903.08726 \[hep-ex\]](#).
- [7] M. Chala, A. Lenz, A. V. Rusov, and J. Scholtz, “ ΔA_{CP} within the Standard Model and beyond,” *JHEP* **07** (2019) 161, [arXiv:1903.10490 \[hep-ph\]](#).
- [8] A. Dery and Y. Nir, “Implications of the LHCb discovery of CP violation in charm decays,” [arXiv:1909.11242 \[hep-ph\]](#).
- [9] A. D. Sakharov, “Violation of CP Invariance, C asymmetry, and baryon asymmetry of the universe,” *Pisma Zh. Eksp. Teor. Fiz.* **5** (1967) 32–35. [Usp. Fiz. Nauk161,no.5,61(1991)].
- [10] **BaBar**, **Belle** Collaboration, A. J. Bevan *et al.*, “The Physics of the B Factories,” *Eur. Phys. J.* **C74** (2014) 3026, [arXiv:1406.6311 \[hep-ex\]](#).
- [11] K. Anikeev *et al.*, “B physics at the Tevatron: Run II and beyond,” in *Workshop on B Physics at the Tevatron: Run II and Beyond Batavia, Illinois, September 23-25, 1999*. 2001. [arXiv:hep-ph/0201071 \[hep-ph\]](#).
http://lss.fnal.gov/cgi-bin/find_paper.pl?pub-01-197.
- [12] G. Borissov, “B-physics results from Tevatron,” *Int. J. Mod. Phys.* **A28** (2013) 1330007, [arXiv:1304.2173 \[hep-ex\]](#).
- [13] **LHCb** Collaboration, R. Aaij *et al.*, “Implications of LHCb measurements and future prospects,” *Eur. Phys. J.* **C73** no. 4, (2013) 2373, [arXiv:1208.3355 \[hep-ex\]](#).
- [14] P. Koppenburg and V. Vagnoni, “Precision physics with heavy-flavoured hadrons,” *Adv. Ser. Direct. High Energy Phys.* **23** (2015) 31–59, [arXiv:1510.04466 \[hep-ex\]](#).
- [15] **ATLAS** Collaboration, G. Aad *et al.*, “Measurement of the CP-violating phase ϕ_s and the B_s^0 meson decay width difference with $B_s^0 \rightarrow J/\psi\phi$ decays in ATLAS,” *JHEP* **08** (2016) 147, [arXiv:1601.03297 \[hep-ex\]](#).
- [16] **CMS** Collaboration, V. Khachatryan *et al.*, “Measurement of the CP-violating weak phase ϕ_s and the decay width difference $\Delta\Gamma_s$ using the $B_s^0 \rightarrow J/\psi\phi(1020)$ decay channel in pp collisions at $\sqrt{s} = 8$ TeV,” *Phys. Lett.* **B757** (2016) 97–120, [arXiv:1507.07527 \[hep-ex\]](#).
- [17] M. Beneke, G. Buchalla, M. Neubert, and C. T. Sachrajda, “QCD factorization for $B \rightarrow \pi\pi$ decays: Strong phases and CP violation in the heavy quark limit,” *Phys. Rev. Lett.* **83** (1999) 1914–1917, [arXiv:hep-ph/9905312 \[hep-ph\]](#).
- [18] M. Beneke, G. Buchalla, M. Neubert, and C. T. Sachrajda, “QCD factorization for exclusive, nonleptonic B meson decays: General arguments and the case of heavy light final states,” *Nucl. Phys.* **B591** (2000) 313–418, [arXiv:hep-ph/0006124 \[hep-ph\]](#).
- [19] M. Beneke, G. Buchalla, M. Neubert, and C. T. Sachrajda, “QCD factorization in $B \rightarrow \pi K, \pi\pi$ decays and extraction of Wolfenstein parameters,” *Nucl. Phys.* **B606** (2001) 245–321, [arXiv:hep-ph/0104110 \[hep-ph\]](#).

- [20] M. Beneke and M. Neubert, “QCD factorization for $B \rightarrow PP$ and $B \rightarrow PV$ decays,” *Nucl. Phys.* **B675** (2003) 333–415, [arXiv:hep-ph/0308039](#) [[hep-ph](#)].
- [21] V. A. Khoze and M. A. Shifman, “HEAVY QUARKS,” *Sov. Phys. Usp.* **26** (1983) 387.
- [22] M. A. Shifman and M. B. Voloshin, “Preasymptotic Effects in Inclusive Weak Decays of Charmed Particles,” *Sov. J. Nucl. Phys.* **41** (1985) 120. [*Yad. Fiz.*41,187(1985)].
- [23] I. I. Y. Bigi and N. G. Uraltsev, “Gluonic enhancements in non-spectator beauty decays: An Inclusive mirage though an exclusive possibility,” *Phys. Lett.* **B280** (1992) 271–280.
- [24] I. I. Y. Bigi, N. G. Uraltsev, and A. I. Vainshtein, “Nonperturbative corrections to inclusive beauty and charm decays: QCD versus phenomenological models,” *Phys. Lett.* **B293** (1992) 430–436, [arXiv:hep-ph/9207214](#) [[hep-ph](#)]. [Erratum: *Phys. Lett.*B297,477(1992)].
- [25] B. Blok and M. A. Shifman, “The Rule of discarding $1/N(c)$ in inclusive weak decays. 1.,” *Nucl. Phys.* **B399** (1993) 441–458, [arXiv:hep-ph/9207236](#) [[hep-ph](#)].
- [26] B. Blok and M. A. Shifman, “The Rule of discarding $1/N(c)$ in inclusive weak decays. 2.,” *Nucl. Phys.* **B399** (1993) 459–476, [arXiv:hep-ph/9209289](#) [[hep-ph](#)].
- [27] J. Chay, H. Georgi, and B. Grinstein, “Lepton energy distributions in heavy meson decays from QCD,” *Phys. Lett.* **B247** (1990) 399–405.
- [28] M. E. Luke, “Effects of subleading operators in the heavy quark effective theory,” *Phys. Lett.* **B252** (1990) 447–455.
- [29] A. Lenz, “Lifetimes and heavy quark expansion,” *Int. J. Mod. Phys.* **A30** no. 10, (2015) 1543005, [arXiv:1405.3601](#) [[hep-ph](#)]. [63(2014)].
- [30] R. Fleischer, “Theoretical prospects for B physics,” *PoS FPCP2015* (2015) 002, [arXiv:1509.00601](#) [[hep-ph](#)].
- [31] M. Artuso, G. Borissov, and A. Lenz, “CP violation in the B_s^0 system,” *Rev. Mod. Phys.* **88** no. 4, (2016) 045002, [arXiv:1511.09466](#) [[hep-ph](#)].
- [32] T. Jubb, M. Kirk, A. Lenz, and G. Tetlalmatzi-Xolocotzi, “On the ultimate precision of meson mixing observables,” *Nucl. Phys.* **B915** (2017) 431–453, [arXiv:1603.07770](#) [[hep-ph](#)].
- [33] **D0** Collaboration, V. M. Abazov *et al.*, “Evidence for an Anomalous Like-Sign Dimuon Charge Asymmetry,” *Phys. Rev.* **D82** (2010) 032001, [arXiv:1005.2757](#) [[hep-ex](#)].
- [34] **D0** Collaboration, V. M. Abazov *et al.*, “Evidence for an Anomalous Like-Sign Dimuon Charge Asymmetry,” *Phys. Rev. Lett.* **105** (2010) 081801, [arXiv:1007.0395](#) [[hep-ex](#)].
- [35] **D0** Collaboration, V. M. Abazov *et al.*, “Measurement of the anomalous like-sign dimuon charge asymmetry with 9 fb^{-1} of $p\bar{p}$ collisions,” *Phys. Rev.* **D84** (2011) 052007, [arXiv:1106.6308](#) [[hep-ex](#)].
- [36] **D0** Collaboration, V. M. Abazov *et al.*, “Study of CP-violating charge asymmetries of single muons and like-sign dimuons in $p\bar{p}$ collisions,” *Phys. Rev.* **D89** no. 1, (2014) 012002, [arXiv:1310.0447](#) [[hep-ex](#)].
- [37] C. W. Bauer and N. D. Dunn, “Comment on new physics contributions to Γ_{12}^s ,” *Phys. Lett.* **B696** (2011) 362–366, [arXiv:1006.1629](#) [[hep-ph](#)].
- [38] **BaBar** Collaboration, J. P. Lees *et al.*, “Evidence for an excess of $\bar{B} \rightarrow D^{(*)}\tau^-\bar{\nu}_\tau$ decays,” *Phys. Rev. Lett.* **109** (2012) 101802, [arXiv:1205.5442](#) [[hep-ex](#)].

- [39] **LHCb** Collaboration, R. Aaij *et al.*, “Measurement of the ratio of branching fractions $\mathcal{B}(\bar{B}^0 \rightarrow D^{*+}\tau^-\bar{\nu}_\tau)/\mathcal{B}(\bar{B}^0 \rightarrow D^{*+}\mu^-\bar{\nu}_\mu)$,” *Phys. Rev. Lett.* **115** no. 11, (2015) 111803, [arXiv:1506.08614 \[hep-ex\]](#). [Erratum: *Phys. Rev. Lett.* 115,no.15,159901(2015)].
- [40] **Belle** Collaboration, M. Huschle *et al.*, “Measurement of the branching ratio of $\bar{B} \rightarrow D^{(*)}\tau^-\bar{\nu}_\tau$ relative to $\bar{B} \rightarrow D^{(*)}\ell^-\bar{\nu}_\ell$ decays with hadronic tagging at Belle,” *Phys. Rev.* **D92** no. 7, (2015) 072014, [arXiv:1507.03233 \[hep-ex\]](#).
- [41] **Belle** Collaboration, A. Abdesselam *et al.*, “Measurement of the branching ratio of $\bar{B}^0 \rightarrow D^{*+}\tau^-\bar{\nu}_\tau$ relative to $\bar{B}^0 \rightarrow D^{*+}\ell^-\bar{\nu}_\ell$ decays with a semileptonic tagging method,” in *Proceedings, 51st Rencontres de Moriond on Electroweak Interactions and Unified Theories: La Thuile, Italy, March 12-19, 2016*. 2016. [arXiv:1603.06711 \[hep-ex\]](#).
- [42] S. Jäger and J. Martin Camalich, “Reassessing the discovery potential of the $B \rightarrow K^*\ell^+\ell^-$ decays in the large-recoil region: SM challenges and BSM opportunities,” *Phys. Rev.* **D93** no. 1, (2016) 014028, [arXiv:1412.3183 \[hep-ph\]](#).
- [43] W. Altmannshofer and D. M. Straub, “Implications of $b \rightarrow s$ measurements,” in *Proceedings, 50th Rencontres de Moriond Electroweak Interactions and Unified Theories: La Thuile, Italy, March 14-21, 2015*, pp. 333–338. 2015. [arXiv:1503.06199 \[hep-ph\]](#).
- [44] S. Descotes-Genon, L. Hofer, J. Matias, and J. Virto, “Global analysis of $b \rightarrow s\ell\ell$ anomalies,” *JHEP* **06** (2016) 092, [arXiv:1510.04239 \[hep-ph\]](#).
- [45] M. Ciuchini, M. Fedele, E. Franco, S. Mishima, A. Paul, L. Silvestrini, and M. Valli, “ $B \rightarrow K^*\ell^+\ell^-$ decays at large recoil in the Standard Model: a theoretical reappraisal,” *JHEP* **06** (2016) 116, [arXiv:1512.07157 \[hep-ph\]](#).
- [46] T. Hurth, F. Mahmoudi, and S. Neshatpour, “On the anomalies in the latest LHCb data,” *Nucl. Phys.* **B909** (2016) 737–777, [arXiv:1603.00865 \[hep-ph\]](#).
- [47] M. Algueró, B. Capdevila, A. Crivellin, S. Descotes-Genon, P. Masjuan, J. Matias, M. Novoa Brunet, and J. Virto, “Emerging patterns of New Physics with and without Lepton Flavour Universal contributions,” *Eur. Phys. J. C* **79** no. 8, (2019) 714, [arXiv:1903.09578 \[hep-ph\]](#). [Addendum: *Eur.Phys.J.C* 80, 511 (2020)].
- [48] M. Ciuchini, A. M. Coutinho, M. Fedele, E. Franco, A. Paul, L. Silvestrini, and M. Valli, “New Physics in $b \rightarrow s\ell^+\ell^-$ confronts new data on Lepton Universality,” *Eur. Phys. J. C* **79** no. 8, (2019) 719, [arXiv:1903.09632 \[hep-ph\]](#).
- [49] A. Datta, J. Kumar, and D. London, “The B anomalies and new physics in $b \rightarrow se^+e^-$,” *Phys. Lett. B* **797** (2019) 134858, [arXiv:1903.10086 \[hep-ph\]](#).
- [50] J. Aebischer, W. Altmannshofer, D. Guadagnoli, M. Reboud, P. Stangl, and D. M. Straub, “ B -decay discrepancies after Moriond 2019,” *Eur. Phys. J. C* **80** no. 3, (2020) 252, [arXiv:1903.10434 \[hep-ph\]](#).
- [51] K. Kowalska, D. Kumar, and E. M. Sessolo, “Implications for new physics in $b \rightarrow s\mu\mu$ transitions after recent measurements by Belle and LHCb,” *Eur. Phys. J. C* **79** no. 10, (2019) 840, [arXiv:1903.10932 \[hep-ph\]](#).
- [52] A. Arbey, T. Hurth, F. Mahmoudi, D. M. Santos, and S. Neshatpour, “Update on the $b \rightarrow s$ anomalies,” *Phys. Rev. D* **100** no. 1, (2019) 015045, [arXiv:1904.08399 \[hep-ph\]](#).
- [53] A. Biswas, S. Nandi, I. Ray, and S. K. Patra, “New physics in $b \rightarrow s\ell\ell$ decays with complex Wilson coefficients,” [arXiv:2004.14687 \[hep-ph\]](#).

- [54] J. Bhom, M. Chruszcz, F. Mahmoudi, M. Prim, P. Scott, and M. White, “A model-independent analysis of $b \rightarrow s\mu^+\mu^-$ transitions with GAMBIT’s FlavBit,” [arXiv:2006.03489 \[hep-ph\]](#).
- [55] C. Bobeth, U. Haisch, A. Lenz, B. Pecjak, and G. Tetlalmatzi-Xolocotzi, “On new physics in $\Delta\Gamma_d$,” *JHEP* **06** (2014) 040, [arXiv:1404.2531 \[hep-ph\]](#).
- [56] C. Bobeth, M. Gorbahn, and S. Vickers, “Weak annihilation and new physics in charmless $B \rightarrow MM$ decays,” *Eur. Phys. J. C* **75** no. 7, (2015) 340, [arXiv:1409.3252 \[hep-ph\]](#).
- [57] J. Brod, A. Lenz, G. Tetlalmatzi-Xolocotzi, and M. Wiebusch, “New physics effects in tree-level decays and the precision in the determination of the quark mixing angle γ ,” *Phys. Rev. D* **92** no. 3, (2015) 033002, [arXiv:1412.1446 \[hep-ph\]](#).
- [58] S. Jäger, M. Kirk, A. Lenz, and K. Leslie, “Charming new physics in rare B-decays and mixing?,” *Phys. Rev. D* **97** no. 1, (2018) 015021, [arXiv:1701.09183 \[hep-ph\]](#).
- [59] J. Aebischer, C. Bobeth, A. J. Buras, and D. M. Straub, “Anatomy of ϵ'/ϵ beyond the standard model,” *Eur. Phys. J. C* **79** no. 3, (2019) 219, [arXiv:1808.00466 \[hep-ph\]](#).
- [60] S. Jäger, M. Kirk, A. Lenz, and K. Leslie, “Charming New B -Physics,” [arXiv:1910.12924 \[hep-ph\]](#).
- [61] A. Crivellin, C. Gross, S. Pokorski, and L. Vernazza, “Correlating ϵ'/ϵ to hadronic B decays via $U(2)^3$ flavour symmetry,” 2019. [arXiv:1909.02101 \[hep-ph\]](#).
- [62] L. Calibbi, A. Crivellin, F. Kirk, C. A. Manzari, and L. Vernazza, “ Z' models with less-minimal flavour violation,” [arXiv:1910.00014 \[hep-ph\]](#).
- [63] M. Wiebusch, “Numerical Computation of p-values with *myFitter*,” *Comput. Phys. Commun.* **184** (2013) 2438–2445, [arXiv:1207.1446 \[hep-ph\]](#).
- [64] D. King, M. Kirk, A. Lenz, and T. Rauh, “ $|V_{cb}|$ and γ from B -mixing,” [arXiv:1911.07856 \[hep-ph\]](#).
- [65] L. Di Luzio, M. Kirk, A. Lenz, and T. Rauh, “ ΔM_s theory precision confronts flavour anomalies,” [arXiv:1909.11087 \[hep-ph\]](#).
- [66] G. Buchalla, A. J. Buras, and M. E. Lautenbacher, “Weak decays beyond leading logarithms,” *Rev. Mod. Phys.* **68** (1996) 1125–1144, [arXiv:hep-ph/9512380 \[hep-ph\]](#).
- [67] M. Beneke, G. Buchalla, C. Greub, A. Lenz, and U. Nierste, “Next-to-leading order QCD corrections to the lifetime difference of B_s mesons,” *Phys. Lett. B* **459** (1999) 631–640, [arXiv:hep-ph/9808385 \[hep-ph\]](#).
- [68] J. Aebischer, M. Fael, C. Greub, and J. Virto, “B physics Beyond the Standard Model at One Loop: Complete Renormalization Group Evolution below the Electroweak Scale,” *JHEP* **09** (2017) 158, [arXiv:1704.06639 \[hep-ph\]](#).
- [69] A. J. Buras, “Weak Hamiltonian, CP violation and rare decays,” in *Probing the standard model of particle interactions. Proceedings, Summer School in Theoretical Physics, NATO Advanced Study Institute, 68th session, Les Houches, France, July 28-September 5, 1997. Pt. 1, 2*, pp. 281–539. 1998. [arXiv:hep-ph/9806471 \[hep-ph\]](#).
- [70] A. J. Buras, P. Gambino, and U. A. Haisch, “Electroweak penguin contributions to nonleptonic $\Delta F = 1$ decays at NNLO,” *Nucl. Phys. B* **570** (2000) 117–154, [arXiv:hep-ph/9911250 \[hep-ph\]](#).

- [71] F. Krinner, A. Lenz, and T. Rauh, “The inclusive decay $b \rightarrow c\bar{c}s$ revisited,” *Nucl. Phys.* **B876** (2013) 31–54, [arXiv:1305.5390 \[hep-ph\]](#).
- [72] E. Bagan, P. Ball, V. M. Braun, and P. Gosdzinsky, “Charm quark mass dependence of QCD corrections to nonleptonic inclusive B decays,” *Nucl. Phys.* **B432** (1994) 3–38, [arXiv:hep-ph/9408306 \[hep-ph\]](#).
- [73] E. Bagan, P. Ball, B. Fiol, and P. Gosdzinsky, “Next-to-leading order radiative corrections to the decay $b \rightarrow ccs$,” *Phys. Lett.* **B351** (1995) 546–554, [arXiv:hep-ph/9502338 \[hep-ph\]](#).
- [74] A. Lenz, U. Nierste, and G. Ostermaier, “Penguin diagrams, charmless B decays and the missing charm puzzle,” *Phys. Rev.* **D56** (1997) 7228–7239, [arXiv:hep-ph/9706501 \[hep-ph\]](#).
- [75] A. Lenz, U. Nierste, and G. Ostermaier, “Determination of the CKM angle γ and $|V_{ub}/V_{cb}|$ from inclusive direct CP asymmetries and branching ratios in charmless B decays,” *Phys. Rev.* **D59** (1999) 034008, [arXiv:hep-ph/9802202 \[hep-ph\]](#).
- [76] C. Greub and P. Liniger, “The Rare decay $b \rightarrow sg$ beyond leading logarithms,” *Phys. Lett.* **B494** (2000) 237–247, [arXiv:hep-ph/0008071 \[hep-ph\]](#).
- [77] C. Greub and P. Liniger, “Calculation of next-to-leading QCD corrections to $b \rightarrow sg$,” *Phys. Rev.* **D63** (2001) 054025, [arXiv:hep-ph/0009144 \[hep-ph\]](#).
- [78] N. G. Uraltsev, “On the problem of boosting nonleptonic b baryon decays,” *Phys. Lett.* **B376** (1996) 303–308, [arXiv:hep-ph/9602324 \[hep-ph\]](#).
- [79] M. Neubert and C. T. Sachrajda, “Spectator effects in inclusive decays of beauty hadrons,” *Nucl. Phys.* **B483** (1997) 339–370, [arXiv:hep-ph/9603202 \[hep-ph\]](#).
- [80] M. Beneke, G. Buchalla, C. Greub, A. Lenz, and U. Nierste, “The $B^+ - B_d^0$ lifetime difference beyond leading logarithms,” *Nucl. Phys.* **B639** (2002) 389–407, [arXiv:hep-ph/0202106 \[hep-ph\]](#).
- [81] E. Franco, V. Lubicz, F. Mescia, and C. Tarantino, “Lifetime ratios of beauty hadrons at the next-to-leading order in QCD,” *Nucl. Phys.* **B633** (2002) 212–236, [arXiv:hep-ph/0203089 \[hep-ph\]](#).
- [82] M. Kirk, A. Lenz, and T. Rauh, “Dimension-six matrix elements for meson mixing and lifetimes from sum rules,” *JHEP* **12** (2017) 068, [arXiv:1711.02100 \[hep-ph\]](#).
- [83] M. Beneke, G. Buchalla, and I. Dunietz, “Width Difference in the $B_s - \bar{B}_s$ System,” *Phys. Rev.* **D54** (1996) 4419–4431, [arXiv:hep-ph/9605259 \[hep-ph\]](#). [Erratum: Phys. Rev.D83,119902(2011)].
- [84] A. S. Dighe, T. Hurth, C. S. Kim, and T. Yoshikawa, “Measurement of the lifetime difference of B(d) mesons: Possible and worthwhile?,” *Nucl. Phys.* **B624** (2002) 377–404, [arXiv:hep-ph/0109088 \[hep-ph\]](#).
- [85] M. Ciuchini, E. Franco, V. Lubicz, F. Mescia, and C. Tarantino, “Lifetime differences and CP violation parameters of neutral B mesons at the next-to-leading order in QCD,” *JHEP* **08** (2003) 031, [arXiv:hep-ph/0308029 \[hep-ph\]](#).
- [86] M. Beneke, G. Buchalla, A. Lenz, and U. Nierste, “CP asymmetry in flavor specific B decays beyond leading logarithms,” *Phys. Lett.* **B576** (2003) 173–183, [arXiv:hep-ph/0307344 \[hep-ph\]](#).

- [87] A. Lenz and U. Nierste, “Theoretical update of $B_s - \bar{B}_s$ mixing,” *JHEP* **06** (2007) 072, [arXiv:hep-ph/0612167](#) [[hep-ph](#)].
- [88] T. Inami and C. S. Lim, “Effects of Superheavy Quarks and Leptons in Low-Energy Weak Processes $K_L \rightarrow \mu\bar{\mu}$, $K^+ \rightarrow \pi^+\nu\bar{\nu}$ and $K^0 \leftrightarrow \bar{K}^0$,” *Prog. Theor. Phys.* **65** (1981) 297. [Erratum: *Prog. Theor. Phys.* 65,1772(1981)].
- [89] A. J. Buras, M. Jamin, and P. H. Weisz, “Leading and Next-to-leading QCD Corrections to ϵ Parameter and $B^0 - \bar{B}^0$ Mixing in the Presence of a Heavy Top Quark,” *Nucl. Phys.* **B347** (1990) 491–536.
- [90] A. G. Grozin, R. Klein, T. Mannel, and A. A. Pivovarov, “ $B^0 - \bar{B}^0$ mixing at next-to-leading order,” *Phys. Rev.* **D94** no. 3, (2016) 034024, [arXiv:1606.06054](#) [[hep-ph](#)].
- [91] D. King, A. Lenz, and T. Rauh, “ B_s mixing observables and $-V_{td}/V_{ts}$ — from sum rules,” *JHEP* **05** (2019) 034, [arXiv:1904.00940](#) [[hep-ph](#)].
- [92] N. H. Christ, J. M. Flynn, T. Izubuchi, T. Kawanai, C. Lehner, A. Soni, R. S. Van de Water, and O. Witzel, “B-meson decay constants from 2+1-flavor lattice QCD with domain-wall light quarks and relativistic heavy quarks,” *Phys. Rev.* **D91** no. 5, (2015) 054502, [arXiv:1404.4670](#) [[hep-lat](#)].
- [93] **ETM** Collaboration, A. Bussone *et al.*, “Mass of the b quark and B -meson decay constants from $N_f = 2 + 1 + 1$ twisted-mass lattice QCD,” *Phys. Rev.* **D93** no. 11, (2016) 114505, [arXiv:1603.04306](#) [[hep-lat](#)].
- [94] C. Hughes, C. T. H. Davies, and C. J. Monahan, “New methods for B meson decay constants and form factors from lattice NRQCD,” *Phys. Rev.* **D97** no. 5, (2018) 054509, [arXiv:1711.09981](#) [[hep-lat](#)].
- [95] A. Bazavov *et al.*, “B- and D-meson leptonic decay constants from four-flavor lattice QCD,” *Phys. Rev.* **D98** no. 7, (2018) 074512, [arXiv:1712.09262](#) [[hep-lat](#)].
- [96] **HPQCD** Collaboration, C. T. H. Davies, J. Harrison, G. P. Lepage, C. J. Monahan, J. Shigemitsu, and M. Wingate, “Lattice QCD matrix elements for the $B_s^0 - \bar{B}_s^0$ width difference beyond leading order,” [arXiv:1910.00970](#) [[hep-lat](#)].
- [97] M. Beneke, J. Rohrer, and D. Yang, “Branching fractions, polarisation and asymmetries of $B \rightarrow VV$ decays,” *Nucl. Phys.* **B774** (2007) 64–101, [arXiv:hep-ph/0612290](#) [[hep-ph](#)].
- [98] M. Bartsch, G. Buchalla, and C. Kraus, “ $B \rightarrow V_L V_L$ Decays at Next-to-Leading Order in QCD,” [arXiv:0810.0249](#) [[hep-ph](#)].
- [99] M. Beneke, T. Huber, and X.-Q. Li, “NNLO vertex corrections to non-leptonic B decays: Tree amplitudes,” *Nucl. Phys.* **B832** (2010) 109–151, [arXiv:0911.3655](#) [[hep-ph](#)].
- [100] V. M. Braun, D. Yu. Ivanov, and G. P. Korchemsky, “The B meson distribution amplitude in QCD,” *Phys. Rev.* **D69** (2004) 034014, [arXiv:hep-ph/0309330](#) [[hep-ph](#)].
- [101] M. Beneke and J. Rohrwild, “B meson distribution amplitude from $B \rightarrow \gamma\ell\nu$,” *Eur. Phys. J.* **C71** (2011) 1818, [arXiv:1110.3228](#) [[hep-ph](#)].
- [102] Y.-M. Wang, “Factorization and dispersion relations for radiative leptonic B decay,” *JHEP* **09** (2016) 159, [arXiv:1606.03080](#) [[hep-ph](#)].
- [103] M. Beneke, V. M. Braun, Y. Ji, and Y.-B. Wei, “Radiative leptonic decay $B \rightarrow \gamma\ell\nu_\ell$ with subleading power corrections,” *JHEP* **07** (2018) 154, [arXiv:1804.04962](#) [[hep-ph](#)].

- [104] Y.-M. Wang and Y.-L. Shen, “Subleading-power corrections to the radiative leptonic $B \rightarrow \gamma \ell \nu$ decay in QCD,” *JHEP* **05** (2018) 184, [arXiv:1803.06667 \[hep-ph\]](#).
- [105] **Belle** Collaboration, A. Heller *et al.*, “Search for $B^+ \rightarrow \ell^+ \nu_\ell \gamma$ decays with hadronic tagging using the full Belle data sample,” *Phys. Rev.* **D91** no. 11, (2015) 112009, [arXiv:1504.05831 \[hep-ex\]](#).
- [106] S. J. Lee and M. Neubert, “Model-independent properties of the B-meson distribution amplitude,” *Phys. Rev.* **D72** (2005) 094028, [arXiv:hep-ph/0509350 \[hep-ph\]](#).
- [107] G. Bell and V. Pilipp, “ $B^- \rightarrow \pi^- \pi^0 / \rho^- \rho^0$ to NNLO in QCD factorization,” *Phys. Rev.* **D80** (2009) 054024, [arXiv:0907.1016 \[hep-ph\]](#).
- [108] L. Hofer, D. Scherer, and L. Vernazza, “ $B_s \rightarrow \phi \rho^0$ and $B_s \rightarrow \phi \pi^0$ as a handle on isospin-violating New physics,” *JHEP* **02** (2011) 080, [arXiv:1011.6319 \[hep-ph\]](#).
- [109] J. D. Bjorken, “Topics in B Physics,” *Nucl. Phys. Proc. Suppl.* **11** (1989) 325–341.
- [110] T. Huber, S. Kränkl, and X.-Q. Li, “Two-body non-leptonic heavy-to-heavy decays at NNLO in QCD factorization,” *JHEP* **09** (2016) 112, [arXiv:1606.02888 \[hep-ph\]](#).
- [111] **HFLAV** Collaboration, Y. Amhis *et al.*, “Averages of b -hadron, c -hadron, and τ -lepton properties as of summer 2016,” *Eur. Phys. J.* **C77** no. 12, (2017) 895, [arXiv:1612.07233 \[hep-ex\]](#).
- [112] G. Banelli, R. Fleischer, R. Jaarsma, and G. Tetlalmatzi-Xolocotzi, “Decoding (Pseudo)-Scalar Operators in Leptonic and Semileptonic B Decays,” *Eur. Phys. J.* **C78** no. 11, (2018) 911, [arXiv:1809.09051 \[hep-ph\]](#).
- [113] M. Beneke and S. Jager, “Spectator scattering at NLO in non-leptonic b decays: Tree amplitudes,” *Nucl. Phys.* **B751** (2006) 160–185, [arXiv:hep-ph/0512351 \[hep-ph\]](#).
- [114] G. Bell, “NNLO vertex corrections in charmless hadronic B decays: Imaginary part,” *Nucl. Phys.* **B795** (2008) 1–26, [arXiv:0705.3127 \[hep-ph\]](#).
- [115] G. Bell, “NNLO vertex corrections in charmless hadronic B decays: Real part,” *Nucl. Phys.* **B822** (2009) 172–200, [arXiv:0902.1915 \[hep-ph\]](#).
- [116] **Particle Data Group** Collaboration, M. Tanabashi *et al.*, “Review of Particle Physics,” *Phys. Rev.* **D98** no. 3, (2018) 030001.
- [117] S. Gonzàlez-Solís and P. Masjuan, “Study of $B \rightarrow \pi \ell \nu_\ell$ and $B^+ \rightarrow \eta^{(\prime)} \ell^+ \nu_\ell$ decays and determination of $|V_{ub}|$,” *Phys. Rev.* **D98** no. 3, (2018) 034027, [arXiv:1805.11262 \[hep-ph\]](#).
- [118] **BaBar** Collaboration, P. del Amo Sanchez *et al.*, “Study of $B \rightarrow \pi \ell \nu$ and $B \rightarrow \rho \ell \nu$ Decays and Determination of $|V_{ub}|$,” *Phys. Rev.* **D83** (2011) 032007, [arXiv:1005.3288 \[hep-ex\]](#).
- [119] **BaBar** Collaboration, J. P. Lees *et al.*, “Branching fraction and form-factor shape measurements of exclusive charmless semileptonic B decays, and determination of $|V_{ub}|$,” *Phys. Rev.* **D86** (2012) 092004, [arXiv:1208.1253 \[hep-ex\]](#).
- [120] **Belle** Collaboration, H. Ha *et al.*, “Measurement of the decay $B^0 \rightarrow \pi^- \ell^+ \nu$ and determination of $|V_{ub}|$,” *Phys. Rev.* **D83** (2011) 071101, [arXiv:1012.0090 \[hep-ex\]](#).
- [121] **Belle** Collaboration, A. Sibidanov *et al.*, “Study of Exclusive $B \rightarrow X_u \ell \nu$ Decays and Extraction of $\|V_{ub}\|$ using Full Reconstruction Tagging at the Belle Experiment,” *Phys. Rev.* **D88** no. 3, (2013) 032005, [arXiv:1306.2781 \[hep-ex\]](#).

- [122] **CLEO** Collaboration, N. E. Adam *et al.*, “A Study of Exclusive Charmless Semileptonic B Decay and $—V(ub)—$,” *Phys. Rev. Lett.* **99** (2007) 041802, [arXiv:hep-ex/0703041 \[HEP-EX\]](#).
- [123] M. Kaminski, M. Misiak, and M. Poradzinski, “Tree-level contributions to $B \rightarrow X_s \gamma$,” *Phys. Rev.* **D86** (2012) 094004, [arXiv:1209.0965 \[hep-ph\]](#).
- [124] M. Czakon, P. Fiedler, T. Huber, M. Misiak, T. Schutzmeier, and M. Steinhauser, “The $(Q_7, Q_{1,2})$ contribution to $\bar{B} \rightarrow X_s \gamma$ at $\mathcal{O}(\alpha_s^2)$,” *JHEP* **04** (2015) 168, [arXiv:1503.01791 \[hep-ph\]](#).
- [125] M. Misiak and M. Steinhauser, “NNLO QCD corrections to the $\bar{B} \rightarrow X_s \gamma$ matrix elements using interpolation in $m(c)$,” *Nucl. Phys.* **B764** (2007) 62–82, [arXiv:hep-ph/0609241 \[hep-ph\]](#).
- [126] K. G. Chetyrkin, M. Misiak, and M. Munz, “Weak radiative B meson decay beyond leading logarithms,” *Phys. Lett.* **B400** (1997) 206–219, [arXiv:hep-ph/9612313 \[hep-ph\]](#).
[Erratum: *Phys. Lett.* B425,414(1998)].
- [127] S. L. Glashow, J. Iliopoulos, and L. Maiani, “Weak Interactions with Lepton-Hadron Symmetry,” *Phys. Rev.* **D2** (1970) 1285–1292.
- [128] A. Lenz and U. Nierste, “Numerical Updates of Lifetimes and Mixing Parameters of B Mesons,” in *CKM unitarity triangle. Proceedings, 6th International Workshop, CKM 2010, Warwick, UK, September 6-10, 2010*. 2011. [arXiv:1102.4274 \[hep-ph\]](#).
- [129] H. M. Asatrian, A. Hovhannisyan, U. Nierste, and A. Yeghiazaryan, “Towards next-to-next-to-leading-log accuracy for the width difference in the $B_s - \bar{B}_s$ system: fermionic contributions to order $(m_c/m_b)^0$ and $(m_c/m_b)^1$,” *JHEP* **10** (2017) 191, [arXiv:1709.02160 \[hep-ph\]](#).
- [130] H.-Y. Cheng, Y.-Y. Keum, and K.-C. Yang, “ $B \rightarrow J/\psi K^*$ decays in QCD factorization,” *Phys. Rev.* **D65** (2002) 094023, [arXiv:hep-ph/0111094 \[hep-ph\]](#).
- [131] A. Lenz, M. L. Piscopo, and A. V. Rusov, “Contribution of the Darwin operator to non-leptonic decays of heavy quarks,” [arXiv:2004.09527 \[hep-ph\]](#).
- [132] T. Mannel, D. Moreno, and A. Pivovarov, “Heavy Quark Expansion for Heavy Hadron Lifetimes: Completing the $1/m_b^3$ Corrections,” [arXiv:2004.09485 \[hep-ph\]](#).
- [133] H. Boos, T. Mannel, and J. Reuter, “The Gold plated mode revisited: $\sin(2\beta)$ and $B^0 \rightarrow J/\psi K_S$ in the standard model,” *Phys. Rev.* **D70** (2004) 036006, [arXiv:hep-ph/0403085 \[hep-ph\]](#).
- [134] M. Misiak *et al.*, “Updated NNLO QCD predictions for the weak radiative B-meson decays,” *Phys. Rev. Lett.* **114** no. 22, (2015) 221801, [arXiv:1503.01789 \[hep-ph\]](#).
- [135] A. Crivellin and L. Mercolli, “ $B \rightarrow X_d \gamma$ and constraints on new physics,” *Phys. Rev.* **D84** (2011) 114005, [arXiv:1106.5499 \[hep-ph\]](#).
- [136] **BaBar** Collaboration, P. del Amo Sanchez *et al.*, “Study of $B \rightarrow X \gamma$ Decays and Determination of $|V_{td}/V_{ts}|$,” *Phys. Rev.* **D82** (2010) 051101, [arXiv:1005.4087 \[hep-ex\]](#).
- [137] W. Wang, “ $b \rightarrow s \gamma$ and $b \rightarrow d \gamma$ (B factories),” in *CKM unitarity triangle. Proceedings, 6th International Workshop, CKM 2010, Warwick, UK, September 6-10, 2010*. 2011. [arXiv:1102.1925 \[hep-ex\]](#).

- [138] A. J. Lenz, “Selected Topics in Heavy Flavour Physics,” *J. Phys.* **G41** (2014) 103001, [arXiv:1404.6197 \[hep-ph\]](#).
- [139] G. Borissov and B. Hoeneisen, “Understanding the like-sign dimuon charge asymmetry in $p\bar{p}$ collisions,” *Phys. Rev.* **D87** no. 7, (2013) 074020, [arXiv:1303.0175 \[hep-ex\]](#).
- [140] I. I. Y. Bigi and A. I. Sanda, “Notes on the Observability of CP Violations in B Decays,” *Nucl. Phys.* **B193** (1981) 85–108.
- [141] M. Gronau and D. London, “How to determine all the angles of the unitarity triangle from $B(d)0 \rightarrow \ell^+ D K(s)$ and $B(s)0 \rightarrow \ell^+ D0$,” *Phys. Lett.* **B253** (1991) 483–488.
- [142] M. Gronau and D. Wyler, “On determining a weak phase from CP asymmetries in charged B decays,” *Phys. Lett.* **B265** (1991) 172–176.
- [143] D. Atwood, I. Dunietz, and A. Soni, “Enhanced CP violation with $B \rightarrow \ell^+ K D0$ (anti- $D0$) modes and extraction of the CKM angle γ ,” *Phys. Rev. Lett.* **78** (1997) 3257–3260, [arXiv:hep-ph/9612433 \[hep-ph\]](#).
- [144] D. Atwood, I. Dunietz, and A. Soni, “Improved methods for observing CP violation in $B \rightarrow \ell^+ K D$ and measuring the CKM phase γ ,” *Phys. Rev.* **D63** (2001) 036005, [arXiv:hep-ph/0008090 \[hep-ph\]](#).
- [145] A. Giri, Y. Grossman, A. Soffer, and J. Zupan, “Determining γ using $B \rightarrow \ell^+ DK$ with multibody D decays,” *Phys. Rev.* **D68** (2003) 054018, [arXiv:hep-ph/0303187 \[hep-ph\]](#).
- [146] **LHCb** Collaboration, M. W. Kenzie and M. P. Whitehead, “Update of the LHCb combination of the CKM angle γ ,”.
- [147] **HFLAV** Collaboration, Y. S. Amhis *et al.*, “Averages of b -hadron, c -hadron, and τ -lepton properties as of 2018,” [arXiv:1909.12524 \[hep-ex\]](#).
- [148] **LHCb** Collaboration, R. Aaij *et al.*, “Physics case for an LHCb Upgrade II - Opportunities in flavour physics, and beyond, in the HL-LHC era,” [arXiv:1808.08865](#).
- [149] M. Blanke and A. J. Buras, “Universal Unitarity Triangle 2016 and the tension between $\Delta M_{s,d}$ and ε_K in CMFV models,” *Eur. Phys. J.* **C76** no. 4, (2016) 197, [arXiv:1602.04020 \[hep-ph\]](#).
- [150] M. Blanke and A. J. Buras, “Emerging ΔM_d -anomaly from tree-level determinations of $|V_{cb}|$ and the angle γ ,” *Eur. Phys. J.* **C79** no. 2, (2019) 159, [arXiv:1812.06963 \[hep-ph\]](#).
- [151] J. Brod and J. Zupan, “The ultimate theoretical error on γ from $B \rightarrow DK$ decays,” *JHEP* **01** (2014) 051, [arXiv:1308.5663 \[hep-ph\]](#).
- [152] J. Brod, “Electroweak effects in the extraction of the CKM angle γ from $B \rightarrow D\pi$ decays,” *Phys. Lett.* **B743** (2015) 56–60, [arXiv:1412.3173 \[hep-ph\]](#).
- [153] **CKMfitter Group** Collaboration, J. Charles, A. Hocker, H. Lacker, S. Laplace, F. R. Le Diberder, J. Malcles, J. Ocariz, M. Pivk, and L. Roos, “CP violation and the CKM matrix: Assessing the impact of the asymmetric B factories,” *Eur. Phys. J.* **C41** no. 1, (2005) 1–131, [arXiv:hep-ph/0406184 \[hep-ph\]](#).
- [154] **UTfit** Collaboration, M. Bona *et al.*, “The Unitarity Triangle Fit in the Standard Model and Hadronic Parameters from Lattice QCD: A Reappraisal after the Measurements of $\Delta m(s)$ and $BR(B \rightarrow \ell^+ \tau \nu(\tau))$,” *JHEP* **10** (2006) 081, [arXiv:hep-ph/0606167 \[hep-ph\]](#).

- [155] A. Cerri *et al.*, “Report from Working Group 4,” *CERN Yellow Rep. Monogr.* **7** (2019) 867–1158, [arXiv:1812.07638 \[hep-ph\]](#).
- [156] A. K. Alok, B. Bhattacharya, D. Kumar, J. Kumar, D. London, and S. U. Sankar, “New physics in $b \rightarrow s\mu^+\mu^-$: Distinguishing models through CP-violating effects,” *Phys. Rev. D* **96** no. 1, (2017) 015034, [arXiv:1703.09247 \[hep-ph\]](#).
- [157] T. Gershon, “ $\Delta\Gamma_d$: A Forgotten Null Test of the Standard Model,” *J. Phys.* **G38** (2011) 015007, [arXiv:1007.5135 \[hep-ph\]](#).
- [158] **ATLAS, CDF, CMS, D0** Collaboration, “First combination of Tevatron and LHC measurements of the top-quark mass,” [arXiv:1403.4427 \[hep-ex\]](#).
- [159] T. Rauh, “Higher-order condensate corrections to Υ masses, leptonic decay rates and sum rules,” *JHEP* **05** (2018) 201, [arXiv:1803.05477 \[hep-ph\]](#).
- [160] P. Ball and R. Zwicky, “SU(3) breaking of leading-twist K and K^* distribution amplitudes: A Reprise,” *Phys. Lett. B* **633** (2006) 289–297, [arXiv:hep-ph/0510338 \[hep-ph\]](#).
- [161] P. Ball, V. M. Braun, and A. Lenz, “Higher-twist distribution amplitudes of the K meson in QCD,” *JHEP* **05** (2006) 004, [arXiv:hep-ph/0603063 \[hep-ph\]](#).
- [162] P. Ball, V. M. Braun, and A. Lenz, “Twist-4 distribution amplitudes of the K^* and ϕ mesons in QCD,” *JHEP* **08** (2007) 090, [arXiv:0707.1201 \[hep-ph\]](#).
- [163] P. Ball and G. W. Jones, “Twist-3 distribution amplitudes of K^* and ϕ mesons,” *JHEP* **03** (2007) 069, [arXiv:hep-ph/0702100 \[HEP-PH\]](#).
- [164] P. Ball and V. M. Braun, “Handbook of higher twist distribution amplitudes of vector mesons in QCD,” in *Continuous advances in QCD. Proceedings, 3rd Workshop, QCD’98, Minneapolis, USA, April 16-19, 1998*, pp. 125–141. 1998. [arXiv:hep-ph/9808229 \[hep-ph\]](#).
- [165] **Flavour Lattice Averaging Group** Collaboration, S. Aoki *et al.*, “FLAG Review 2019,” [arXiv:1902.08191 \[hep-lat\]](#).
- [166] P. Ball, G. W. Jones, and R. Zwicky, “ $B \rightarrow V\gamma$ beyond QCD factorisation,” *Phys. Rev. D* **75** (2007) 054004, [arXiv:hep-ph/0612081 \[hep-ph\]](#).
- [167] P. Ball and R. Zwicky, “ $B_{d,s} \rightarrow \rho, \omega, K^*, \phi$ decay form-factors from light-cone sum rules revisited,” *Phys. Rev. D* **71** (2005) 014029, [arXiv:hep-ph/0412079 \[hep-ph\]](#).
- [168] **ETM** Collaboration, V. Lubicz, A. Melis, and S. Simula, “Masses and decay constants of $D_{(s)}^*$ and $B_{(s)}^*$ mesons with $N_f = 2 + 1 + 1$ twisted mass fermions,” *Phys. Rev. D* **96** no. 3, (2017) 034524, [arXiv:1707.04529 \[hep-lat\]](#).
- [169] A. Bharucha, “Two-loop Corrections to the $B \rightarrow \pi$ Form Factor from QCD Sum Rules on the Light-Cone and $|V_{ub}|$,” *JHEP* **05** (2012) 092, [arXiv:1203.1359 \[hep-ph\]](#).
- [170] A. Bharucha, D. M. Straub, and R. Zwicky, “ $B \rightarrow V\ell^+\ell^-$ in the Standard Model from light-cone sum rules,” *JHEP* **08** (2016) 098, [arXiv:1503.05534 \[hep-ph\]](#).
- [171] F. U. Bernlochner, Z. Ligeti, M. Papucci, and D. J. Robinson, “Combined analysis of semileptonic B decays to D and D^* : $R(D^{(*)})$, $|V_{cb}|$, and new physics,” *Phys. Rev. D* **95** no. 11, (2017) 115008, [arXiv:1703.05330 \[hep-ph\]](#). [erratum: Phys. Rev. D **97**, no. 5, 059902(2018)].
- [172] Y. Sakaki, M. Tanaka, A. Tayduganov, and R. Watanabe, “Testing leptoquark models in $\bar{B} \rightarrow D^{(*)}\tau\bar{\nu}$,” *Phys. Rev. D* **88** no. 9, (2013) 094012, [arXiv:1309.0301 \[hep-ph\]](#).

- [173] F. Herren and M. Steinhauser, “Version 3 of RunDec and CRunDec,” *Comput. Phys. Commun.* **224** (2018) 333–345, [arXiv:1703.03751 \[hep-ph\]](#).
- [174] A. G. Grozin and R. N. Lee, “Three-loop HQET vertex diagrams for B^0 - anti- B^0 mixing,” *JHEP* **02** (2009) 047, [arXiv:0812.4522 \[hep-ph\]](#).
- [175] **ETM** Collaboration, N. Carrasco *et al.*, “B-physics from $N_f = 2$ tmQCD: the Standard Model and beyond,” *JHEP* **03** (2014) 016, [arXiv:1308.1851 \[hep-lat\]](#).
- [176] Y. Aoki, T. Ishikawa, T. Izubuchi, C. Lehner, and A. Soni, “Neutral B meson mixings and B meson decay constants with static heavy and domain-wall light quarks,” *Phys. Rev.* **D91** no. 11, (2015) 114505, [arXiv:1406.6192 \[hep-lat\]](#).
- [177] **Fermilab Lattice, MILC** Collaboration, A. Bazavov *et al.*, “ $B_{(s)}^0$ -mixing matrix elements from lattice QCD for the Standard Model and beyond,” *Phys. Rev.* **D93** no. 11, (2016) 113016, [arXiv:1602.03560 \[hep-lat\]](#).
- [178] **RBC/UKQCD** Collaboration, P. A. Boyle, L. Del Debbio, N. Garron, A. Juttner, A. Soni, J. T. Tsang, and O. Witzel, “SU(3)-breaking ratios for $D_{(s)}$ and $B_{(s)}$ mesons,” [arXiv:1812.08791 \[hep-lat\]](#).
- [179] R. J. Dowdall, C. T. H. Davies, R. R. Horgan, G. P. Lepage, C. J. Monahan, J. Shigemitsu, and M. Wingate, “Neutral B-meson mixing from full lattice QCD at the physical point,” [arXiv:1907.01025 \[hep-lat\]](#).